Preferred Frequencies for Coupling of Seismic Waves and Vibrating Tall Buildings

by

Sergey Zheltukhin

A Thesis

Submitted to the Faculty

of

WORCESTER POLYTECHNIC INSTITUTE

In partial fulfillment of the requirements for the

Degree of Doctor of Philosophy

in

Mathematical Sciences

April, 2013

APPROVED:

Professor Darko Volkov, Advisor Department of Mathematical Sciences Worcester Polytechnic Institute	Professor Ioan Ionescu Institut Galilée Université Paris
Professor Marcus Sarkis Department of Mathematical Sciences Worcester Polytechnic Institute	Professor Suzanne Weekes Department of Mathematical Sciences Worcester Polytechnic Institute
Professor Bogdan Vernescu Department of Mathematical Sciences Worcester Polytechnic Institute	

Contents

Acknowledgements

I am very grateful for the opportunity to be a part of Worcester Polytechnic Institute, and Department of Mathematical Sciences in particular. It was a challenging experience which contributed greatly to my self development. This would not be possible without help of many people to whom I would like to express my gratitude.

To my advisor, Darko Volkov, for introducing me to interesting and demanding problems and guidance in their solving, for his support, patience, and time he dedicated to me.

To the members of my dissertation committee, Professor Volkov, Professor Ionescu, Professor Sarkis, Professor Weekes, and Professor Vernescu, for the time they spent reading and correcting my thesis.

To all of the professors I have taken classes with or worked with as a teaching assistant for the lessons I learned, both practical and theoretical, and especially to Roger Lui who guided me through the first years in the program.

To Ellen Mackin, Rhonda Podell, Deborah Riel, Linda Bullens, and Mike Malone for taking care of all the organizational matters. To my fellow graduate students for making life and studies easier.

Introduction

Background

It has been observed, that when an earthquake strikes a large city, the seismic activity is altered by the collective response of the buildings of the city. This phenomenon is called the "city-effect", and in our dissertation we study this problem. The evaluation of seismic risk in urban environments is crucial because of high population densities as well as the factories and offices situated in those areas whose contribution to our economy is vital. Studying the city-effect problem may help safety agencies and policy makers in the future assess seismic risk specific to urban areas and it may lead to setting new guidelines for local building codes. The traditional approach to evaluating seismic risk in urban areas is to consider seismic waves in the underground as the only cause for motion at the top. Accordingly, in earlier studies, seismic wave propagation was evaluated in a separate step and then impacts on man made structures above ground were calculated. However, observational evidence has since then demonstrated that structures built on the earth surface may in turn impact seismic waves, see [4, 19, 11]. The 1985 Michoacan earthquake in Mexico City led Wirgin and Bard [31] to hypothesize that city buildings may collectively affect the ground motion during an earthquake. That idea was supported by several other technical and computational studies, see [2, 6, 7]. The starting point of this thesis is a paper on the city-effect problem by Ghergu and Ionescu, [15], with a stronger theoretical and mathematical flavor. Ghergu and Ionescu proposed a model derived from the equations of physics and a solution algorithm relying on solid mathematics. Our contribution is to extend their work and to provide a mathematical analysis for proving the existence of preferred frequencies coupling vibrations of buildings to underground seismic waves.

Ghergu and Ionescu were able to compute a city frequency constant, that is, given the geometry and the specific physical constants of an idealized two dimensional city, they computed a frequency that will lead to the resonance between vibrating buildings and underground seismic waves. This is an impressive achievement, but that city frequency constant was obtained by simply increasing the number of buildings at the expense of solving larger and larger systems. Our idea is instead to use a periodic Green's function and perform computations on a single period. That allows for much faster computations, and in turn makes it possible to consider more complex geometries within a single period.

This thesis includes theoretical considerations related to the city-effect problem. We

solve a system of integral equations to determine the (anti-plane) vibrations of the ground, so that potential theory, partial differential equations and integral equations are important underlying mathematical objects that we will have to manipulate throughout this thesis. We investigated regularity results for double-layer potentials, given in appendix. Although related results are certainly considered to be standard, we have not found in the literature the precise regularity result that we are interested in. Later in this thesis we provide a rather in depth and proof based account of different formulations for the periodic Green's function that we need. Although the actual formulas that we use have been known for some time, see [23], we prove that they are indeed fundamental solutions to the Helmholtz operator and we analyze their convergence rate. Finally we devote the last chapter of this thesis to the mathematical proof of existence of preferred frequencies coupling vibrations of buildings to underground seismic waves.

Thesis outline

The first chapter of the thesis is an introduction to the city-effect model developed by Ghergu and Ionescu. They pertain to the case of a city with a finite number of equally spaced and identical buildings located along a straight line. We describe the physical statement and corresponding mathematical problem, which leads to the two-dimensional Helmholtz equation.

Chapter II is dedicated to periodic Green's function for the Helmholtz operator. We examine three ways of defining these Green's functions. The first way uses infinite sums of Bessel functions. This formulation is straightforward but suffers from a very slow convergence rate. The second way is done in a spectral form which appears as a series which converges very fast at points (x_0, y_0, x, y) where $|x - x_0|$ is large enough. We provide a complete argument proving that this second form is indeed a fundamental solution to the Helmholtz equation. The third way relies on the so called Ewald method. We show that this method converges remarkably fast and independently of $|x - x_0|$. Eventually we will use either the second or the third form depending on $|x - x_0|$.

In the second part of chapter II, we proceed to work on numerical solutions to interior Neumann problems for Helmholtz equations *whose solutions in closed form are known*. Our goal is two fold. First, we want to gain a solid grasp of weakly singular boundary integral equations since they will be essential in our city-effect computations. Second, this is an excellent opportunity to use periodic Green's functions in our codes and verify how accurately we can solve integral equations with those special Green's functions.

The third chapter of this thesis is entirely devoted to numerical computations for the city-effect problem. We begin by reproducing the computational method introduced by Ghergu and Ionescu in [15]. Ghergu and Ionescu realized that the search for coupling frequencies in that case can be greatly accelerated by finding the eigenvalues of a relevant symmetric matrix T. As the number of buildings in a city grows large their study seemed to indicate that the smallest eigenvalue of that matrix converges to some limit value. In our approach,

cities are directly modeled to be periodic, so the search for coupling frequencies is performed on a single cell and thus our search is even less computationally intensive. We are able to recover the same value as in the large number of buildings case. As we explored different values of relative spacing between buildings, a more complex picture arose. It turned out that if buildings are closer together it is the *largest* eigenvalue of T which is convergent to the periodic case.

In the second part of chapter III we investigate the case of buildings of different geometries, which are no longer required to be equally spaced. In that case the matrix T is no helpful anymore and the solution method proposed by Ghergu and Ionescu in [15] is no longer applicable. A free space calculation is particularly burdensome in that case and may quickly become intractable. Clearly, our periodic formulation statement becomes especially helpful in that case. We simply impose a pattern of buildings of different sizes on each cell and assume that this pattern is repeated on each period.

The last chapter of this thesis pertains to the theoretical proof that preferred, that is, coupling frequencies for the city-effect problem do exist. The proof is done in the simpler case of a single building. We do not believe that this simplifying assumption is too restrictive, it is rather done as a matter of simplifying notations and statements. This existence result ensues from asymptotics at high and low frequencies and continuity in the frequency variable. These asymptotics are proved using variational formulations and boundary Dirichlet to Neumann operators which involve rather delicate manipulations of series of Hankel functions.

The first part of the appendices is about C^α regularity results for single and double layer potentials. These kinds of results are certainly standard, however, we have not found in the literature the exact case that we wanted to cover: C^α regularity all the way to the boundary for a double-layer potential defined on the C^2 boundary of a bounded domain in $\mathbb{R}^2$ (most texts focus exclusively on the three dimensional case, or are merely on C^α continuity on the boundary, or on the case where that boundary is *only approached in a normal direction*). In the end we provide our $Matlab$ code for the cases of a city with non-identical buildings, both free-space and periodic, and $Maple$ code for calculation of the particular limits we use during the periodic model derivation.

Chapter 1

City-Effect Seismic Problem

1.1 Introduction

Seismic vibrations of the earth may impact structures built on its surface, and throughout history people have experienced how destructive earthquakes can be. This phenomenon is called "soil-structure interaction". The fact that structures, in their turn, can cause or alter earth vibration is subtle and much less noticeable, and only recently has evidence been found to support this. Several cases are stated in [2].

In 1970 vibrations of the Millikan library on the Caltech campus caused by roof actuators were registered by seismographs located a few kilometers away (actually, there were several testings, the last one in 2002, see [4]). Several times a shock wave from a space shuttle which was entering the atmosphere was recorded by different seismic networks near Edwards Air Force Base (Columbia, 1989; Atlantis, 1991; Discovery, 1991; see [19]). In particular, a shock wave from the shuttle Columbia hit high buildings in Los Angeles and induced seismic waves which were recorded by stations in Pasadena, CA (the distance is about 15 kilometers). During the terrorist attacks against the Twin Towers of the World Trade Center in New York in 2001 the impact was felt several tens of kilometers away. This phenomenon is called structure-soil interaction. All these events were possible because the natural frequencies of the structures happened to be very close to the frequencies of the soil layers in these areas.

A more complicated phenomenon occurred in Sweden, when the audience of a rock concert at the Ullevi stadium in Gothenburg started to jump in accord with the beat. Resulting waves transmitted to the soil, were trapped in it, and propagated back as the surface waves. These waves in turn, resonating with the crowd jumping, made the stadium shake (see [11]).

The most significant observation was made during destructive Michoacan earthquake in Mexico city in 1985 (see, for example, [17]). The classical computational methods failed to explain all the features of the seismic records. This case led Wirgin and Bard in [31] to suggest that "the ground motion is significantly contaminated in the immediate vicinity of a building", because Mexico City is a densely urbanized area. Bard et al. showed experimen-

tally in [2] that "the idea itself is not stupid, [...] the buildings do talk to each other through the ground." This is called "city-effect".

One of the crucial common factors for all these observations was that the frequency of the structures coincided with the frequency of the soil layers. Our main objective in this thesis will be studying city frequencies.

The following section is a summary of [15]. It describes a model for the city-effect problem and a solution algorithm introduced by Ghergu and Ionescu (2009). This model deals with cities of finite size with identical evenly spaced buildings. Here we will briefly discuss the statement of the physical problem and the associated spectral problem. The mathematical method of its solution will be presented in Chapter III.

1.2 Cities with a finite number of equal-sized, uniformly spaced, buildings

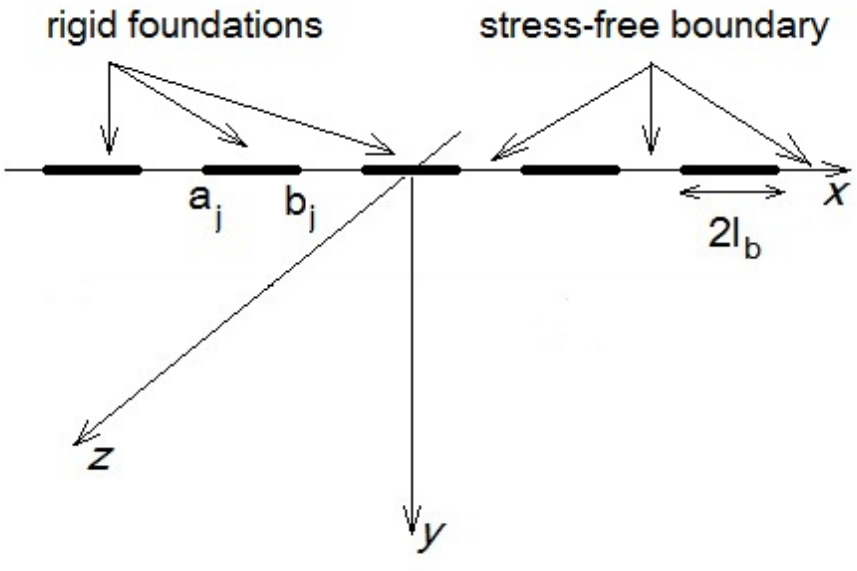

Fig. 1.1: *Geometrical model of a city.*

1.2.1 Physical model

We consider soil as an elastic half-space $\Omega \times \mathbb{R}$, where $\Omega = \mathbb{R} \times (0, \infty)$. A city, consisting of N buildings of width $2l_b$ and height h each, and the distance between two consecutive buildings is *space*. The rigid foundations of the buildings are located along the x-axis and denoted as $\Gamma_j = [a_j, b_j] \times 0$ in Ω. Now, let us denote

- $\Gamma = \bigcup_{j=1}^{N} \Gamma_j$, the set of foundations;
- $\Gamma_{free} = \mathbb{R} \times 0 \backslash \Gamma$, the stress free soil boundary;
- $\vec{\mathbf{w}} = \big(0, 0, w(t, x, y)\big)$, the displacement field; **anti-plane shearing** is assumed in this model.

Other physical parameters of the buildings and soil are:

- ρ, ρ_b - soil and building mass densities;
- S, S_b - soil and building shear rigidities;
- $\beta = \sqrt{S/\rho}$, $\beta_b = \sqrt{S_b/\rho_b}$ - soil and building shear velocities;
- $u_j(t)$ - the displacement of the rigid building foundation Γ_j;

- $v_j(t)$ - the displacement of the top of the j^{th} building;
- $m_1,\ m_0$ - the masses of the top and of the foundation correspondingly;
- $R_j(w)$ - the soil force acting on the foundation Γ_j.

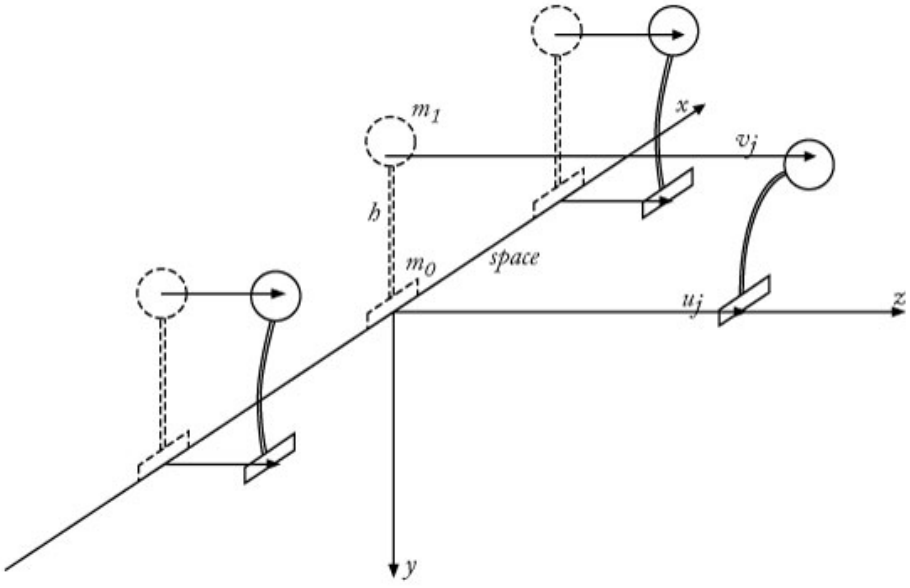

Fig. 1.2: *The displacements of the city buildings.*

Using fundamental laws of solid physics, we obtain the following equations:

$$\rho\ddot{w}(t) = S\Delta w(t) \text{ in } \Omega \times \mathbb{R}, \tag{1.1}$$

$$w(t,x,0) = u_j(t)\ \forall (x,0) \in \Gamma_j,\ \frac{\partial w}{\partial y}(t,x,0) = 0\ \forall (x,0) \in \Gamma_{free}, \tag{1.2}$$

$$m_1\ddot{v}_j(t) = -k(v_j(t) - u_j(t)), \tag{1.3}$$

$$R_j(w) = \int_{\Gamma_j} S\frac{\partial w}{\partial y}(s,0)ds, \tag{1.4}$$

$$m_0\ddot{u}_j(t) = \int_{\Gamma_j} S\frac{\partial w}{\partial y}(t,s,0)ds + k(v_j(t) - u_j(t)). \tag{1.5}$$

Here (1.1) is the wave equation for the displacement; (1.2) shows that the displacement is constant for each rigid foundation and the space between the buildings is stress free; (1.3) and (1.5) are the second Newton law for the buildings' tops and foundations.

1.2.2 The associated spectral problem

We are interested in time harmonic solution for the system (1.1)-(1.5):

$$w(t,x,y) = \Phi(x,y)e^{-i\mu t}. \tag{1.6}$$

Here $\Phi : \Omega \to \mathbb{R}$ represents the soil displacement; $\mu^2 > 0$ is the related frequency. Let us denote $\alpha,\ \eta \in \mathbb{R}^N$ as the displacements of the foundations and the tops of the buildings correspondingly. After performing the necessary differentiation in (1.1)-(1.5), we obtain the corresponding eigenvalue problem:

$$-S\Delta\Phi = \rho\mu^2\Phi \text{ in } \Omega, \tag{1.7}$$

$$k(\eta-\alpha) = \mu^2 m_1\eta,\ \ R(\Phi) - k(\eta-\alpha) = \mu^2 m_0\alpha, \tag{1.8}$$

$$\Phi = \alpha_j \text{ on } \Gamma_j,\ \ \frac{\partial\Phi}{\partial y} = 0 \text{ on } \Gamma_{free}. \tag{1.9}$$

The last step is the non-dimensionalization of the problem above. We introduce a characteristic length l. The non-dimensional spatial coordinates and non-dimensional frequency are:

$$x' = \frac{x}{l},\ y' = \frac{y}{l},\ \xi = \mu\frac{l}{\beta}, \tag{1.10}$$

Notice, that we will omit primes and write x and y in future, but these are the **non-dimensional** coordinates. Sets $\Omega,\ \Gamma,\ \Gamma_{free}$ change accordingly, but we will keep the notation. The non-dimensional city parameters are:

$$\gamma_b = \frac{m_1}{m_0},\ f_b = \frac{l_b}{h},\ c_b = \frac{l_b}{l},\ r = \frac{\rho_b}{\rho},\ b = \frac{\beta_b}{\beta}. \tag{1.11}$$

We set up

$$p(\xi^2) = c_b^2\xi^2 - b^2 f_b^2,\ \ q(\xi^2) = \frac{2rc_b^2\xi^2}{f_b}\big(c_b^2\xi^2 - \frac{\gamma_b+1}{\gamma_b}p(\xi^2)\big); \tag{1.12}$$

we can calculate $\alpha,\ \eta$ as

$$\alpha_j = \Phi(x,0) \text{ for (x,0)} \in \Gamma_j,\ \eta_j = -\frac{b^2 f_b^2\alpha_j}{p(\xi^2)}.$$

Finally, we are getting the following non-linear eigenvalue problem:

$$\Delta\Phi + \xi^2\Phi = 0 \text{ in } \Omega, \tag{1.13}$$

$$\frac{\partial\Phi}{\partial y} = 0 \text{ on } \Gamma_{free}, \tag{1.14}$$

$$q(\xi^2)\Phi(x,0) = p(\xi^2)\int_{\Gamma_j}\frac{\partial\Phi}{\partial y}(s,0)ds \text{ for } (x,0) \in \Gamma_j,\ 1 \le j \le N. \tag{1.15}$$

Our main objective is to find values of the non-dimensionalized frequency ξ for which system (1.13)-(1.15) will be solvable. In Chapter III we will describe the mathematical solution of this problem and its numerical implemetation, both given by Ghergu and Ionescu. Then we will modify the model to extend it to a wider variety of city types and to improve the speed and the accuracy of the numerical algorithm.

Chapter 2

Helmholtz Equation in 2-D. Periodic Green's Function

In this chapter we develop numerical tools to work with the city-effect problem. For its solution we need to calculate a periodic Green's function for a range of arguments. The fundamental solution of the Helmholtz equation in periodic domains is a well-known function, we present it in Section 2.1. However, its standard form is hardly applicable numerically, because of its extremely slow rate of convergence. We will study two other representations of the periodic Green's function in Sections 2.2 and 2.3, and will work with them later in Chapter III. Additionally, we will calculate its gradient in Section 2.4. It is not required for the present city-effect model, but it is an interesting problem by itself, and we believe it will be useful for future work on the subject. In the final section of this chapter, an example will be solved to check the accuracy of our derivations and numerics.

2.1 Fundamental solution of the Helmholtz equation

The"city-effect" phenomenon involves a scattering of seismic waves in a viscoelastic medium. The Helmholtz equation represents the time-independent form of a corresponding partial differential equation. In this section we will assume that we have an unbounded region in 2-D. Let us assume $\zeta = (x, y),\ \zeta_0 = (x_0, y_0) \in \mathbb{R}^2$; we will define $r = |\zeta - \zeta_0| = \big|(x, y) - (x_0, y_0)\big|$. The Green's function will satisfy

$$(\Delta + \kappa^2) G_{sp}(\zeta, \zeta_0) = 0,\ \zeta \neq \zeta_0, \tag{2.1}$$

$$G_{sp}(\zeta, \zeta_0) \approx \frac{1}{2\pi} \ln r^{-1},\ \text{as } r \to 0. \tag{2.2}$$

Since we are interested in outgoing waves, function G should also subject to a Sommerfeld radiation condition. In 2-D it takes the form

$$\frac{\partial G_{sp}}{\partial r} - i\kappa G_{sp} = o(r^{-1/2}),\ \text{as } r \to \infty. \tag{2.3}$$

In the case when there is no periodicity, which we call the "free-space" case, the fundamental solution is (A.17), as is mentioned in Section A.3. However, the scatterers in our problem are the buildings of a city. Eventually we want to assume that there exists some periodic pattern, which means periodicity in one variable for the Green's function. We notice that in this case condition (2.3) is not valid. Let us suppose that the periodicity is in the second coordinate, and the period is d, such that

$$G\big(x, y, x_0, y_0\big) = G\big(x, y + nd, x_0, y_0 + md\big)$$

for $n,\ m \in \mathbb{Z}$. Then, informally

$$G(\zeta, \zeta_0) = \frac{i}{4} \sum_{m=-\infty}^{\infty} H_0^{(1)}(\kappa r_m), \tag{2.4}$$

where

$$r_m = \big|(x, y) - (x_0, y_0 + md)\big| = \sqrt{(x - x_0)^2 + (y - y_0 - md)^2},\ m \in \mathbb{Z}, \tag{2.5}$$

solves

$$(\Delta + \kappa^2) G(\zeta, \zeta_0) = 0,\ \zeta \neq \zeta_0. \tag{2.6}$$

This is the standard form, but it is not suitable for use computationally, because (2.4) converges very slowly (like $\sum_{m=-\infty}^{\infty} m^{-1/2} e^{im\theta}$). For example, if the infinite series (2.4) is approximated by a sum with index from -10^4 to 10^4, we will not obtain even a second decimal digit precision. We will consider two other representations below, and they will be used in our numerical simulations.

Remark 2.1. *The representations we use here are taken from [23]. The formulas in that paper depend on parameter β which characterizes the incident wave. In our work $\beta = 0$, that is why all the formulas appear without a $e^{im\beta d}$ factor.*

2.2 Spectral form of the periodic Green's function

In this section we will introduce another form of the periodic Green's function. In the literature it is often referred to as the spectral representation, see [23]. Here we will show that it is, indeed, a fundamental solution of the Helmholtz equation in periodic two-dimensional domains.

For simplicity we first assume $d = 1$. Set

$$\gamma_m = \begin{cases} \sqrt{4\pi^2 m^2 - \kappa^2}, & \text{if } 4\pi^2 m^2 - \kappa^2 > 0 \\ -i\sqrt{\kappa^2 - 4\pi^2 m^2}, & \text{otherwise} \end{cases} \tag{2.7}$$

Here we assume that κ is such that for every integer m, γ_m is non zero. The case where γ_m may be zero is beyond the scope of this thesis. Set

$$G_1(x,y,x_0,y_0) = \sum_{m=-\infty}^{\infty} \frac{1}{2\gamma_m} e^{-\gamma_m|x-x_0|} e^{2i\pi m(y-y_0)}, \tag{2.8}$$

Proposition 2.2. *The series in (2.8) converges absolutely for all $x \neq x_0$. G_1 is locally Lebesgue integrable. More precisely, G_1 satisfies the estimate*

$$|G_1(x,y,x_0,y_0)| \leq C - \frac{1}{2\pi}\ln(1-e^{-2\pi|x-x_0|}), \tag{2.9}$$

where the constant C depends only on the wave number κ.

Proof:
Set $M = \left[\frac{\kappa}{2\pi}\right] + 1$, where $[t]$ is the integer part of $t \in \mathbb{R}$. Note that γ_m is real if $|m| \geq M$, and imaginary otherwise; $m - M < m - \frac{\kappa}{2\pi}$; also, if $|m| \geq M$, then $\kappa < 2\pi|m|$, so that $0 < 2\pi|m| - \kappa < \sqrt{4\pi^2|m|^2 - \kappa^2}$.

$$\begin{aligned}
\left|G_1(x,y,x_0,y_0)\right| &\leq \sum_{m=-\infty}^{\infty} \left|\frac{1}{2\gamma_m} e^{-\gamma_m|x-x_0|} e^{2i\pi m(y-y_0)}\right| = \sum_{m=-\infty}^{\infty} \frac{1}{2|\gamma_m|}\left|e^{-\gamma_m|x-x_0|}\right| = \\
&\sum_{|m|<M} \frac{1}{2\sqrt{\kappa^2 - 4\pi^2 m^2}} + \sum_{|m|\geq M} \frac{e^{-\sqrt{4\pi^2m^2-\kappa^2}|x-x_0|}}{2\sqrt{4\pi^2m^2-\kappa^2}} \leq \\
&C + \sum_{m\geq M} \frac{e^{-(2\pi m-\kappa)|x-x_0|}}{2\pi m - \kappa} < \\
&C + \frac{e^{-(2\pi M-\kappa)|x-x_0|}}{2\pi M - \kappa} + \sum_{m\geq M+1} \frac{e^{-2\pi(m-M)|x-x_0|}}{2\pi(m-M)} \leq \\
&C + \sum_{m\geq 1} \frac{e^{-2\pi m|x-x_0|}}{2\pi m} = C - \frac{1}{2\pi}\ln\left(1-e^{-2\pi|x-x_0|}\right)
\end{aligned}$$

Here we used the Taylor series of the logarithmic function. Notice, that C depends on M only, which, in its turn, depends only on κ. Estimate (2.9) clearly implies that G_1 is locally integrable. □

Remark 2.3. *It can be shown that (2.8) is conditionally convergent when $x = x_0$ and $y \neq y_0$. In our work, however, we will use a different Green's function representation in this case.*

Proposition 2.4. *Let function $G_1(x,y,x_0,y_0)$ be defined as in (2.8). Then it is a fundamental solution of the Helmholtz equation, that is,*

$$\int_0^1 \int_{-\infty}^{\infty} G_1(x,y,x_0,y_0)(\Delta + \kappa^2)\varphi(x,y)dxdy = \varphi(x_0,y_0), \tag{2.10}$$

where $\varphi(x,y)$ is a test function with compact support in $(-\infty,\infty)\times(0,1)$.

Proof:

Let

$$g^{(m)}(x,y,x_0,y_0) = \frac{1}{2\gamma_m} e^{-\gamma_m|x-x_0|} e^{2i\pi m(y-y_0)}, \tag{2.11}$$

so that $G_1(x,y,x_0,y_0) = \sum_{m=-\infty}^{\infty} g^{(m)}(x,y,x_0,y_0)$. We will omit (x,y,x_0,y_0) for simplicity. Each function $g^{(m)}$ is in $C^\infty\big((-\infty,x_0)\cup(x_0,\infty)\big)$ with respect to the variable x, and in $C^\infty(\mathbb{R})$ with respect to variable the y (though here we are interested in just two continuous derivatives for each variable). We will denote $g_x^{(m)+}$, $g_{xx}^{(m)+}$, $g_x^{(m)-}$, $g_{xx}^{(m)-}$ right and left derivatives at $x = x_0$ respectively. We need to calculate the first derivatives:

$$g_x^{(m)+} = -\frac{1}{2} e^{-\gamma_m(x-x_0)} e^{2i\pi m(y-y_0)},\ g_x^{(m)-} = \frac{1}{2} e^{\gamma_m(x-x_0)} e^{2i\pi m(y-y_0)}$$

One more fact we will use is that φ has a compact support, from which we deduce $\lim_{x\to\pm\infty} \varphi = \lim_{x\to\pm\infty} \varphi_x = 0$. Keeping all the above in mind, we proceed to integrate by parts:

$$\int_{-\infty}^{\infty} g^m \varphi_{xx} dx = \int_{-\infty}^{x_0} g^{(m)} \varphi_{xx} dx + \int_{x_0}^{\infty} g^{(m)} \varphi_{xx} dx = g^{(m)} \varphi_x\big|_{-\infty}^{x_0} - \int_{-\infty}^{x_0} g_x^{(m)-} \varphi_x dx +$$

$$g^{(m)} \varphi_x\big|_{x_0}^{\infty} - \int_{x_0}^{\infty} g_x^{(m)+} \varphi_x dx = - g_x^{(m)-} \varphi\big|_{-\infty}^{x_0} + \int_{-\infty}^{x_0} g_{xx}^{(m)-} \varphi dx - g_x^{(m)+} \varphi\big|_{x_0}^{\infty} + \int_{x_0}^{\infty} g_{xx}^{(m)+} \varphi dx =$$

$$-\frac{1}{2} e^{\gamma_m(x-x_0)} e^{2i\pi m(y-y_0)} \varphi\Big|_{-\infty}^{x_0} - \frac{1}{2} e^{-\gamma_m(x-x_0)} e^{2i\pi m(y-y_0)} \varphi\Big|_{x_0}^{\infty} + \int_{-\infty}^{x_0} g_{xx}^{(m)-} \varphi dx + \int_{x_0}^{\infty} g_{xx}^{(m)+} \varphi dx =$$

$$e^{2i\pi m(y-y_0)} \varphi(x_0,y) + \int_{-\infty}^{x_0} g_{xx}^{(m)-} \varphi dx + \int_{x_0}^{\infty} g_{xx}^{(m)+} \varphi dx.$$

Analogously, $\int_0^1 g^{(m)} \varphi_{yy} dy = \int_0^1 g_{yy}^{(m)} \varphi dy$.

Now, since $(\Delta + \kappa^2) g^{(m)} = 0$:

$$\int_0^1 \int_{-\infty}^{\infty} g^{(m)} (\Delta + \kappa^2) \varphi dx dy = \int_0^1 \int_{-\infty}^{\infty} g^{(m)} (\varphi_{xx} + \varphi_{yy}) dx dy + \int_0^1 \int_{-\infty}^{\infty} \kappa^2 g^{(m)} \varphi dx dy =$$

$$\int_0^1 e^{2i\pi m(y-y_0)} \varphi(x_0,y) dy + \int_0^1 \left(\int_{-\infty}^{x_0} (\Delta + \kappa^2) g^{(m)} \varphi dx + \int_{x_0}^{\infty} (\Delta + \kappa^2) g^{(m)} \varphi dx \right) dy =$$

$$\int_0^1 e^{2i\pi m(y-y_0)} \varphi(x_0,y) dy.$$

Using Fourier series representation, $\varphi(x,y) = \sum_{n=-\infty}^{\infty} a_n(x) e^{-2i\pi n y}$, where this sum is convergent in $L^2\big(y \in (0,1)\big)$ for a fixed $x \in \mathbb{R}$. Thus,

$$\int_0^1 e^{2i\pi m(y-y_0)}\left(\sum_{n=-\infty}^{\infty} a_n(x_0)e^{-2i\pi ny}\right)dy = \sum_{n=-\infty}^{\infty} a_n(x_0)\int_0^1 e^{-2i\pi my_0}e^{2i\pi y(m-n)}dy =$$

$$a_m(x_0)e^{-2i\pi my_0} + \sum_{n=-\infty, n\neq m}^{\infty} a_n(x_0)\int_0^1 e^{2i\pi y(m-n)}dy = a_m(x_0)e^{-2i\pi my_0}.$$

We have thus proved that

$$\sum_{m=-\infty}^{\infty}\int_0^1\int_{-\infty}^{\infty} g^{(m)}(\Delta+\kappa^2)\varphi dxdy = \varphi(x_0,y_0),$$

and there only remains to argue that the infinite sum and the double integral in the left hand side of that identity can be interchanged. According to Fubini's theorem this is possible if

$$\int_0^1\int_{-\infty}^{\infty}\sum_{m=-\infty}^{\infty}|g^{(m)}||(\Delta+\kappa^2)\varphi|dxdy < \infty \tag{2.12}$$

Looking back into the proof of Proposition 2.2 we see that

$$\sum_{m=-\infty}^{\infty}|g^{(m)}| \leq C - \frac{1}{2\pi}\ln\left(1-e^{-2\pi|x-x_0|}\right)$$

Since φ is smooth and has compact support, estimate (2.12) is now clear. □

Remark 2.5. *Both propositions 2.2 and 2.4 are valid for any positive period d:*

$$G(x,y,x_0,y_0) = \frac{1}{2d}\sum_{m=-\infty}^{\infty}\frac{1}{2\gamma_m}e^{-\gamma_m|x-x_0|}e^{2i\pi m(y-y_0)/d}, \tag{2.13}$$

where

$$\gamma_m = \begin{cases}\sqrt{4\pi^2m^2/d^2-\kappa^2}, & \text{if } 4\pi^2m^2/d^2-\kappa^2\geq 0\\ -i\sqrt{\kappa^2-4\pi^2m^2/d^2}, & \text{otherwise.}\end{cases} \tag{2.14}$$

For our numerical application we want to reduce the number of input parameters as much as we can. Keeping remark 2.5 in mind, in the programming code we will use period $d = 1$ only. The following lemma justifies our choice.

Lemma 2.6. *Let function $G(x,y,x_0,y_0)$ be a solution of (2.6) in a periodic domain with period d; let $\tilde{x} = x/d$, $\tilde{y} = y/d$, $\tilde{x_0} = x_0/d$, $\tilde{y_0} = y_0/d$, and $\tilde{G}(\tilde{x_0},\tilde{y_0}) = G(x_0,y_0)$. Then $\Delta_{\tilde{x_0},\tilde{y_0}}\tilde{G} + (\kappa d)^2 G = 0$, if $(\tilde{x_0},\tilde{y_0}) \neq (\tilde{x},\tilde{y})$, in a periodic domain with period 1.*

Proof:
We notice that function $\tilde{G}$ is periodic with period 1; for $m \in \mathbb{Z}$

$$\tilde{G}(\tilde{x},\tilde{y},\tilde{x_0},\tilde{y_0}+m) = G\big(d\tilde{x},d\tilde{y},d\tilde{x_0},d(\tilde{y_0}+m)\big) = G(d\tilde{x},d\tilde{y},d\tilde{x_0},d\tilde{y_0}) = \tilde{G}(\tilde{x},\tilde{y},\tilde{x_0},\tilde{y_0}).$$

Then

$$\Delta_{\tilde{x_0},\tilde{y_0}}\tilde{G} = \frac{1}{d^2}\Delta_{x_0,y_0}\tilde{G},$$

and it is obvious that $\tilde{G}$ solves the Helmholtz equation with wave number κd in terms of new variables. □

For example, if we want to calculate periodic Green's function $green(M, d, kappa, x, y, ksi, eta)$ (here M is the number of grid points, d is the period, $kappa$ is the wavenumber, and x, y, ksi, eta are the points) using our code, then

$$green(M, d, kappa, x, y, ksi, eta) = green(M, 1, kappa * d, x/d, y/d, ksi/d, eta/d).$$

For numerical purposes (2.13) is much better than (2.4), and it gives a very rapid convergence rate when $|x - x_0| >> 0$, like the series $C \sum_{m=-\infty}^{\infty} e^{-Km}$. But it is still slow for very small $|x - x_0|$ and is not applicable at all when $x = x_0$. We will need one more representation which will be discussed in the next section.

2.3 Ewald's method

The following form of the periodic Green's function was originally devised by Ewald in [12]. We will use the formulation given by Linton in [23], with the only difference that we take it with the minus sign to be consistent throughout the thesis. Its derivation can be found in [23, 29, 8], and here we introduce the result only. Let $X = x - x_0$, $Y = y - y_0$, $p = 2\pi/d$, γ_m defined as in (2.14), and r_m as in (2.5).

$$\begin{aligned} G(X,Y) = \frac{1}{4d}\sum_{m=-\infty}^{\infty}\frac{e^{ipmY}}{\gamma_m}\left[e^{\gamma_m X}erfc\left(\frac{\gamma_m d}{2a}+\frac{aX}{d}\right)+e^{-\gamma_m X}erfc\left(\frac{\gamma_m d}{2a}-\frac{aX}{d}\right)\right] \\ +\frac{1}{4\pi}\sum_{m=-\infty}^{\infty}\sum_{n=0}^{\infty}\frac{1}{n!}\left(\frac{\kappa d}{2a}\right)^{2n}E_{n+1}\left(\frac{a^2 r_m^2}{d^2}\right), \end{aligned} \tag{2.15}$$

where a is called "splitting parameter",

$$erfc(z) = \frac{2}{\sqrt{\pi}}\int_z^{\infty} e^{-t^2}dt \tag{2.16}$$

is the complementary error function, and

$$E_n(z) = \int_1^{\infty} t^{-n}e^{-zt}dt \tag{2.17}$$

is the exponential integral.

Remark 2.7. *Computation of the complementary error function deserves a special mention. Currently, Matlab does not have a built-in function for $z \in \mathbb{C}$. We could have used Maple for the matter, but for the sake of uniformity we decided to code it in Matlab. For algorithm details we refer to [25].*

We would like to discuss briefly the rate of convergence of series (2.15). We notice that when m is large, γ_m tends to $p|m|$. If we assume that $z > 1$ is purely real, then for the complementary error function we have

$$erfc(z) \leq \int_z^\infty te^{-t^2}dt = \frac{1}{2}e^{-z^2}.$$

For the exponential integral, using formula 5.1.19 from [1], it follows

$$E_n(z) \leq \frac{e^{-z}}{z+n-1}.$$

Using these bounds and keeping only the dominant factors, we conclude that when all the indices go to infinity, series (2.15) behaves as

$$C_1 \sum_{m=-\infty}^{\infty} e^{-C_2 m^2} + C_3 \sum_{m=-\infty}^{\infty} \sum_{n=0}^{\infty} \frac{1}{n \cdot n!} \left(\frac{\kappa d}{2a}\right)^{2n} e^{-C_4 m^2}.$$

This is a significant improvement compared to $C \sum_{m=-\infty}^{\infty} e^{-Km}$ rate of convergence for (2.13) (C and K are positive constants). Most importantly, if $x \neq x_0$ are in $(0, d)$, positive constants C_1, C_2, C_3, C_4 are independent of $|x - x_0|$.

The splitting parameter a is of a particular importance. Large values of a favor the convergence of the second series of (2.15), while making the first one slowly convergent, and visa versa. Discussion about the optimum splitting parameter can be found in [8].

Later we will consider the Neumann problem for the Helmholtz equation in a periodic domain, and use periodic Green's function to solve it. We will work on this sample problem to check the accuracy of the numerical implementation of the introduced representations. This will require some additional calculations.

As will be shown later in details, Nyström's method uses limiting values of particular parts of the Green's function and its gradient as $r_0 \to 0$. That is why (2.4) minus the zeroth term will be of interest in the periodic case. When $r_0 \to 0$, $|x - x_0| \to 0$ too, and this is the time when we choose Ewald form. Our goal now is to rewrite $\sum_{m \neq 0} \frac{i}{4} H_0^{(1)}(\kappa r_m)$ in a form similar to (2.15).

First, we notice that all the terms of (2.4), but zeroth, are nonsingular as $r_0 \to 0$. If we subtract (A.17) from (2.15), the result will be nonsingular too. Let's extract the only singular part from (2.15). It is contained in the second series when $m = n = 0$; we use

formula 5.1.11 from [1] to get

$$E_1\left(\frac{a^2r_0^2}{d^2}\right) = -\left\{C + \ln\frac{a^2r_0^2}{d^2} + \sum_{k=1}^{\infty}\frac{(-1)^k}{k\cdot k!}\left(\frac{a^2r_0^2}{d^2}\right)^k\right\}. \tag{2.18}$$

Formula 8.444 from [16] gives us the series representation for $\frac{i}{4}H_0^{(1)}(\kappa r_0)$:

$$\begin{aligned}\frac{i}{4}H_0^{(1)}(\kappa r_0) =& \frac{i}{4}\big(J_0(\kappa r_0) + iY(\kappa r_0)\big)\\ =& \frac{i}{4}J_0(\kappa r_0) - \frac{1}{4}\left\{\frac{2}{\pi}(\ln\frac{\kappa r_0}{2} + C)J_0(\kappa r_0) - \frac{2}{\pi}\sum_{m=1}^{\infty}a_m\frac{(-1)^m}{(m!)^2}\left(\frac{\kappa r_0}{2}\right)^{2m}\right\},\end{aligned} \tag{2.19}$$

where $a_m = \sum_{j=1}^{m}\frac{1}{j}$.
Finally, we substitute E_1 in (2.15) by (2.18), and subtract (2.19). Logarithmic singularities both in (2.18) and (2.19) will cancel each other, as expected:

$$\begin{aligned}\sum_{m\neq 0}\frac{i}{4}H_0^{(1)}(\kappa r_m) =& \frac{1}{4d}\sum_{m=-\infty}^{\infty}\frac{e^{ipmY}}{\gamma_m}\left[e^{\gamma_m X}erfc\left(\frac{\gamma_m d}{2a} + \frac{aX}{d}\right) + e^{-\gamma_m X}erfc\left(\frac{\gamma_m d}{2a} - \frac{aX}{d}\right)\right] +\\ & \frac{1}{4\pi}\sum_{m\neq 0}\sum_{n=0}^{\infty}\frac{1}{n!}\left(\frac{\kappa d}{2a}\right)^{2n}E_{n+1}\left(\frac{a^2r_m^2}{d^2}\right) + \frac{1}{4\pi}\sum_{n=1}^{\infty}\frac{1}{n!}\left(\frac{\kappa d}{2a}\right)^{2n}E_{n+1}\left(\frac{a^2r_0^2}{d^2}\right) -\\ & \frac{1}{2\pi}\left\{(\ln\frac{\kappa}{2} + C)J_0(\kappa r_0) - \sum_{m=1}^{\infty}a_m\frac{(-1)^m}{(m!)^2}\left(\frac{\kappa r_0}{2}\right)^{2m}\right\} +\\ & \frac{1}{4\pi}\left\{C + \ln\frac{a^2}{d^2} + \sum_{m=1}^{\infty}\frac{(-1)^m}{m\cdot m!}\left(\frac{a^2r_0^2}{d^2}\right)^m\right\} - \frac{i}{4}J_0(\kappa r_0) - \frac{1}{2\pi}\ln r_0\left(1 - J_0(\kappa r_0)\right).\end{aligned} \tag{2.20}$$

We notice that $\lim_{r_0\to 0} r_m = |m|d$ and conclude:

$$\begin{aligned}\sum_{m\neq 0}H_0^{(1)}(\kappa d|m|) =& \\ & \frac{2}{id}\sum_{m=-\infty}^{\infty}\frac{erfc\frac{\gamma_m d}{2a}}{\gamma_m} + \frac{1}{i\pi}\sum_{m\neq 0}\sum_{n=0}^{\infty}\frac{1}{n!}\left(\frac{\kappa d}{2a}\right)^{2n}E_{n+1}(a^2m^2) +\\ & \frac{1}{i\pi}\sum_{n=1}^{\infty}\frac{1}{n\cdot n!}\left(\frac{\kappa d}{2a}\right)^{2n} + \frac{2}{i\pi}\ln\frac{\kappa d}{2a} - 1 + \frac{C}{i\pi}\end{aligned} \tag{2.21}$$

2.4 Gradient of the periodic Green's function

We need a rapidly convergent summation formula for the gradient of the periodic Green's function too. We have to calculate partial derivatives of the Green's function, and some corresponding limits as r_0 goes to zero.
To begin with, let us think of spectral form 2.13. Proposition 2.2 allows us termwise differentiation of this series. By direct calculations, we get

$$\begin{aligned}\frac{\partial G}{\partial x_0}(X,Y) &= \frac{1}{2d}\frac{X}{|X|}\sum_{m=-\infty}^{\infty} e^{-\gamma_m|X|}e^{2i\pi mY/d}\\ \frac{\partial G}{\partial y_0}(X,Y) &= \frac{1}{2di}\sum_{m=-\infty}^{\infty}\frac{2i\pi m}{\gamma_m d}e^{-\gamma_m|X|}e^{2i\pi mY/d}\end{aligned} \tag{2.22}$$

One more time we notice that we can not use this form when $x = x_0$, because the series is not differentiable with respect to x variable.
Ewald's formula is more involved. First, we notice that the derivatives of the complimentary error function 2.16 and the exponential integral 2.17 are, correspondingly,

$$\frac{\partial}{\partial z}\left(erfc(z)\right) = -\frac{2}{\sqrt{\pi}}e^{-z^2},$$

$$\frac{\partial}{\partial z}\left(E_n(z)\right) = \int_1^\infty t^{-n}e^{-zt}(-t)dt = -\int_1^\infty t^{-(n-1)}e^{-zt}dt = -E_{n-1}(z).$$

Now, if we denote

$$\begin{aligned}\lambda_+ &= \frac{\gamma_m d}{2a} + \frac{aX}{d}\\ \lambda_- &= \frac{\gamma_m d}{2a} - \frac{aX}{d}\end{aligned}$$

the formula for the gradient of the Ewald's form is calculated as follows:

$$\frac{\partial G}{\partial x_0}(X,Y) =$$
$$\frac{1}{4d}\sum_{m=-\infty}^{\infty}\frac{e^{impY}}{\gamma_m}\Big[-\gamma_m e^{\gamma_m X} erfc(\lambda_+) + \frac{2a}{d\sqrt{\pi}}e^{\gamma_m X-\lambda_+^2} + \gamma_m e^{-\gamma_m X} erfc(\lambda_-) -$$
$$\frac{2a}{d\sqrt{\pi}}e^{-\gamma_m X-\lambda_-^2}\Big] + \frac{1}{4\pi}\sum_{m=-\infty}^{\infty}\sum_{n=0}^{\infty}\frac{1}{n!}\left(\frac{\kappa d}{2a}\right)^{2n} E_n\Big(\frac{a^2 r_m^2}{d^2}\Big)\frac{2a^2 X}{d^2} =$$
$$\frac{1}{4d}\sum_{m=-\infty}^{\infty} e^{impY}\left(e^{-\gamma_m X} erfc(\lambda_-) - e^{\gamma_m X} erfc(\lambda_+)\right) +$$
$$\frac{a^2 X}{2\pi d^2}\sum_{m=-\infty}^{\infty}\sum_{n=0}^{\infty}\frac{1}{n!}\left(\frac{\kappa d}{2a}\right)^{2n} E_n\left(\frac{a^2 r_m^2}{d^2}\right)$$
$$\frac{\partial G}{\partial y_0}(X,Y) =$$
$$\frac{1}{4d}\sum_{m=-\infty}^{\infty}(-imp)\frac{e^{impY}}{\gamma_m}\left[e^{\gamma_m X} erfc(\lambda_+) + e^{-\gamma_m X} erfc(\lambda_-)\right] +$$
$$\frac{a^2}{2\pi d^2}\sum_{m=-\infty}^{\infty}\sum_{n=0}^{\infty}\frac{1}{n!}\left(\frac{\kappa d}{2a}\right)^{2n} E_n\left(\frac{a^2 r_m^2}{d^2}\right)(Y-md) \tag{2.23}$$

Now we will have to calculate $\lim_{r_0\to 0}\nabla_{x_0y_0}G(X,Y)$.

Lemma 2.8. $\lim_{r_0\to 0}\nabla_{x_0y_0}(G-G_{sp}) = 0.$

Proof:

The lemma becomes obvious if we use form (2.4). By direct calculation, we get:

$$\frac{\partial(G-G_{sp})}{\partial x_0} = \frac{i\kappa}{4}\sum_{m\neq 0}H_1^{(1)}(\kappa r_m)\frac{x-x_0}{r_m}$$
$$\frac{\partial(G-G_{sp})}{\partial y_0} = \frac{i\kappa}{4}\sum_{m\neq 0}H_1^{(1)}(\kappa r_m)\frac{y-y_0-md}{r_m}.$$

Statement for ∂x_0 follows from the fact that $\lim_{r_0\to 0}\frac{x-x_0}{r_m} = 0$ if $m\neq 0$. For the derivative with respect to y_0 variable we notice

$$\lim_{r_0\to 0}\frac{y-y_0-md}{r_m} = \frac{-md}{|md|} = \begin{cases}-1, \text{ if } m>0\\ 1, \text{ if } m<0.\end{cases} \tag{2.24}$$

□

Below we will apply all of our calculated results.

2.5 Application to integral equations

In this section we will solve the Neumann problem for the Helmholtz equation in dimension 2 using Nyström's method. We want to do this here mainly to check the efficiency of our numerical methods for the different forms of periodic Green's function, but we also believe that this problem can be applied for future work on the city-effect model.

We start by briefly introducing Nyström's method. We apply it to computing the numerical solution of an interior Neumann problem for the Helmholtz equation, which is a standard technique. Then, we solve the same problem, using the periodic Green's function. We do this to verify that we possess an efficient computation method and that we will be able to rely on it when later in this thesis when we tackle computations pertaining to the city-effect problem.

2.5.1 Nyström's method

Nyström's method is used for finding approximate solutions to integral equations. The idea is to substitute an integral operator by quadrature rules, and then solve the resulting linear system of equations. In our work, we apply it for an integral equation of the second kind with singular kernels of the form

$$\big(A\varphi\big)(\mathbf{x}) = \int_{\partial D} \omega\big(|\mathbf{x}-\mathbf{y}|\big) K(\mathbf{x},\mathbf{y})\varphi(\mathbf{y}) d\mathbf{y},\ \mathbf{x} \in \partial D \subset \mathbb{R}^2. \tag{2.25}$$

Here ∂D is of class C^2. The weight function $\omega : (0,\infty) \to \mathbb{R}$ is assumed to be weakly singular, i.e., it is continuous and satisfies $|\omega(t)| \leq Mt^{\alpha-1}$, where t is the arclength, for some positive constant M and $\alpha > 0$. The remaining kernel K is continuous.
A sequence of quadrature rules

$$\big(Q_n g\big)(\mathbf{x}) = \sum_{j=1}^{n} \alpha_j^{(n)}(\mathbf{x}) g(\mathbf{x}_j^{(n)}),\ \mathbf{x} \in \partial D$$

is chosen to approximate the weighted integral

$$\big(Qg\big)(\mathbf{x}) = \int_{\partial D} \omega\big(|\mathbf{x}-\mathbf{y}|\big) g(\mathbf{y}) d\mathbf{y},\ \mathbf{x} \in \partial D.$$

Then the operator from (2.25) is approximated by a sequence of numerical integral operators

$$\big(A_n\varphi\big)(\mathbf{x}) = \sum_{k=1}^{n} \alpha_k^{(n)}(\mathbf{x}) K(\mathbf{x},\mathbf{x}_k^{(n)})\varphi(\mathbf{x}_k^{(n)}),\ \mathbf{x} \in \partial D.$$

As was pointed out in the previous section, we will have to deal with logarithmic singularities. This is a well-known case. Let us consider an operator

$$\big(A_n\varphi\big)(\mathbf{x}) = \frac{1}{2\pi} \int_0^{2\pi} \ln\big(4\sin^2(\frac{t-\tau}{2})\big) K(t,\tau)\varphi(\tau) d\tau,\ 0 \leq t \leq 2\pi \tag{2.26}$$

The kernel K is assumed to be continuous and 2π-periodic with respect to both variables. To approximate this operator, Kress constructed the following numerical quadratures in [21]:

$$\big(Q_n g\big)(t) = \sum_{j=0}^{2n-1} R_j^{(n)} g(t_j) \tag{2.27}$$

with the quadrature points $t_j = j\pi/n$ and the quadrature weights

$$R_j^{(n)}(t) = -\frac{1}{n}\left\{\sum_{m=1}^{n-1}\frac{1}{m}\cos m(t-t_j) + \frac{1}{2n}\cos n(t-t_j)\right\},\ 0 \le j \le 2n-1. \tag{2.28}$$

From Theorem 11.7 from [21] it follows that these quadratures give exponential rate of convergence, if the boundary ∂D is real analytic.

2.5.2 The free-space case

The interior Neumann problem for the Helmholtz equation is stated as follows:

$$\begin{cases} \Delta u + \kappa^2 u = 0 \text{ in } D, \\ \dfrac{\partial u}{\partial \nu} = g \text{ on } \partial D, \end{cases} \tag{2.29}$$

where $D \subset \mathbb{R}^2$ is simply connected, bounded domain, and ν is an outward normal to the boundary ∂D.
In Chapter 12 of [21], Kress illustrates Nyström's method by solving (2.29) in the open unit disk. We will elaborate this example and enlarge the set of possible domain geometries. Then we will compare the numerical results for different domains and different wave numbers. We will apply Nyström method, as Kress did.
It can be shown (for details we refer to [9]) that the unknown boundary values $\varphi = u$ on ∂D of the solution of the interior Neumann BVP satisfies the integral equation

$$\varphi(\mathbf{x}) + 2\int_{\partial D}\varphi(\mathbf{y})\frac{\partial\Phi(\mathbf{x},\mathbf{y})}{\partial\nu(\mathbf{y})}ds(\mathbf{y}) = 2\int_{\partial D} g(\mathbf{y})\Phi(\mathbf{x},\mathbf{y})ds(\mathbf{y}),\ \text{for } \mathbf{x}\in\partial D, \tag{2.30}$$

where $\Phi(\mathbf{x},\mathbf{y})$ is a fundamental solution of the Helmholtz equation (since we do not specify if it is free-space or periodic yet, we denote it Φ).
We introduce the boundary parameterization $\mathbf{s}(\cdot) = \big(s_1(\cdot), s_2(\cdot)\big)$, such that for $\mathbf{x},\mathbf{y}\in\partial D$

$$\begin{aligned} \mathbf{x}(t) &= \mathbf{s}(t) = \big(s_1(t), s_2(t)\big),\ t\in[0,2\pi) \\ \mathbf{y}(\tau) &= \mathbf{s}(\tau) = \big(s_1(\tau), s_2(\tau)\big),\ \tau\in[0,2\pi). \end{aligned}$$

We assume that for this parameterization the outward normal to the boundary at the point $\mathbf{y}$ is given by

$$\nu(\tau) = \big(-\dot{s_2}(\tau), \dot{s_1}(\tau)\big).$$

Using this parameterization, (2.30) is transformed into

$$\tilde{\varphi}(t) - \frac{1}{2\pi}\int_0^{2\pi} K(t,\tau)\tilde{\varphi}(\tau)d\tau = \frac{1}{2\pi}\int_0^{2\pi} L(t,\tau)\tilde{g}(\tau)d\tau \tag{2.31}$$

in order to match the form of (2.26) (we omit tildes in future).
The kernels in the last integral equation are singular for $t = \tau$, and this is where Nyström's method comes into play. To apply it we want split the integral kernels $K(t,\tau)$ and $L(t,\tau)$ into

$$\begin{aligned} K(t,\tau) &= K_1(t,\tau)\ln\big(4\sin^2\frac{t-\tau}{2}\big) + K_2(t,\tau), \\ K(t,\tau) &= L_1(t,\tau)\ln\big(4\sin^2\frac{t-\tau}{2}\big) + L_2(t,\tau), \end{aligned}$$

where $K_1,\ K_2,\ L_1,\ L_2$ are all real analytic functions if ∂D is such that s_1 and s_2 are real analytic. Then the parts K_2 and L_2 are handled by regular mid-point rule, while K_1 and L_1 are treated with the help of quadratures (2.27). This is exactly how we get the linear system

$$\begin{aligned} \varphi_j - \sum_{k=0}^{2n-1}\left\{R^{(n)}_{|j-k|}K_1(t_j,t_k) + \frac{1}{2n}K_2(t_j,t_k)\right\}\varphi_k \\ = \sum_{k=0}^{2n-1}\left\{R^{(n)}_{|j-k|}L_1(t_j,t_k) + \frac{1}{2n}L_2(t_j,t_k)\right\}g(t_k), \end{aligned} \tag{2.32}$$

where the grid points $t_j = j\pi/n,\ 0 \le j \le 2n-1$, and quadraters $R^{(n)}_{|j-k|}$ are defined at (2.27). Its solution $\{\varphi_j\}$ will be an approximate solution of (2.31) on the boundary ∂D. We expect exponential rate of convergence with respect to number of grid points $2n$, as long as $\mathbf{x}$ and $\mathbf{y}$ are real analytic, see [21]. This will be illustrated later by our numerical results.

Going back to our particular problem (2.31), we calculate kernels K and L. Notice, that

$$\nu(\tau) = \big(-\dot{s}_2(\tau), \dot{s}_1(\tau)\big)$$

is the normal (not unit!) directed into the exterior of D, such that

$$\frac{\partial\Phi(\mathbf{x}(t),\mathbf{y}(\tau))}{\partial\nu} = \nabla_y\Phi(\mathbf{x}(t),\mathbf{y}(\tau))\cdot\frac{\big(-\dot{s}_2(\tau),\dot{s}_1(\tau)\big)}{\sqrt{\big(\dot{s}_1(\tau)\big)^2 + \big(\dot{s}_2(\tau)\big)^2}}.$$

When we introduce the parameterization and go from (2.30) to (2.31),

$$ds\big(\mathbf{y}(\tau)\big) = \sqrt{\big(\dot{s}_1(\tau)\big)^2 + \big(\dot{s}_2(\tau)\big)^2}d\tau.$$

Now, it is obvious that

$$K(t,\tau) = -4\pi\nabla_y\Phi(\mathbf{x}(t),\mathbf{y}(\tau))\cdot\nu(\tau) \tag{2.33}$$

We will reserve $\sqrt{\big(\dot{s}_1(\tau)\big)^2+\big(\dot{s}_2(\tau)\big)^2}$ on the right side for the boundary condition g, and set

$$L(t,\tau)=4\pi\Phi(\mathbf{x}(t),\mathbf{y}(\tau)). \tag{2.34}$$

Finally, in the free-space case fundamental solution Φ is defined by (A.17). We set up K_1 and L_1, and calculate $K,\ K_2,\ L,\ L_2$ as follows:

$$\begin{aligned}
K\big(\mathbf{x},\mathbf{y}\big)&=\frac{i\pi\kappa}{|\mathbf{x}-\mathbf{y}|}H_1^{(1)}\left(\kappa|\mathbf{x}-\mathbf{y}|\right)\big(\mathbf{y}-\mathbf{x}\big)\cdot\nu(\tau),\\
L\big(\mathbf{x},\mathbf{y}\big)&=i\pi H_0^{(1)}\left(\kappa|\mathbf{x}-\mathbf{y}|\right),\\
K_1\big(\mathbf{x},\mathbf{y}\big)&=\kappa|\mathbf{x}-\mathbf{y}|\cdot J_1(\kappa|\mathbf{x}-\mathbf{y}|)\cdot\frac{(\mathbf{x}-\mathbf{y})\cdot\nu(\tau)}{|\mathbf{x}-\mathbf{y}|^2},\\
L_1\big(\mathbf{x},\mathbf{y}\big)&=-J_0(\kappa|\mathbf{x}-\mathbf{y}|),\\
K_2\big(\mathbf{x},\mathbf{y}\big)&=K\big(\mathbf{x},\mathbf{y}\big)-K_1\big(\mathbf{x},\mathbf{y}\big)\cdot\ln(4\sin^2\frac{t-\tau}{2}),\\
L_2\big(\mathbf{x},\mathbf{y}\big)&=L\big(\mathbf{x},\mathbf{y}\big)-L_1\big(\mathbf{x},\mathbf{y}\big)\cdot\ln(4\sin^2\frac{t-\tau}{2}).
\end{aligned} \tag{2.35}$$

As we said, kernels $K_1,\ K_2,\ L_1,\ L_2$ are real analytic if boundary ∂D is real analytic. But we can not use these formulas when $t=\tau$, that is why we have to calculate the limit values. Since $J_0(0)=1,\ J_1(0)=0$, we get

$$\begin{aligned}
&\lim_{t\to\tau}K_1(t,\tau)=0,\\
&\lim_{t\to\tau}L_1(t,\tau)=-1.
\end{aligned}$$

Using the fact that

$$\lim_{z\to0}\left(H_0^{(1)}(z)-\frac{2i}{\pi}\ln z J_0(z)\right)=\frac{2i}{\pi}\big(C-\ln 2\big)+1, \tag{2.36}$$

where C is the Euler's constant, we deduce

$$\begin{aligned}
\lim_{\tau\to t}L_2(t,\tau)&=\lim_{\tau\to t}\left(i\pi H_0^{(1)}\left(\kappa|\mathbf{x}-\mathbf{y}|\right)+J_0(\kappa|\mathbf{x}-\mathbf{y}|)\ln\big(4\sin^2\frac{t-\tau}{2}\big)\right)\\
&=\lim_{\tau\to t}i\pi\left(H_0^{(1)}\left(\kappa|\mathbf{x}-\mathbf{y}|\right)-\frac{2i}{\pi}\ln\big(\kappa|\mathbf{x}-\mathbf{y}|\big)J_0\big(\kappa|\mathbf{x}-\mathbf{y}|\big)\right)+\lim_{\tau\to t}\ln\frac{2\big|\sin\frac{t-\tau}{2}\big|}{\kappa|\mathbf{x}-\mathbf{y}|}\\
&=-2\ln\frac{\kappa}{2}-2C+i\pi+\ln\lim_{\tau\to t}\frac{4\sin^2\frac{t-\tau}{2}}{|\mathbf{x}-\mathbf{y}|^2}
\end{aligned} \tag{2.37}$$

From

$$\lim_{z\to0}zH_1^{(1)}(z)=\frac{2}{i\pi}$$

we calculate

$$\lim_{\tau\to t} K(t,\tau) = \lim_{\tau\to t} i\pi\kappa|\mathbf{x}-\mathbf{y}|H_1^{(1)}\big(\kappa|\mathbf{x}-\mathbf{y}|\big)\frac{(\mathbf{y}-\mathbf{x})\cdot\nu(\tau)}{|\mathbf{x}-\mathbf{y}|^2} = 2\lim_{\tau\to t}\frac{(\mathbf{y}-\mathbf{x})\cdot\nu(\tau)}{|\mathbf{x}-\mathbf{y}|^2} \tag{2.38}$$

At this point we notice that limits $\lim\limits_{t\to\tau}\dfrac{(\mathbf{y}-\mathbf{x})\cdot\nu(\tau)}{|\mathbf{x}-\mathbf{y}|^2}$ and $\lim\limits_{t\to\tau}\dfrac{4\sin^2\frac{t-\tau}{2}}{|\mathbf{x}-\mathbf{y}|^2}$ exist for the smooth boundary ∂D, and depend on D only. They can be computed by hand for any particular parameterization, but since we tried many different domains, to save time we wrote a short code which calculates them in *Maple*.

The last limit we have to find is of K_2. Again, for a smooth boundary $\lim\limits_{\tau\to t}\dfrac{|\mathbf{x}-\mathbf{y}|}{|t-\tau|} < \infty$, and

$$\lim_{\tau\to t}\left\{|\mathbf{x}-\mathbf{y}|\cdot\ln\big|\sin\frac{t-\tau}{2}\big|\right\} = \lim_{\tau\to t}\left\{\frac{|\mathbf{x}-\mathbf{y}|}{|t-\tau|}\cdot\frac{|t-\tau|}{\big|\sin\frac{t-\tau}{2}\big|}\cdot\ln\big|\sin\frac{t-\tau}{2}\big|\cdot\big|\sin\frac{t-\tau}{2}\big|\right\} = 0.$$

This shows that

$$\lim_{\tau\to t} K_2(t,\tau) = \lim_{\tau\to t} K(t,\tau) = 2\lim_{\tau\to t}\frac{(\mathbf{y}-\mathbf{x})\cdot\nu(\tau)}{|\mathbf{x}-\mathbf{y}|^2}. \tag{2.39}$$

There is a connection between the latter limit and the boundary's curvature, and we will show it now. In terms of our parameterization, the curvature is defined (see [3]) as

$$Curv(\tau) = \frac{\|\dot{\mathbf{s}}(\tau)\times\ddot{\mathbf{s}}(\tau)\|}{\|\dot{\mathbf{s}}(\tau)\|^3} = \frac{|-\ddot{s}_1(\tau)\dot{s}_2(\tau)+\dot{s}_1(\tau)\ddot{s}_2(\tau)|}{|\dot{\mathbf{s}}(\tau)|^3} \tag{2.40}$$

Using Taylor series, for the numerator of (2.39) we obtain

$$\begin{aligned}(\mathbf{y}-\mathbf{x})\cdot\nu(\tau) &= \left(\dot{\mathbf{s}}(\tau)(t-\tau)+\frac{1}{2}\ddot{\mathbf{s}}(\tau)(t-\tau)^2+\big(O_1((t-\tau)^3),O_2((t-\tau)^3)\big)\right)\cdot\big(-\dot{s}_2(\tau),\dot{s}_1(\tau)\big)\\ &= \frac{1}{2}\big(-\ddot{s}_1(\tau)\dot{s}_2(\tau)+\dot{s}_1(\tau)\ddot{s}_2(\tau)\big)(t-\tau)^2+O(\tau)\big((t-\tau)^3\big).\end{aligned}$$

From the mean-value theorem, the denominator

$$\big|(s)(t)-(s)(\tau)\big|^2 = \big|(\dot{s}_1(\eta_1),\dot{s}_2(\eta_2))\big|^2\cdot|t-\tau|^2.$$

where η_1, η_2 are between t and τ. As $t\to\tau$, both $\eta_1,\ \eta_2\to\tau$, $\big|(\dot{s}_1(\eta_1),\dot{s}_2(\eta_2))\big|\to|\dot{\mathbf{s}}(\tau)|$, and we can rewrite (2.39) as

$$\lim_{t\to\tau} K_2(t,\tau) = \frac{-\ddot{s}_1(\tau)\dot{s}_2(\tau)+\dot{s}_1(\tau)\ddot{s}_2(\tau)}{|\dot{\mathbf{s}}(\tau)|^2}+D,$$

where D is a constant which depends on τ. It is easy to see that

$$Curv(\tau) = \frac{\big|\lim\limits_{t\to\tau}K_2(t,\tau)-D\big|}{|\dot{\mathbf{s}}(\tau)|}.$$

Now we get back to our problem to set up boundary conditions, and this finishes our analytical preparations. For a numerical example, we will consider a case with a known exact solution on the boundary. We compute its normal derivative on the boundary to complete the Neumann problem statement. This way we can evaluate the accuracy of our approximate solution when we find it. Let

$$u(\mathbf{x}) = Y_0\big(\kappa|\mathbf{x}-\mathbf{x}_0|\big),\ \mathbf{x}\in\partial D, \tag{2.41}$$

where Y_0 is the Neumann function of order zero, and $\mathbf{x}_0 = (q,0)$ with $q>1$, such that

$$g(\mathbf{y})ds(\mathbf{y}) = \frac{\kappa Y_1\big(\kappa|\mathbf{y}-\mathbf{x}_0|\big)}{|\mathbf{y}-\mathbf{x}_0|}(\mathbf{x}_0-\mathbf{y})\cdot\nu(\tau)d\tau. \tag{2.42}$$

Here the part we reserved earlier canceled out with $|\nu|$.

We solve the system (2.32) to find the approximate solution φ_j at the grid points. Then we can calculate the exact solution u_j at the same points, and find the relative error $\dfrac{\|u_j-\varphi_j\|}{\|u_j\|}$, where we mean $\|\cdot\|_{L^\infty}$.

The results of our numerical simulations are presented in Tables 2.1 and 2.2. We vary the wavelength κ to illustrate the computational problem of large and very small frequencies. In each case we observe the expected exponential rate of convergence (see [21]) for the relative error as a function of the number of grid points. And of course, domain geometry also influences the accuracy of our method. The presence of the limits (2.37) and (2.39) implies that the boundary's curvature matters. It can be seen that the lasso-shaped geometry is harder to handle which is likely due to higher values for the curvature. Figure 2.3 graphs the curvatures of our two boundaries for $t\in[0;2\pi]$. Here we used formula (2.40). The maximum for the kite-shaped domain is only 50, while in case of the lasso-shaped domain the curvature attains 700 at its peak.

Remark 2.9. *When we know the solution u on the boundary ∂D, we can apply Green's formula, or the Helmholtz representation, to find u in D*

$$u(\boldsymbol{x}) = \int_{\partial D}\left\{\frac{\partial u}{\partial\nu}(\boldsymbol{y})\Phi(\boldsymbol{x},\boldsymbol{y}) - u(\boldsymbol{y})\frac{\partial\Phi(\boldsymbol{x},\boldsymbol{y})}{\partial\nu(\boldsymbol{y})}\right\}ds(\boldsymbol{y}),\ \boldsymbol{x}\in D. \tag{2.43}$$

2.5.3 The periodic case

We can now proceed to the periodic domain case, which is, of course, more involved. At this point we have everything ready, and the only things we have to do is to change the domain of (2.29) and calculate new kernels. The domain D is defined as follows:

$$D = \bigcup_{n=-\infty}^{\infty} D_n,\ \partial D_n = \big\{\big(s_1(t), s_2(t)+n\big),\ t\in[0,2\pi)\big\},\ n\in\mathbb{Z}, \tag{2.44}$$

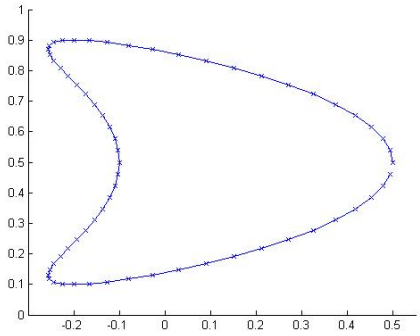

Fig. 2.1: *Kite-shaped:* $\big(s_1(t), s_2(t)\big) = \big(0.3\cos t + 0.2\cos(2t), 0.4\sin t + 0.5\big)$

	$2n$	*error*		$2n$	*error*
	8	0.03143304		8	4.50012988
$\kappa = 1$	16	0.01900763	$\kappa = 20$	16	1.77371600
$q = 2$	32	0.00011168	$q = 2$	32	0.36939184
	64	0.00000000		64	0.00004393
	8	0.26655901		8	1.06178163
$\kappa = 0.1$	16	1.74291470	$\kappa = 10^{-3}$	16	0.98121367
$q = 2$	32	0.00411267	$q = 2$	32	0.93568783
	64	0.00000016		64	0.00080421

Tab. 2.1: *Numerical results for a kite-shaped domain (free-space case).*

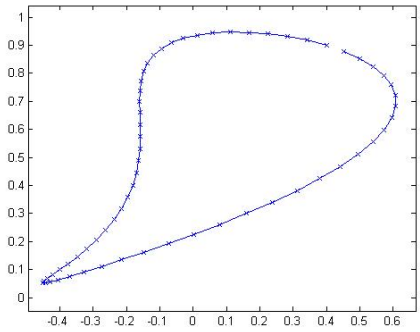

Fig. 2.2: *Lasso-shaped:* $\big(s_1(t), s_2(t)\big) = \big(0.4\cos t - 0.16\sin t - 0.2\sin(2t), 0.4\cos t + 0.2\sin t + 0.5\big)$

where each D_n is compact, ∂D_n is of class C^2. We point out that this domain is periodic with respect to second variable, and its period is $d = 1$.

The difference in the kernels is caused by the periodic Green's function (2.4), which is the fundamental solution in this case. Kernels K and L are defined by (2.33) and (2.34) correspondingly, where $\Phi = G$ is the periodic Green's function. We will not provide the exact formulas here, because we will use its different forms. As we noted before, the only

	$2n$	$error$		$2n$	$error$
	16	7.53711645		32	2.02101627
$\kappa = 1$	32	1.04811013	$\kappa = 20$	64	0.04786721
$q = 2$	64	0.01733972	$q = 2$	128	0.00028352
	128	0.00009830		256	0.00000001
	16	0.90874789		32	0.97348623
$\kappa = 0.1$	32	0.82196203	$\kappa = 10^{-3}$	64	0.97196461
$q = 2$	64	0.13985500	$q = 2$	128	0.79337920
	128	0.00084181		256	0.00015702

Tab. 2.2: *Numerical results for a lasso-shaped domain (free-space case).*

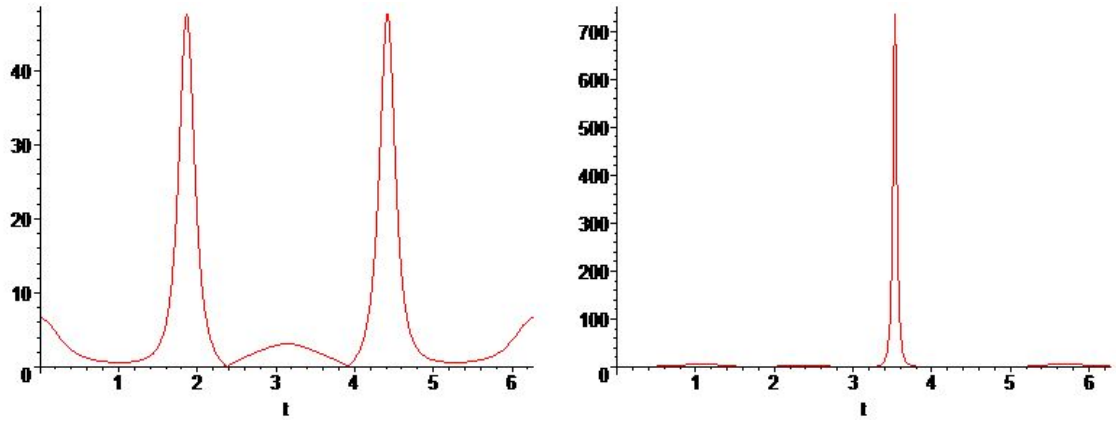

Fig. 2.3: *Graphs of the curvatures for kite-shaped (left) and lasso-shaped (right) domains;* $t \in [0; 2\pi]$.

singularities are contained in $H_0^{(1)}$ and $H_1^{(1)}$ for L and K correspondingly, while the rest of the series (2.4) and its gradient are real analytic. That is why we define K_1, L_1, K, and L exactly in the same way we did for a free-space case at (2.35).

Now, that we know all the kernels, the last preparation step is to find the limits as $\tau \to t$. By definition, limits for K_1 and L_1 are 0 and -1 correspondingly. Due to Lemma 2.8, limit for K_2 is the same as in free-space case too. The only difference we have for L_2:

$$\lim_{t\to\tau} L_2(t,\tau) = i\pi - 2C - 2\ln\frac{\kappa}{2} + \ln\lim_{t\to\tau}\frac{4\sin^2\frac{t-\tau}{2}}{|\mathbf{x}-\mathbf{y}|^2} + i\pi\sum_{m\neq 0} H_0^{(1)}(\kappa d|m|).$$

The rest is the same as for the free-space case. We define the exact solution on the boundary as in (2.41), solve the problem and compare it with the approximate numerical solution. Tables 2.3 and 2.4 show the numerical results for kite- and lasso-shaped domains. We notice that periodic case is more susceptible to the high-frequency problem than free-space case.

	$2n$	*error*		$2n$	*error*
	8	0.03861128		8	1.47799492
$\kappa = 1$	16	0.01293977	$\kappa = 4$	16	0.06532509
$q = 2$	32	0.00008567	$q = 2$	32	0.00055507
	64	0.00000000		64	0.00000054
	8	0.19783325		8	2.49406221
$\kappa = 0.1$	16	0.08372353	$\kappa = 10^{-3}$	16	0.97529350
$q = 2$	32	0.00050190	$q = 2$	32	0.05299212
	64	0.00000002		64	0.00000222

Tab. 2.3: *Numerical results for a kite-shaped domain (periodic case).*

	$2n$	*error*		$2n$	*error*
	16	2.37524649		32	0.31698280
$\kappa = 1$	32	1.31084706	$\kappa = 7$	64	0.00945118
$q = 2$	64	0.01798966	$q = 2$	128	0.00206184
	128	0.00010120		256	0.00021316
	32	0.92469278		32	0.97353357
$\kappa = 0.1$	64	0.03219351	$\kappa = 10^{-3}$	64	0.92871590
$q = 2$	128	0.00016927	$q = 2$	128	0.01595815
	256	0.00000001		256	0.00000058

Tab. 2.4: *Numerical results for a lasso-shaped domain (periodic case).*

Chapter 3

Solution of the City-Effect Problem

In this chapter we continue discussion of the city-effect problem. In Chapter I we described the model which was introduced by Ghergu and Ionescu in [15]. It deals with cities of finite size with equal evenly spaced buildings. Ghergu and Ionescu also developed a solution algorithm, which opens our Chapter III. In Section 3.1 we solve this problem numerically and collect data for frequencies of cities with different parameters. Using our numerical implementation, we check that the model by Ghergu and Ionescu agrees with the real cases in Subsection 3.1.3.

After this, we proceed with our contribution to the city-effect problem. In Section 3.2 we assume that our city is infinite, and apply periodic Green's function to solve the associated problem. Our goal is to compare frequencies of both periodic and corresponding finite cities. Next, in Section 3.3 we modify algorithm to solve for cities with non-homogeneous layout. It is assumed that a city consists of periodic clusters of buildings. Again we consider finite and infinite cities, and compare the results.

3.1 Mathematical solution

The system (1.13)-(1.15) has infinitely many solutions, but not all of them satisfy the physical problem of structure-soil-structure interaction. To find the solutions related to the presence of the buildings Ghergu and Ionescu introduced the following algorithm in [15]. Recalling the boundary conditions on the building foundations and outgoing Sommerfeld radiation condition, we are interested in the solution of the Helmholtz equation with the mixed boundary conditions:

$$\Delta\Psi + \xi^2\Psi = 0 \text{ in } \Omega, \tag{3.1}$$

$$\Psi = \alpha_j \text{ on } \Gamma_j, \frac{\partial\Psi}{\partial y} = 0 \text{ on } \Gamma_{free}, \tag{3.2}$$

$$\frac{\partial\Psi}{\partial r} - i\xi\Psi = o(r^{-1/2}) \text{ as } r = |x| \to +\infty. \tag{3.3}$$

We will denote solution of this system as $\Psi_{\xi,\alpha}$.

Remark 3.1. *If function Ψ satisfies equations (3.1) and (3.3), then the following asymptotics is valid:*

$$\Psi = O(r^{-1/2}),\ r \to +\infty. \tag{3.4}$$

Now we introduce the operator $T(\xi^2) : \mathbb{R}^N \to \mathbb{R}^N$:

$$\left(T(\xi^2)\alpha\right)_j = Re \int_{\Gamma_j} \frac{\partial \Psi_{\xi,\alpha}}{\partial y}(s,0)ds,\ 1 \le j \le N,\ \alpha \in \mathbb{R}^N. \tag{3.5}$$

We will be interested in its matrix in the natural basis of $\mathbb{R}^N$, whose entries will be defined by

$$T(\xi^2)_{kl} = Re \int_{\Gamma_k} \frac{\partial \Psi_{\xi,e_l}}{\partial y}(s,0)ds, \tag{3.6}$$

where e_l is the l^{th} basis vector in $\mathbb{R}^N$. The following fact was mentioned in [15] without proof, which we introduce below.

Lemma 3.2.

$$\int_{\Gamma_i} \frac{\partial \Psi_j}{\partial y} ds = \int_{\Gamma_j} \frac{\partial \Psi_i}{\partial y} ds,$$

where $\Psi_i = \Psi_{\xi,e_i}$ and $\Psi_j = \Psi_{\xi,e_j}$ are the system (3.1)-(3.3) solutions corresponding i^{th} and j^{th} basis vectors in $\mathbb{R}^N$ for a given ξ. By taking the real parts, it follows that matrix (3.6) is symmetric.

Proof:

We notice that

$$\Psi_k(s,0) = \begin{cases} 1, \text{ if } s \in \Gamma_k, \\ 0, \text{ if } s \in \Gamma_l,\ l \neq k. \end{cases}$$

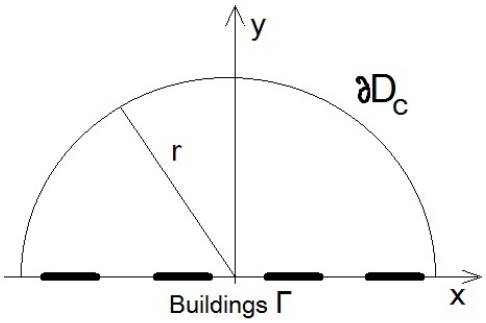

Then it is enough to show that

$$\int_{\Gamma_i} \Psi_i \frac{\partial \Psi_j}{\partial y} ds = \int_{\Gamma_j} \Psi_j \frac{\partial \Psi_i}{\partial y} ds.$$

We consider the half-circle $D = \{(x,y) : x^2 + y^2 \le r^2, y \ge 0\}$. Due to Green's theorem,

$$\int_D \left(\Psi_i \Delta \Psi_j - \Psi_j \Delta \Psi_i\right) dV = \int_{\partial D} \left(\Psi_i \frac{\partial \Psi_j}{\partial \nu} - \Psi_j \frac{\partial \Psi_i}{\partial \nu}\right) ds.$$

Since both functions satisfy (3.1), the integral on the left side is zero. Let us denote ∂D_c

half-circumference part of the boundary ∂D and I the line segment $(x,0) : |x| \le r$. Then

$$\int_{\Gamma_i} \Psi_i \frac{\partial \Psi_j}{\partial y} ds - \int_{\Gamma_j} \Psi_j \frac{\partial \Psi_i}{\partial y} ds = \int_I \left(\Psi_i \frac{\partial \Psi_j}{\partial \nu} - \Psi_j \frac{\partial \Psi_i}{\partial \nu} \right) ds = \int_{\partial D_c} \left(\Psi_j \frac{\partial \Psi_i}{\partial \nu} - \Psi_i \frac{\partial \Psi_j}{\partial \nu} \right) ds$$
$$= \int_{\partial D_c} \left(\Psi_j (i\xi \Psi_i + o(r^{-1/2})) - \Psi_i (i\xi \Psi_j + o(r^{-1/2})) \right) ds$$
$$= \int_{\partial D_c} \left\{ \Psi_j o(r^{-1/2}) - \Psi_i o(r^{-1/2}) \right\} ds = r \cdot O(r^{-1/2}) \cdot o(r^{-1/2}),$$

if we assume $r \to \infty$. Taking the real parts, we see that $\big(T(\xi)e_i\big)_j = \big(T(\xi)e_j\big)_i$. □

Now we continue with explanation how we use this matrix. Since it is symmetric, it can be diagonalized, and all its eigenvalues are **real**. For every $\xi^2 > 0$ we can find the eigenvalues of $T(\xi^2)$ defined in (3.6)

$$\tau_1(\xi^2) \le \tau_2(\xi^2) \le \ldots \le \tau_N(\xi^2), \tag{3.7}$$

and corresponding normalized eigenvectors $\theta_1(\xi^2), \ldots, \theta_N(\xi^2)$.
Assume that for some i

$$p(\xi^2)\tau_i(\xi^2) = q(\xi^2), \tag{3.8}$$

where p and q are defined in (1.12). Since all the non-dimensional parameters (1.11) are the same for all the buildings, then $p(\xi^2)$ and $q(\xi^2)$ do not depend on i. We find solution $\Psi_{\xi,\theta_i(\xi^2)}$ of (3.1)-(3.3). Now, if we take $\Phi = Re\Psi_{\xi,\theta_i(\xi^2)}$, it will satisfy (1.15), and solve the system (1.13)-(1.15).

To be more precise, we pick i and solve nonlinear equation (3.8) for the unknown ξ using *Matlab* solver. We find $\Psi_{\xi,\theta_i(\xi^2)}$ which satisfies the system (3.1)-(3.3). Then $\Phi = Re\Psi_{\xi,\theta_i(\xi^2)}$ will solve the non-linear eigenvalue problem (1.13)-(1.15).

The crucial step in this method is to solve the Helmholtz problem (3.1)-(3.3).

3.1.1 Solution of the Helmholtz equation

We will fix $\xi^2 > 0$ and $\alpha \in \mathbb{R}^N$, and look for a solution to (3.1) as a single-layer potential

$$\Psi(x,y) = \int_\Gamma G\big(\xi\sqrt{(x-s)^2 + y^2}\big)\psi(s)ds, \tag{3.9}$$

where G is the fundamental solution of the Helmholtz equation in the half-plane

$$G(z) = \frac{i}{4} H_0^{(1)}(z). \tag{3.10}$$

As in [22], we assume that

$$\psi(s) = \frac{\varphi(s)}{\sqrt{(s-a_j)(b_j-s)}}, \text{ where } s \in (a_j, b_j),\ 1 \le j \le N, \tag{3.11}$$

and φ is a continuous function. Our solution will look like

$$\Psi(x,y) = \frac{i}{4}\sum_{j=1}^{N}\int_{a_j}^{b_j} H_0^{(1)}(\xi\sqrt{(x-s)^2+y^2})\psi(s)ds, \tag{3.12}$$

Using proposition A.8, we have

$$\left(\frac{\partial\Psi}{\partial y}\right)^{+}(s,0) = -\frac{1}{2}\psi(s) = -\frac{1}{2}\frac{\varphi(s)}{\sqrt{(b_j-s)(s-a_j)}},\ \text{for all } a_j < s < b_j,$$

where we mean the right-hand derivative

$$\left(\frac{\partial\Psi}{\partial y}\right)^{+}(s,0) = \lim_{t\to 0^+}\frac{\partial\Psi}{\partial y}(s,t).$$

To employ the same numerical mesh for each building foundation Γ_j, we introduce a new variable $-1 \le t \le 1$, and for every $[a_j, b_j]$ we define a transformation such that:

$$s = g_j(t) = \frac{b_j - a_j}{2}t + \frac{b_j + a_j}{2},\ s \in [a_j, b_j]. \tag{3.13}$$

In terms of φ and t we rewrite operator T:

$$\big(T(\xi^2)\alpha\big)_j = \frac{1}{2}\int_{-1}^{1}\frac{\varphi\big(g_j(t)\big)}{\sqrt{1-t^2}}dt. \tag{3.14}$$

Using the first part of boundary conditions (3.2), we get N equations

$$\frac{i}{4}\sum_{j=1}^{N}\int_{-1}^{1} H_0^{(1)}(\xi|x-g_j(t)|)\frac{\varphi\big(g_j(t)\big)}{\sqrt{1-t^2}}dt = \alpha_k,\ 1 \le k \le N,\ x \in \Gamma_k. \tag{3.15}$$

For a numerical solution we discretize each of N intervals $[-1;1]$ with grid points

$$\bar{x}_p = -1 + \frac{2p-1}{2M},\ 1 \le p \le 2M. \tag{3.16}$$

Then, we get $2MN$ equations

$$\frac{i}{4}\sum_{j=1}^{N}\int_{-1}^{1} H_0^{(1)}\big(\xi g_{kj}(\bar{x}_p,t)\big)\frac{\varphi\big(g_j(t)\big)}{\sqrt{1-t^2}}dt = \alpha_k, \tag{3.17}$$

where $1 \le k \le N,\ 1 \le p \le 2M$, and $g_{kj}(x,t) = |g_k(x) - g_j(t)|$.
Function $H_0^{(1)}(z)$ is singular for $z = 0$; to deal with these singularities, we decompose it as follows:

$$\frac{i}{4}H_0^{(1)}(z) = A_0(z)\ln\big(\frac{z}{2}\big) + B_0(z), \tag{3.18}$$

$A_0(z) = -\dfrac{1}{2\pi} J_0(z)$), where $J_0(z)$ is the Bessel function of the first kind and order zero, and

$$B_0(z) = \begin{cases} \dfrac{i}{4} H_0^{(1)}(z) + \dfrac{1}{2\pi} J_0(z) \ln\left(\dfrac{z}{2}\right), & \text{if } z \neq 0, \\ \dfrac{i\pi - 2C}{4\pi}, & \text{if } z = 0. \end{cases} \tag{3.19}$$

$C \approx 0.5772156649015328$ is the Euler constant. In order to approximate the integrals we introduce the division points

$$\bar{t}_q = -1 + \frac{q}{M},\ 1 \le q \le 2M. \tag{3.20}$$

To find the approximation for the unknown function φ we propose to solve the system of linear equations:

$$\begin{aligned} \alpha_k = & \sum_{j=1}^{N} \sum_{q=1}^{M} \frac{A_0\big(\xi g_{kj}(\bar{x}_p, \bar{x}_q)\big)}{\sqrt{1-\bar{x}_q}} \varphi\big(g_j(\bar{x}_q)\big) \int_{\bar{t}_{q-1}}^{\bar{t}_q} \frac{\ln\big(g_{kj}(\bar{x}_p, t)\big)}{\sqrt{1+t}} dt \\ & + \sum_{j=1}^{N} \sum_{q=1}^{M} \left(A_0\big(\xi g_{kj}(\bar{x}_p, \bar{x}_q)\big) \ln\frac{\xi}{2} + B_0\big(\xi g_{kj}(\bar{x}_p, \bar{x}_q)\big) \right) \int_{\bar{t}_{q-1}}^{\bar{t}_q} \frac{\varphi\big(g_j(\bar{x}_q)\big)}{\sqrt{1-t^2}} dt \\ & + \sum_{j=1}^{N} \sum_{q=M+1}^{2M} \frac{A_0\big(\xi g_{kj}(\bar{x}_p, \bar{x}_q)\big)}{\sqrt{1+\bar{x}_q}} \varphi\big(g_j(\bar{x}_q)\big) \int_{\bar{t}_{q-1}}^{\bar{t}_q} \frac{\ln\big(g_{kj}(\bar{x}_p, t)\big)}{\sqrt{1-t}} dt \\ & + \sum_{j=1}^{N} \sum_{q=M+1}^{2M} \left(A_0\big(\xi g_{kj}(\bar{x}_p, \bar{x}_q)\big) \ln\frac{\xi}{2} + B_0\big(\xi g_{kj}(\bar{x}_p, \bar{x}_q)\big) \right) \int_{\bar{t}_{q-1}}^{\bar{t}_q} \frac{\varphi\big(g_j(\bar{x}_q)\big)}{\sqrt{1-t^2}} dt. \end{aligned} \tag{3.21}$$

For every $1 \le j, k \le N,\ 1 \le p \le 2M$ matrix of the system (3.21) is given by

$$M_{p+2M(k-1),q+2M(j-1)} = \begin{cases} \dfrac{A_0\big(\xi g_{kj}(\bar{x}_p, \bar{x}_q)\big)}{\sqrt{1-\bar{x}_q}} \displaystyle\int_{\bar{t}_{q-1}}^{\bar{t}_q} \frac{\ln\big(g_{kj}(\bar{x}_p, t)\big)}{\sqrt{1+t}} dt \\ \quad + \left(A_0\big(\xi g_{kj}(\bar{x}_p, \bar{x}_q)\big) \ln\dfrac{\xi}{2} + B_0\big(\xi g_{kj}(\bar{x}_p, \bar{x}_q)\big) \right) \\ \quad \times (\arcsin \bar{t}_{q-1} - \arcsin \bar{t}_q),\ \text{for } 1 \le q \le M \\ \dfrac{A_0\big(\xi g_{kj}(\bar{x}_p, \bar{x}_q)\big)}{\sqrt{1+\bar{x}_q}} \displaystyle\int_{\bar{t}_{q-1}}^{\bar{t}_q} \frac{\ln\big(g_{kj}(\bar{x}_p, t)\big)}{\sqrt{1-t}} dt \\ \quad + \left(A_0\big(\xi g_{kj}(\bar{x}_p, \bar{x}_q)\big) \ln\dfrac{\xi}{2} + B_0\big(\xi g_{kj}(\bar{x}_p, \bar{x}_q)\big) \right) \\ \quad \times (\arcsin \bar{t}_{q-1} - \arcsin \bar{t}_q),\ \text{for } M+1 \le q \le 2M. \end{cases} \tag{3.22}$$

The integrals in (3.22) are computed using the formula

$$\int \frac{\ln|at-b|}{\sqrt{1-t}} dt = 4\sqrt{1-t} - 2I, \tag{3.23}$$

where

$$I = \begin{cases} \sqrt{1-t}\ln|at-b| + 2\sqrt{\dfrac{b-a}{a}}\arctan\sqrt{\dfrac{a-at}{b-a}}, & \text{if } b > a \\ \sqrt{1-t}\ln|at-a|, & \text{if } b = a \\ \left(\sqrt{1-t} - \sqrt{\dfrac{a-b}{a}}\right)\ln|at-b| + 2\sqrt{\dfrac{a-b}{a}}\ln|\sqrt{a-at}+\sqrt{a-b}|, & \text{if } b < a. \end{cases}$$

3.1.2 Results

We open this section by validating our numerical code. In order to do this, we repeat some of the calculations from [15]. Using the same city/soil parameters $l_b = 1$, $space = 0.4$, $l_{char} = l_b$, $\gamma_b = 1.5$, $f_b = 0.5$, $c_b = 1$, $r = 0.1$, $b = 1.5$, $M = 5$, we observed the same asymptotic convergence of the smallest eigenvalue ξ_1 to 0.7792 as number of buildings N grows, just the same as on Fig. 5 of [15]. For one-building system, the computed eigenvalue $\tau(\xi^2)$ of (3.6) exhibits convergent behavior identical to Fig. 10 from [15] as number of gridpoints $2M$ increases.

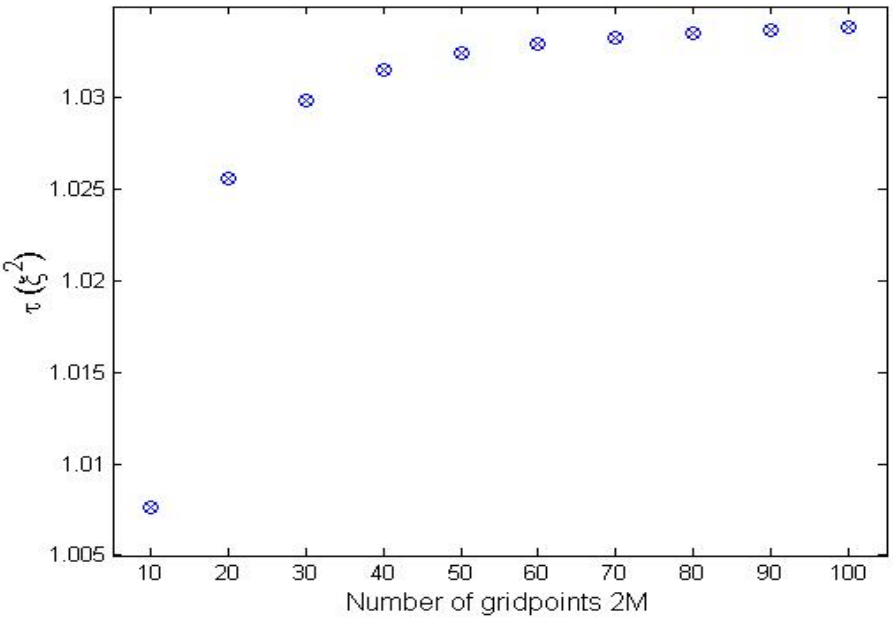

Fig. 3.1: *One-building city:* $l_b = 1$, $space = 0.4$, $l_{char} = l_b$, $\gamma_b = 1.5$, $f_b = 0.5$, $c_b = 1$, $r = 0.1$, $b = 1.5$. *Convergence of the eigenvalue* $\tau(\xi^2)$ *of (3.6) for* $\xi = 1.3$ *as number of gridpoints increases.*

Now we aim to perform further analysis of the model. For this, we will consider several geometries and present some of their eigenvectors along with corresponding eigenvalues. Each city consists of the same number of 51 buildings, has the same building halfwidth

$l_b = 1$, and we have denoted by *space* the distance between consecutive buildings, which is different for each city; $M = 5$, where $2M$ is the number of grid points. If it is not stated otherwise, characteristic length $l = l_b$, and for our numerics we use the following values for the non-dimensional parameters (1.11):

$$\gamma_b = 1.5,\ f_b = 0.5,\ c_b = 1,\ r = 0.1,\ b = 1.5. \tag{3.24}$$

It was conjectured in [15] that the smallest eigenvalue ξ of the spectral problem (1.13)-(1.15) converges as the number of buildings N increases, and this limit was expected to coincide with the first (smallest) frequency of a periodic city. In [5] for a similar problem it was shown that the corresponding eigenvector keeps a constant sign. That is why we want to look at the asymptotic behavior of different eigenvalues, and at the shapes of eigenvectors, and in particular, we want to examine whether some of them remain of constant sign.

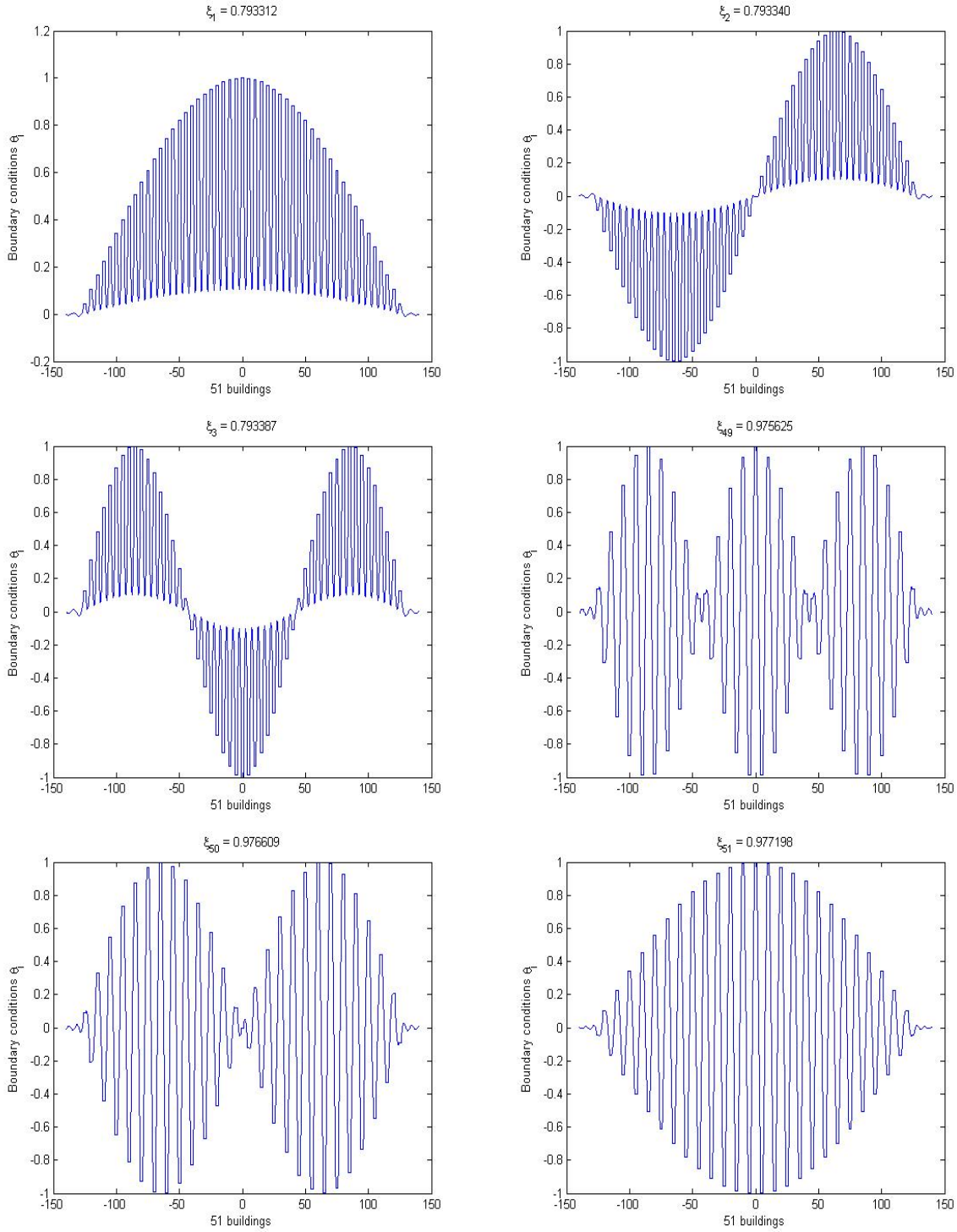

Tab. 3.1: *Different solutions (ξ_j, θ_j) for the free-space problem (1.13)-(1.15). The foundation displacements $\alpha = \theta_j$ are shown on graphs, the corresponding frequency ξ_j is stated above each picture; building halfwidth $l_b = 1$; the distance between consecutive buildings space $= 3$. The number of buildings $N = 51$; $M = 5$.*

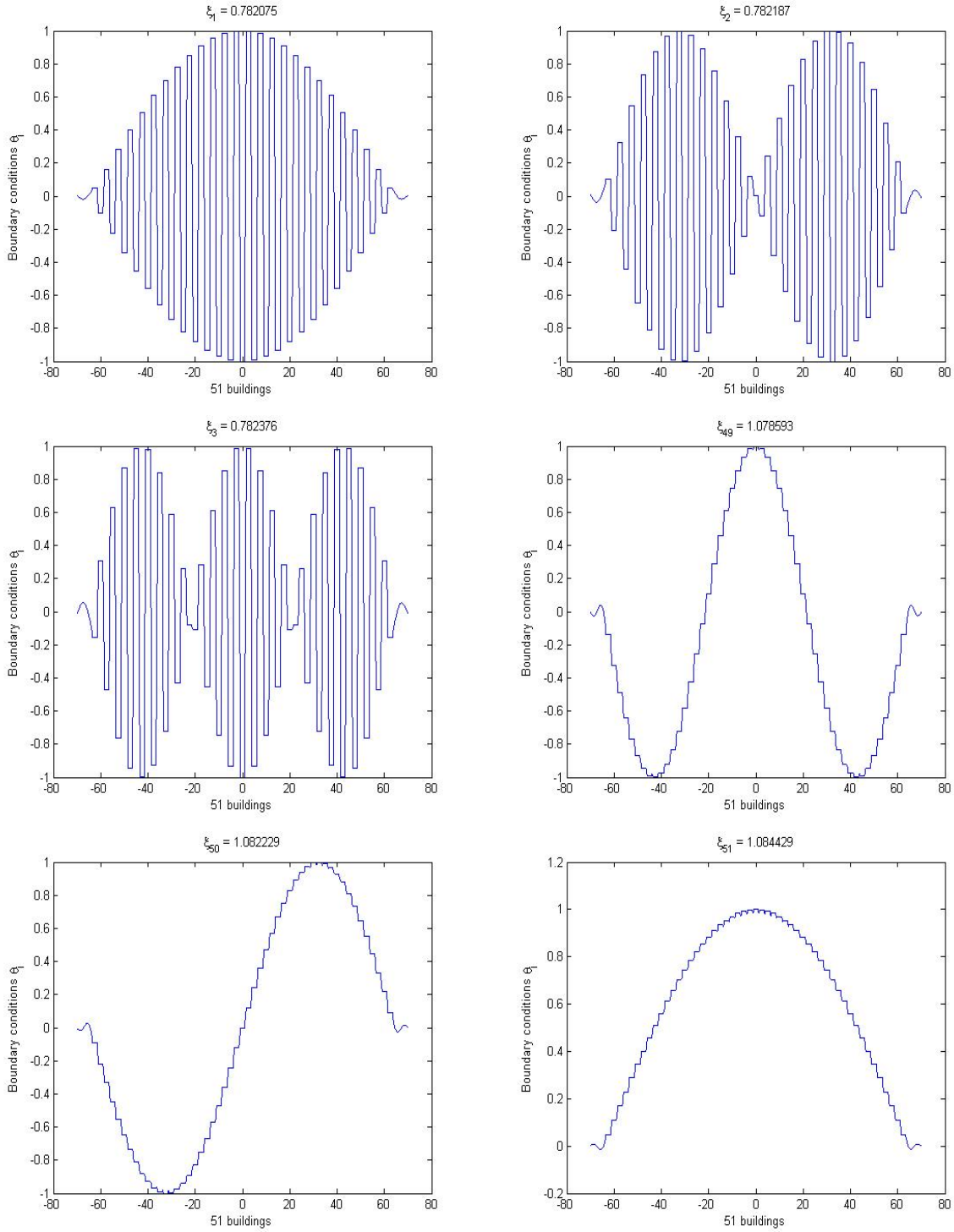

Tab. 3.2: *Different solutions (ξ_j, θ_j) for the free-space problem (1.13)-(1.15). The foundation displacements $\alpha = \theta_j$ are shown on graphs, the corresponding frequency ξ_j is stated above each picture; building halfwidth $l_b = 1$; the distance between consecutive buildings space $= 0.5$. The number of buildings $N = 51$; $M = 5$.*

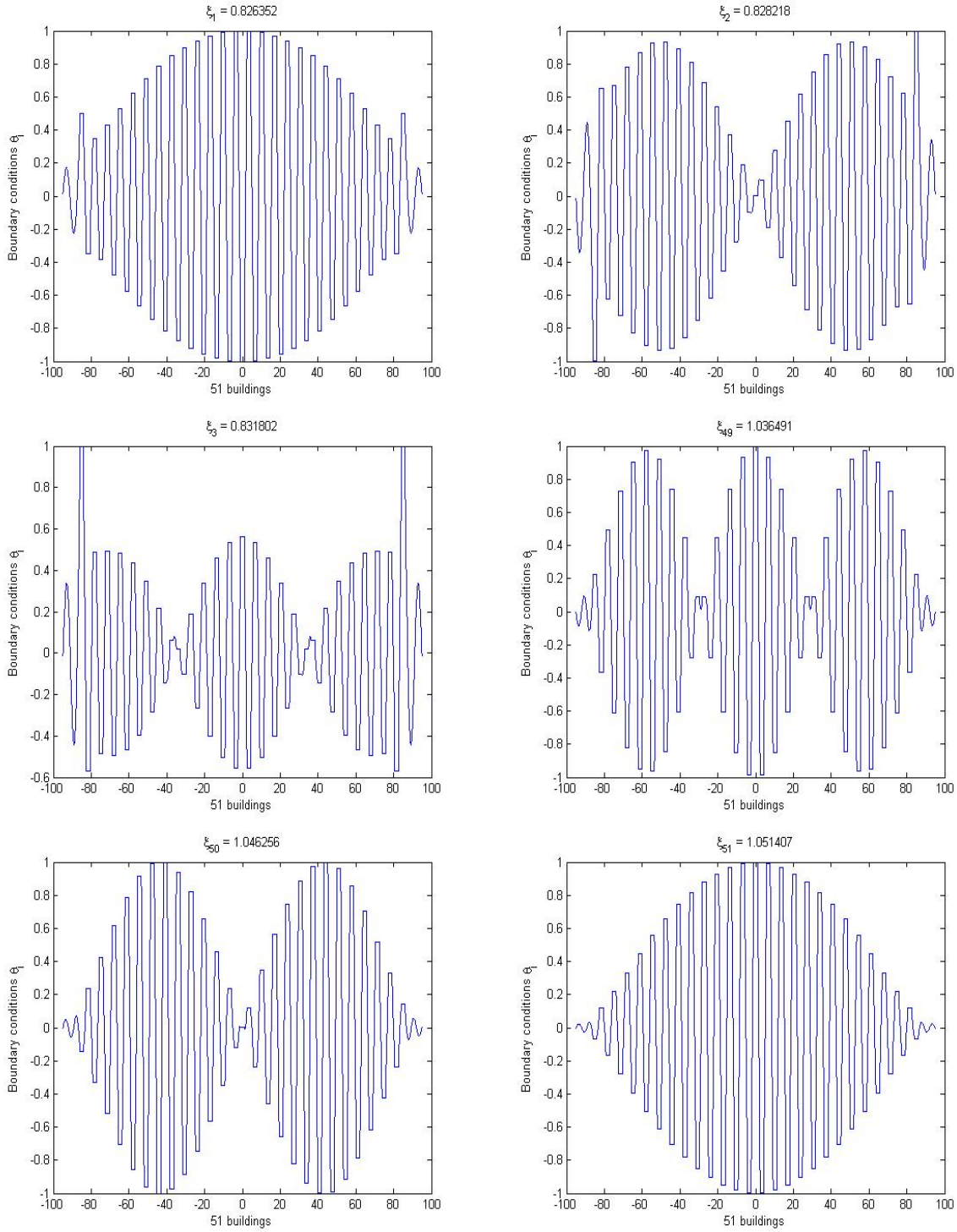

Tab. 3.3: *Different solutions (ξ_j, θ_j) for the free-space problem (1.13)-(1.15). The foundation displacements $\alpha = \theta_j$ are shown on graphs, the corresponding frequency ξ_j is stated above each picture; building halfwidth $l_b = 1$; the distance between consecutive buildings space $= 1.4$. The number of buildings $N = 51$; $M = 5$.*

3.1.3 Calculation of a natural city frequency range for the real data

In this section we want to use our numerical code to estimate the range of the natural city frequencies μ which satisfy the time harmonic solution (1.6). We do it in order to determine which types of seismic waves will favor the city-effect. Notice, that a natural city frequency before the non-dimensionalization is

$$\mu = \xi \frac{\beta}{l},$$

where β is the soil shear velocity, l is the characteristic length, and ξ is a non-dimensional frequency. The first value can be measured for a given region, the second is set by us, and the last one is found using our numerical methods. Note, that ξ depends on l.

We will fix the number of buildings $N = 21$, and calculate the minimum and the maximum frequencies ξ. Then the natural city frequencies μ will vary between $\xi_{min}\beta/l$ and $\xi_{max}\beta/l$. The solutions ξ depend on the city characteristics, that is, the parameters (1.11), the building halfwidth l_b, and the distance between two adjacent buildings which is denoted by *space*. As before, we will consider $l = l_b$, which makes $c_b = 1$. Therefore, in order to calculate the desired range, we need to know the soil shear velocity β, the building shear velocity β_b, and their ratio $b = \beta_b/\beta$; the ratio between building top and foundation masses $\gamma_b = m_1/m_0$; building halfwidth l_b, its height h, and their ratio $f_b = l_b/h$; and finally, the ratio between building and soil mass densities $r = \rho_b/\rho$. We will start with the real values corresponding to the case of Michoacan earthquake, which can be found, for instance, in [2]:

$$\beta_b = 120 \text{ m/s}; \ \beta = 80 \text{ m/s}; \ r = 0.15; \ \gamma_b = 1.5.$$

We will vary all of the ratios to determine which are dominant, and which are negligible; among others, the parameters of the cities Grenoble and Nice (found in [2]) will be tested. For all the simulations let us assume $l_b = 5$m, *space* $= 3$m.

№	h (m)	f_b	β (m/s)	β_b (m/s)	b	γ_b	r	$[\xi_{min},\ \xi_{max}]$	$[\mu_{min},\ \mu_{max}]$(Hz)
1	10	0.5	80	120	1.5	1.5	0.15	[0.81; 1.05]	[13.0; 16.8]
2	10	0.5	80	120	1.5	3	0.15	[0.82; 1.15]	[13.1; 18.4]
3	10	0.5	80	120	1.5	1.5	0.2	[0.83; 1.07]	[13.3; 17.1]
4	10	0.5	700	400	4/7	1.5	0.15	[0.29; 0.31]	[40.6; 43.4]
5	10	0.5	700	120	6/35	1.5	0.15	[0.09; 0.09]	[12.6; 12.6]
6	10	0.5	250	400	8/5	1.5	0.15	[0.87; 1.12]	[43.5; 56.0]
7	10	0.5	200	400	2	1.5	0.15	[1.30; 1.38]	[52.0; 55.2]
8	25	0.2	80	120	1.5	1.5	0.15	[0.32; 0.34]	**[5.1; 5.4]**
9	50	0.1	80	120	1.5	1.5	0.15	[0.15; 0.18]	**[2.4; 2.9]**
10	5	1	250	400	8/5	1.5	0.15	[2.42; 3.11]	[121.0; 155.5]

Tab. 3.4: *The range of the natural city frequencies for the real data; number of buildings $N = 21$, $M = 10$. In cases 8 and 9 the natural city frequency range overlaps with the range of the seismic waves, which makes the city-effect pronounced.*

As was mentioned earlier, the cases when structures caused or altered the seismic activity near them exhibit the same soil and structure frequencies. Therefore, for the city-effect to be pronounced, we need the city and the soil frequencies to coincide and be within the range of the seismic waves.

Natural frequency of a soil layer depends on its thickness and shear velocity, and ranges approximately from 0.1 Hz to 35 Hz (see, for example, [28]). There are two types of seismic activity which displays the same frequencies: seismic primary waves (P-waves), from 0.1Hz to 5Hz, and microearthquakes, from 2Hz to 50Hz (see [18]). Microearthquakes are very low intensity earthquakes of magnitude less then 2.0 on the Richter scale, and rarely felt more than 8 kilometers from the epicenter. That is why we will neglect them. It leaves us with P-waves, and, therefore, the natural city frequencies range should intertwine with $(0.1; 5)$Hz.

We stress that Table 3.4 provides the results for **natural city frequencies**; we can draw several conclusions:

- a change in the ratio r between the soil and the building mass densities or in the ratio γ_m between the building top and foundation masses does not result in a noticeable difference in the natural frequency range: simulations 1, 2, and 3 give almost the same results;
- buildings with low shear velocities favor the onset of the city-effect: compare simulations 4 and 5;
- the ratio b between the soil and buildings shear velocities does not influence the frequency range by itself, for any particular case we have to look at each shear velocity separately: see simulations 4, 5, and 6.
- another crucial factor is the ratio f_b between the building halfwidth and its height, and higher buildings will facilitate the onset of the city-effect: compare simulations 1, 8, and 9.

From Table 3.4 we may conclude that the soil shear velocity is not important (compare simulations 1 and 5, 4 and 6). But for the city-effect to be pronounced, natural soil frequencies should also fall in the interval $(0.1; 5)$Hz, and that is why low soil shear velocities facilitate the phenomenon.

Overall, our calculations alone with the previous results in literature confirm the common sense assumption that both soil and buildings characteristics are important in the city-effect phenomenon: a soil with low shear velocity and buildings high enough are needed for this effect to be noticeable. This is the case of the Michoacan earthquake, where buildings are high, and both shear velocities are low. Simulations 8 and 9 in Table 3.4 represent this case. Simulations 7 and 10 correspond to Nice and Grenoble, where buildings are low, and the building shear velocities are large. There the city-effect is not likely to occur. We conclude, that the model by Ghergu and Ionescu provides solutions which agree with the frequencies expected in reality.

3.1.4 Conclusions

We looked at several cities with different ratios between the width of a building and the distance between two adjacent buildings. Results are presented in Tables 3.1, 3.2, 3.3, and 3.6. As in [15], we see that the smallest eigenvalue is convergent as the number of buildings N grows bigger; but the biggest eigenvalue looks to have a limit too. We notice that for some cases there exists an eigenvector which keeps the sign, and for some cases - does not. Later, when we investigate the case of a periodic city, we will get back to this observation. We will also address the issue of convergence, as the number of buildings N grows, of the smallest eigenvalue to a periodic city frequency.

The method described above gives fast and precise results for a city with a finite number of equal-sized evenly-spaced buildings. To obtain less then 1% error we need to use at least $M = 10$, that is, 20 grid points. For a large number of buildings (more than 20, for example) the calculations become very time-consuming.

What happens when we have a really big city with a thousand equal-sized evenly-spaced buildings? In the next section we will apply periodic Green's function to study a city with infinitely many buildings. We will find its frequency and compare it to the eigenvalues of (3.14).

3.2 Periodic city

3.2.1 Modified algorithm

Let us assume that we have a city with infinitely many buildings. Assume that all the buildings are of equal size that they are evenly spaced; the conditions on their foundations are the same. We can assume $\alpha_j = 1$ for all j and consider only one building of width $2l_b$ located at $[-l_b, l_b]$ with the distance between two adjacent buildings *space*. Let

$$\begin{aligned}\Gamma_{per} &= [-l_b, l_b] \times \{0\},\\ \Gamma_{per}^{free} &= \{[-l_b - \frac{1}{2}space, -l_b] \cup [l_b, l_b + \frac{1}{2}space]\} \times \{0\},\\ \Omega_{per} &= [-l_b - \frac{1}{2}space, l_b + \frac{1}{2}space] \times (0, +\infty).\end{aligned}$$

Instead of (3.1)-(3.3) we will have to solve Helmholtz equation in a periodic domain. For a single period it is formulated as follows:

$$\Delta\Psi + \xi^2\Psi = 0 \text{ in } \Omega_{per}, \tag{3.25}$$

$$\Psi = 1 \text{ on } \Gamma_{per}, \ \frac{\partial\Psi}{\partial y} = 0 \text{ on } \Gamma_{per}^{free}. \tag{3.26}$$

The equation (1.15) will simplify to

$$q(\xi^2) = p(\xi^2) \int_{\Gamma_{per}} \frac{\partial\Phi}{\partial y}(s, 0)ds, \tag{3.27}$$

and the matrix (3.6) reduces to a scalar. In this case we do not have several eigenvalues and do not have to calculate an $N \times N$ matrix. We still have a nonlinear equation (3.27) for the unknown ξ which we can solve using Newton's method. On each iteration we still will have to solve a linear system of equations corresponding to condition $\Psi = 1$, but only $2M \times 2M$ size.

The solution to (3.25)-(3.26) is given by the single-layer potential (3.9), except that the integration kernel will be different. The fundamental solution in this case is given by the periodic Green's function (2.4) with period $d = 2l_b + space$, though we will have to use Ewald representation (2.15) for the numerical calculations. The analog of (3.18) is

$$\frac{i}{4} \sum_{n=-\infty}^{\infty} H_0^{(1)}(\xi r_n) = A_0(r_0) \ln \frac{\xi r_0}{2} + B_0(z_1, z_2), \tag{3.28}$$

where $z_1 = y$, $z_2 = x - s$, $r_n = \sqrt{y^2 + (x - s - nd)^2}$, $A_0(r_0) = -\dfrac{1}{2\pi} J_0(\xi r_0)$, and

$$B_0(z_1, z_2) = \begin{cases} \dfrac{i}{4} \displaystyle\sum_{n=-\infty}^{\infty} H_0^{(1)}(\xi r_n) + \frac{1}{2\pi} J_0(\xi r_0) \ln \frac{\xi r_0}{2}, & \text{if } r_0 \neq 0, \\ \dfrac{i\pi - 2C}{4\pi} + \dfrac{i}{4} \displaystyle\sum_{n \neq 0} H_0^{(1)}(\xi |n| d), & \text{if } r_0 = 0, \end{cases} \tag{3.29}$$

where C is the Euler constant. $B_0(0,0)$ is calculated using formula (2.21).

3.2.2 Numerical results. Comparison with the finite case

Below we provide the table comparing solutions of periodic problem with maximum and minimum eigenvalues of the corresponding free-space case. For all the city patterns $l_b = 1$, *space* is different. Free-space case: $N = 51,\ M = 5$; periodic case: $M = 10$. We highlight the values if they look to coincide.

space	0.5	1	1.3	1.4	1.5	2	3
ξ_{per}	**1.0864**	**0.9420**	0.8873	0.8737	0.8619	**0.8225**	**0.7934**
ξ_{min}	0.7821	0.7990	0.8156	0.8264	0.8418	**0.8222**	**0.7933**
ξ_{max}	**1.0844**	**0.9408**	1.0391	1.0514	1.0602	1.0635	0.9772

Tab. 3.5: *Comparison of the free-space and periodic frequencies ξ_{per} vs ξ_{min}, ξ_{max}; building halfwidth $l_b = 1$; the number of buildings $N = 51$, $M = 5$ for the free-space case, $M = 10$ for the periodic case.*

It can be seen that when *space* is small enough, ξ_{per} coincides with ξ_{max}, and when it is big enough - with ξ_{min}. Tables 3.1 and 3.2 show that the corresponding eigenvectors keep the sign. Then, for some range of *space* $\xi_{min} < \xi_{per} < \xi_{max}$. It was noticed before that for such cities no eigenvector keeps the sign.

We would like to look deeper into this matter. Is there any connection between ξ_{per} and eigenvalues for such cities? First, let us consider the city where $l_b = 1,\ space = 1.7$ and find all of its eigenvalues. We will do it for different number of buildings $N = 11;\ 31;\ 51$. Again, for every simulation $M = 5$. It appears that $\xi_{per} \approx \xi_3$. Also, we show all the eigenvalues for $space = 0.5,\ space = 3$. All the results are presented in Table 3.6.

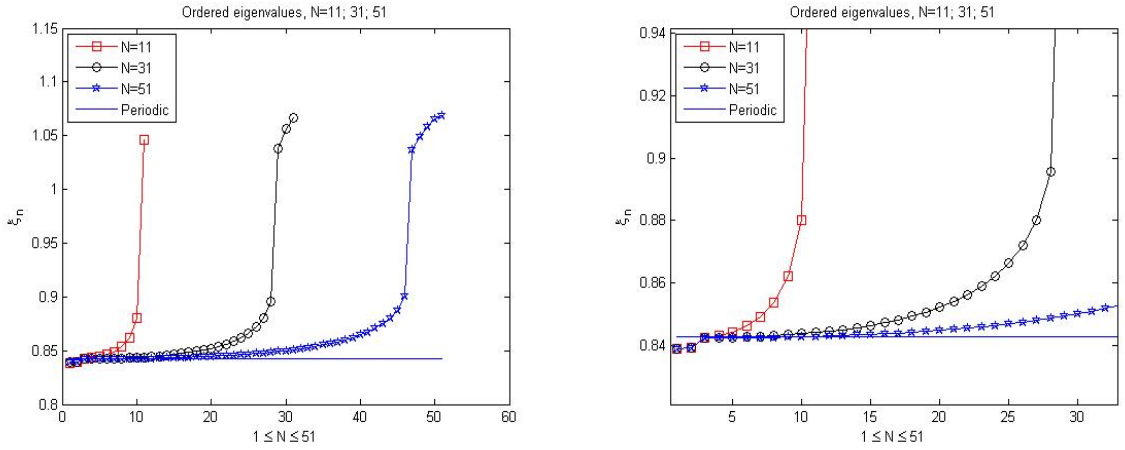

$space = 1.7$

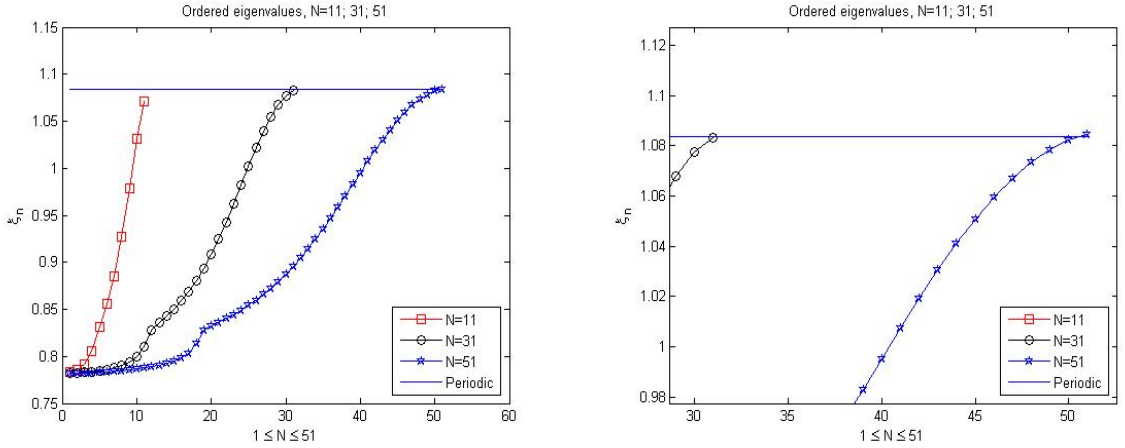

$space = 0.5$

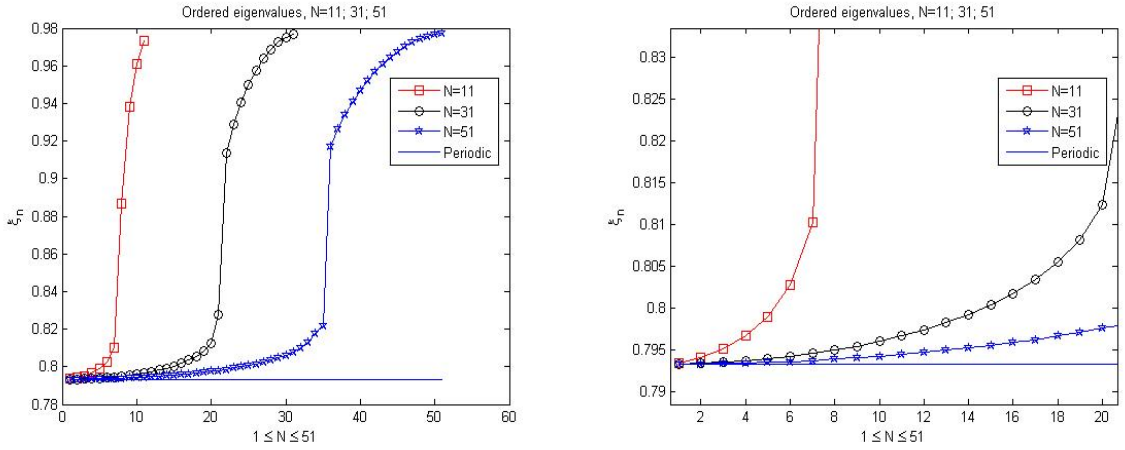

$space = 3$

Tab. 3.6: *Ordered eigenvalues (frequencies) for the free-space problem (1.13)-(1.15) compared to the frequency of the periodic problem (3.25)-(3.27). Cities have building halfwidth $l_b = 1$; the distance between consecutive buildings "space" is a specific for every city constant. The number of buildings N is* 11, 31, *and* 51*; $M = 5$. The pictures on the right are blow ups of the pictures on the left.*

3.3 Cities with different buildings

3.3.1 Small size city

The previous results were obtained under stringent assumptions. It is more realistic to allow buildings to be of different size and rigidity. We now allow buildings to have different heights, foundation areas, distances between each other, and to be built from various materials. In terms of our physical model, it means that not only displacements, but all the other parameters defined in section 1.2.1 depend now on the building number j. The same is true for non-dimensional parameters (1.11), and the polynomials p and q defined by (1.12). It is reasonable to conjecture that eigenvalues and eigenvectors of (3.5) do not solve problem (3.1) - (3.3). We will illustrate this for a 2-building city with building left endpoints $a = [-2.5; 1.5]$, building right endpoints $b = [-1.5; 3]$, and distance between the buildings $space = 3$.

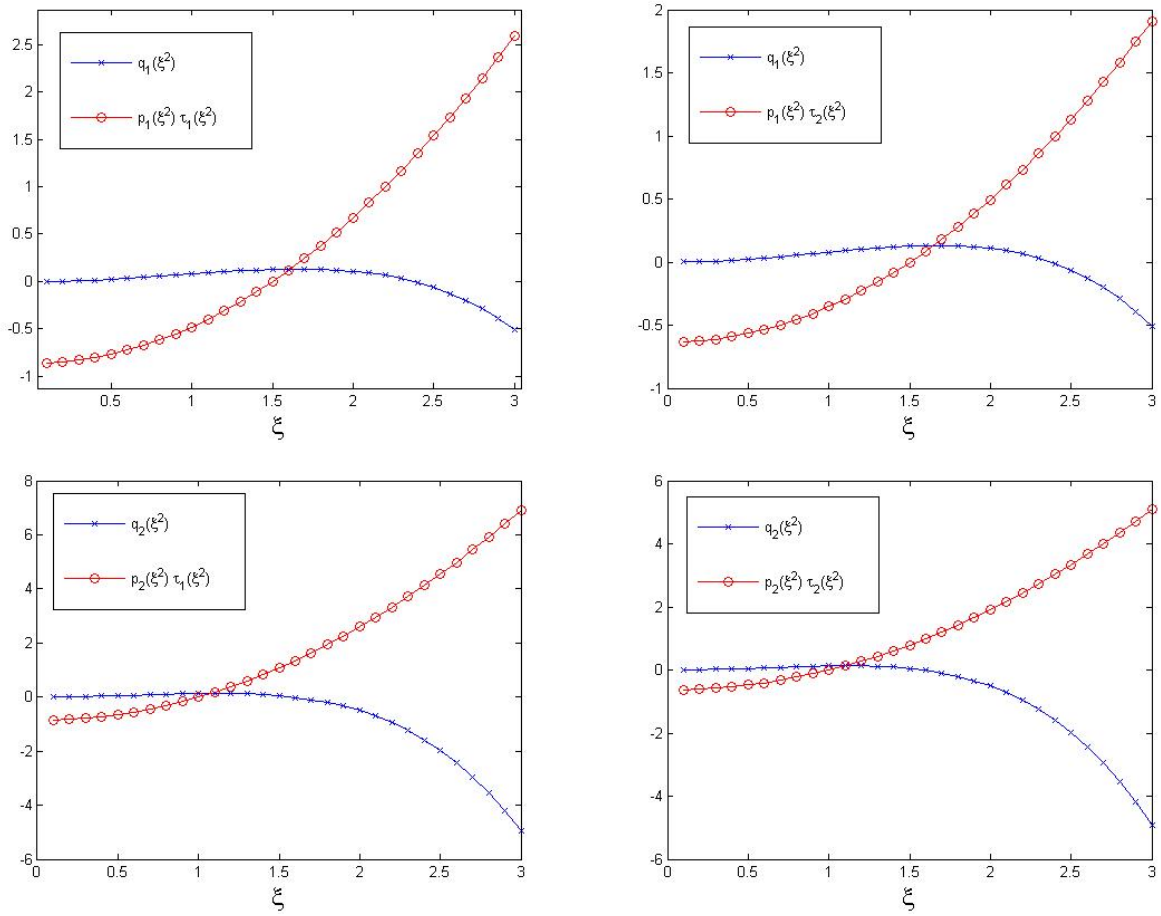

Fig. 3.2: *A 2-building city:* $a = [-2.5; 1.5]$, $b = [-1.5; 3]$*;* $q_j(\xi^2)$ *and* $p_j(\xi^2)\tau_i(\xi^2)$ *intersect at different points.*

In terms of 2-building city, if we want one of the eigenvalues τ_1, τ_2 of the matrix (3.6) to satisfy (1.15), then one of the systems ought to hold:

$$\begin{cases} q_1(\xi^2) = p_1(\xi^2)\tau_1(\xi^2) \\ q_2(\xi^2) = p_2(\xi^2)\tau_1(\xi^2) \end{cases} \qquad \begin{cases} q_1(\xi^2) = p_1(\xi^2)\tau_2(\xi^2) \\ q_2(\xi^2) = p_2(\xi^2)\tau_2(\xi^2) \end{cases}$$

Figure 3.2 illustrates that neither system has a solution. Pictures on the right correspond to the equations of the left system, and pictures on the right correspond to the right system. It is clear that the points of intersection are different for each pair of graphs.

It follows that we can not use pairs of eigenvalues and eigenvectors to solve our problem, and we have to modify the solution algorithm from section 3.1. In case of different buildings (1.15) takes form

$$q_j(\xi^2)\Phi(x,0) = p_j(\xi^2)\int_{\Gamma_j}\frac{\partial\Phi}{\partial y}(s,0)ds \text{ for } (x,0)\in\Gamma_j,\ 1\le j\le N, \tag{3.30}$$

and it defines system of N nonlinear equations with $N+1$ unknowns $\{\alpha,\xi\}$. The number of variables was reduced. We notice that if $[\Psi,\xi,\alpha]$ solves (3.1) - (3.3), then $[C\Psi,\xi,C\alpha]$ solves it too. It means that without loss of generality we can assume $\alpha_j = 1$ for some fixed j. This leaves us with N unknowns and the system (3.30) can be solved using one of the iterative methods. In the case of a finite city function Φ is found using the free-space Green's function (A.17).

We will vary building halfwidths l_{bj} and distances between the buildings $space_j$. This will lead us to different $p_j(\xi^2)$ and $q_j(\xi^2)$. We recall that for the homogeneous case characteristic length l was set up equal to l_b, such that $c_b = 1$ (see (3.24)). We can not proceed in the same manner, because l_{bj} are different, and l should be unique for our problem. That is why we choose to assign $l = 1$, and it follows that $c_{bj} = l_{bj}$. All the other parameters (3.24) will be unchanged and equal for all the buildings, but we notice that altering them will not change anything in our methods and reasoning. We observe distinctive solutions when we prescribe $\alpha_j = 1$ for different j. Table 3.7 presents the solutions (ξ,α) for a 6-building city sketched on figure 3.3, where $a = [0; 1.3; 3; 4; 5.4; 6.8]$, $b = [1; 2.6; 3.5; 5; 6.2; 7.4]$ for $M = 10$ ($2M$ is the number of grid points in our numerical calculations). Conditions on the building foundations α are shown as bar graphs, and coupled wavenumbers ξ are stated below each graph.

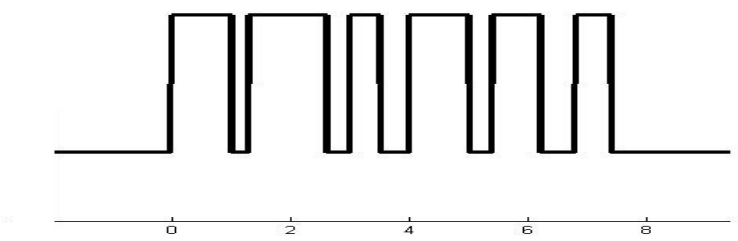

Fig. 3.3: *A sketch illustrating the relative size of the foundations and the spacing between the buildings for the 6-building city defined by* $a = [0; 1.3; 3; 4; 5.4; 6.8]$, $b = [1; 2.6; 3.5; 5; 6.2; 7.4]$.

Remark 3.3. *We use Matlab to solve the nonlinear systems of equations. The termination conditions are set up in such a way that the final answer accuracy is* 10^{-6}. *We notice that this is not the accuracy of our method.*

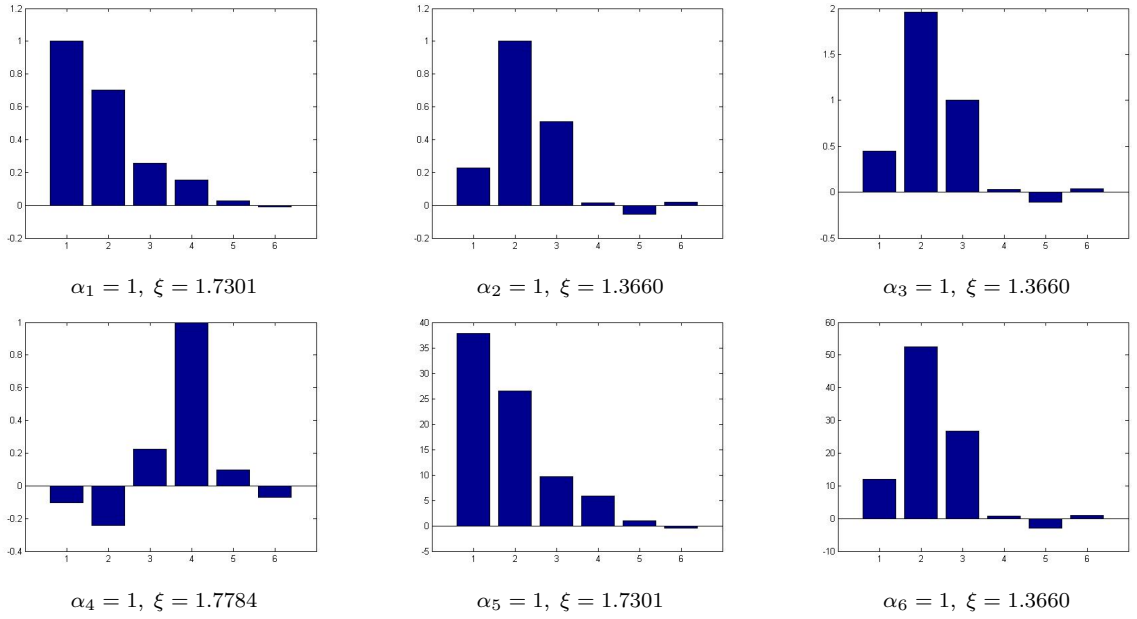

$\alpha_1 = 1,\ \xi = 1.7301$ $\alpha_2 = 1,\ \xi = 1.3660$ $\alpha_3 = 1,\ \xi = 1.3660$

$\alpha_4 = 1,\ \xi = 1.7784$ $\alpha_5 = 1,\ \xi = 1.7301$ $\alpha_6 = 1,\ \xi = 1.3660$

Tab. 3.7: *Solutions for the 6-building city:* $a = [0; 1.3; 3; 4; 5.4; 6.8]$, $b = [1; 2.6; 3.5; 5; 6.2; 7.4]$, $M = 10$.

We notice that the solution for each case $\alpha_j = 1$ may not be unique. The results in Table 3.7 are achieved for an initial guess for the wavenumber $\xi_0 = 1$. If we take $\xi_0 = 2.5$, we obtain the following:
if we impose $\alpha_1 = 1$, or $\alpha_2 = 1$, or $\alpha_3 = 1$, then our computation results in $\xi = 1.7301$;
if we impose $\alpha_4 = 1$, or $\alpha_5 = 1$, then our computation results in $\xi = 2.1861$;
if we impose $\alpha_6 = 1$, then our computation results in $\xi = 2.8057$.

We also notice that the initial guess for α does not influence the resulting solution, it may only accelerate or slow down its retrieving.

Ultimately we want to assume that some building cluster is repeated periodically in a city, and apply periodic Green's function to find city frequencies. That is why in the free-space case we will consider cities with several equal clusters of a few buildings. Then number of buildings in the city N equals $N_b N_c$, where N_b is the number of buildings in one cluster, and N_c is the number of clusters. Below we present the results for three different geometries. First, it will be the 2-building city that we have already mentioned. Then we consider two 3-building cities. We will refer to them as city7.5, city7 and city6.5, because their lengths of the periodic clusters are 7.5, 7 and 6.5.

1. City7.5: $a = [-2.5; 1.5],\ b = [-1.5; 3],\ space = [3; 2]$.

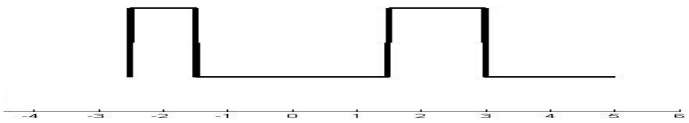

Fig. 3.4: *A sketch illustrating the relative size of the foundations and the spacing between the buildings for the city7.5 defined by* $a = [-2.5; 1.5]$, $b = [-1.5; 3]$, *space* $= [3; 2]$

.

2. City7: $a = [0; 2; 5],\ b = [1.2; 3; 6.7],\ space = [0.8; 2; 0.3]$.

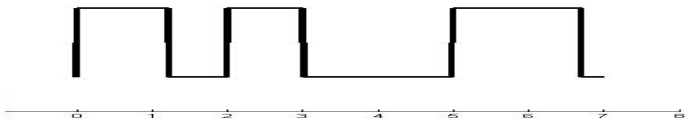

Fig. 3.5: *A sketch illustrating the relative size of the foundations and the spacing between the buildings for the city7 defined by* $a = [0; 2; 5]$, $b = [1.2; 3; 6.7]$, *space* $= [0.8; 2; 0.3]$

.

3. City6.5: $a = [0; 2.2; 4.7]; b = [1.8; 4.2; 6.2],\ space = [0.4; 0.5; 0.3]$.

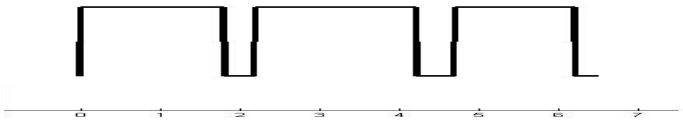

Fig. 3.6: *A sketch illustrating the relative size of the foundations and the spacing between the buildings for the city6.5 defined by* $a = [0; 2.2; 4.7]$, $b = [1.8; 4.2; 6.2]$, $space = [0.4; 0.5; 0.3]$

.

Tables 3.8 and 3.9 simply show the solutions we obtain. In the next subsection we will present the data that demonstrates that they converge as the number of clusters increases (see Tables 3.16 and 3.17). Also, at this point we would like to emphasize $\xi = 1.1584$ for city7.5 and $\xi = 1.0349$ for city7. We will meet these again when we solve the periodic problem.

Tables 3.10, 3.11, and 3.12 illustrate the convergence of the wavenumbers ξ and the foundation displacements α as the number of grid points $2M$ grows. Tables 3.13 and 3.14 give a more visual demonstration of this fact. Also, Table 3.14 seems to suggest that we are able to capture the first two decimal digits for the value of ξ for $M = 10$.

The last thing we would like to notice about the free-space case is that when the number of buildings increases, we obtain more solutions. This is similar to the case of equal buildings. For example, if we take the number of clusters $N_{cl} = 5$ and $M = 5$ for city6.5, we will find the following solutions for the wavenumber: 0.9801; 0.9865; 0.9906; 1.1427; 1.1986; 1.2302. Recall that we had just four solutions for $N_{cl} = 3$ (if $M = 10$ or $M = 20$). Table 3.15 provides the corresponding α, and we see that even though first three solutions for the frequency ξ appear to be very close to each other, these are indeed distinct solutions.

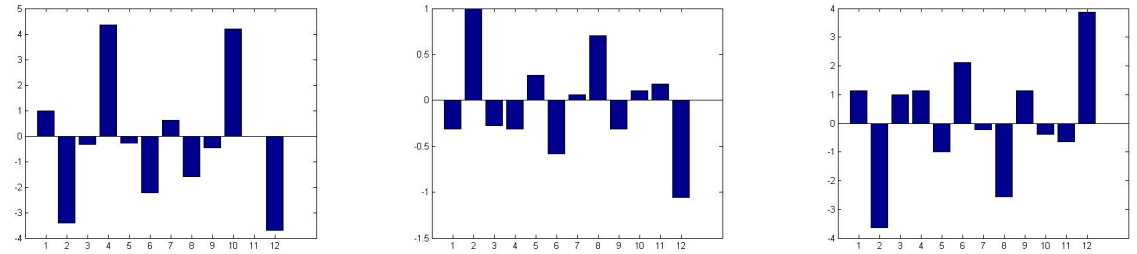

$\alpha_1 = 1,\ \xi = 1.0778$

$\alpha_2 = 1,\ \xi = 1.1212$

$\alpha_3 = 1,\ \xi = 1.1212$

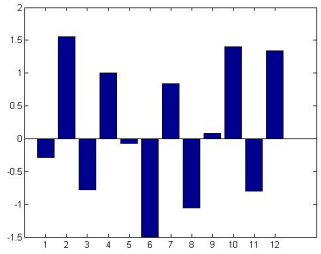

$\alpha_4 = 1,\ \xi = 1.1489$

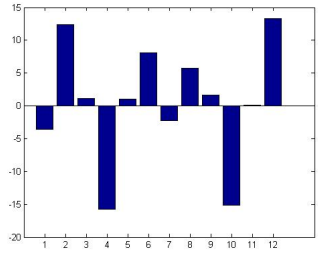

$\alpha_5 = 1,\ \xi = 1.0778$

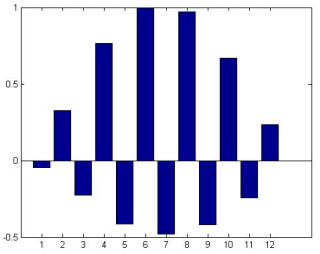

$\alpha_6 = 1,\ \xi = 1.1584$

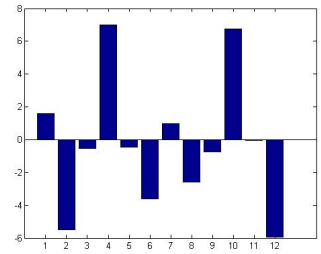

$\alpha_7 = 1,\ \xi = 1.0778$

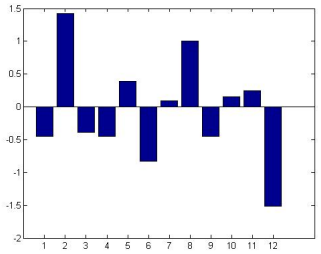

$\alpha_8 = 1,\ \xi = 1.1212$

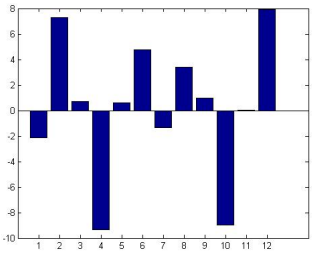

$\alpha_9 = 1,\ \xi = 1.0778$

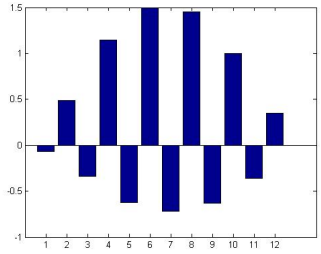

$\alpha_{10} = 1,\ \xi = 1.1584$

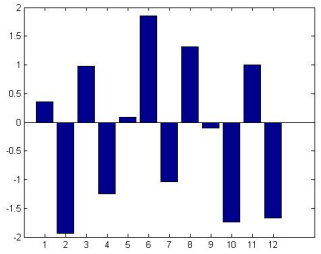

$\alpha_{11} = 1,\ \xi = 1.1489$

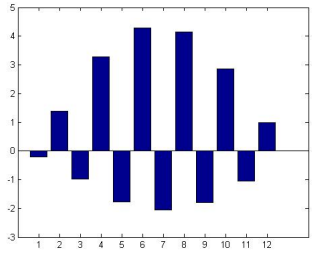

$\alpha_{12} = 1,\ \xi = 1.1584$

Tab. 3.8: *Two-building city7.5; number of clusters is 6, $M = 5$. The foundation displacements α are depicted as bar graphs, ξ are the wavenumbers.*

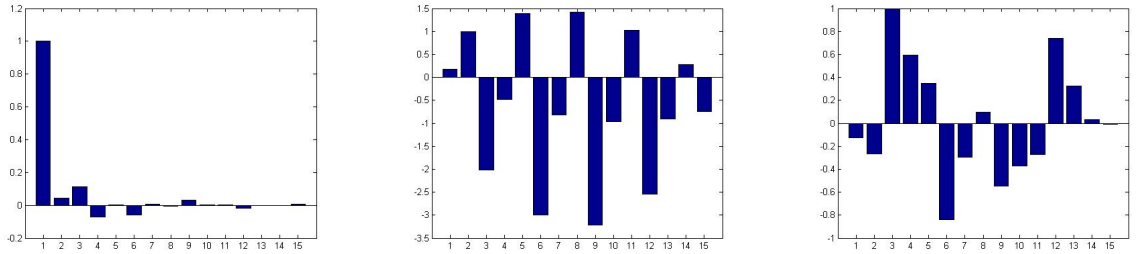

$\alpha_1 = 1,\ \xi = 1.4119$

$\alpha_2 = 1,\ \xi = 1.0349$

$\alpha_3 = 1,\ \xi = 1.0043$

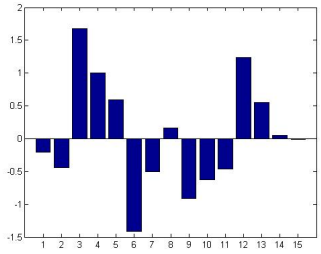

$\alpha_4 = 1,\ \xi = 1.0043$

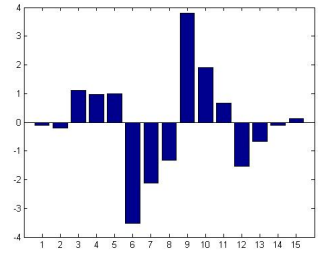

$\alpha_5 = 1,\ \xi = 1.0048$

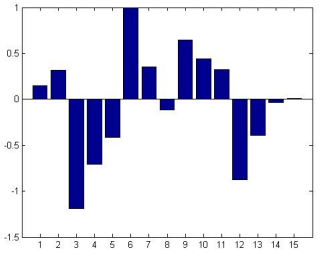

$\alpha_6 = 1,\ \xi = 1.0043$

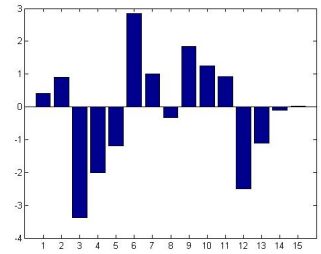

$\alpha_7 = 1,\ \xi = 1.0043$

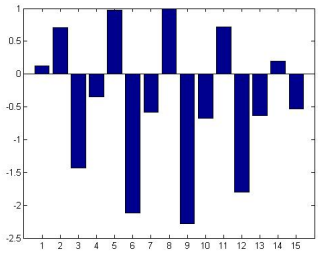

$\alpha_8 = 1,\ \xi = 1.0349$

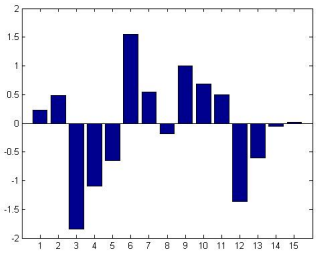

$\alpha_9 = 1,\ \xi = 1.0043$

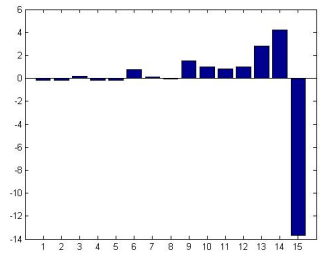

$\alpha_{10} = 1,\ \xi = 0.9837$

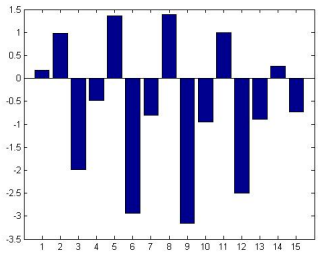

$\alpha_{11} = 1,\ \xi = 1.0349$

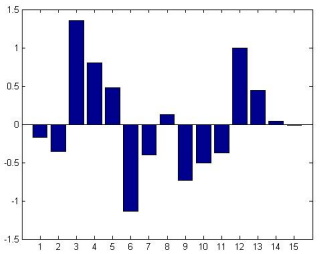

$\alpha_{12} = 1,\ \xi = 1.0043$

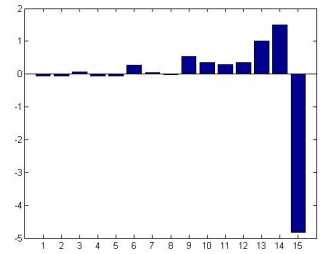

$\alpha_{13} = 1,\ \xi = 0.9837$

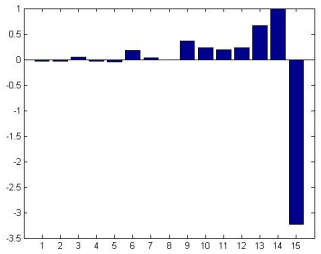

$\alpha_{14} = 1,\ \xi = 0.9837$

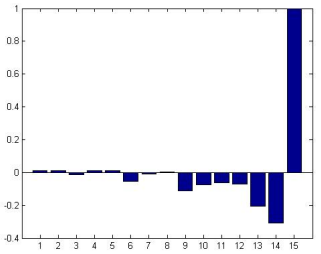

$\alpha_{15} = 1,\ \xi = 0.9837$

Tab. 3.9: *Three-building city7; number of clusters is 5, $M = 5$. The foundation displacements α are depicted as bar graphs, ξ are the wavenumbers.*

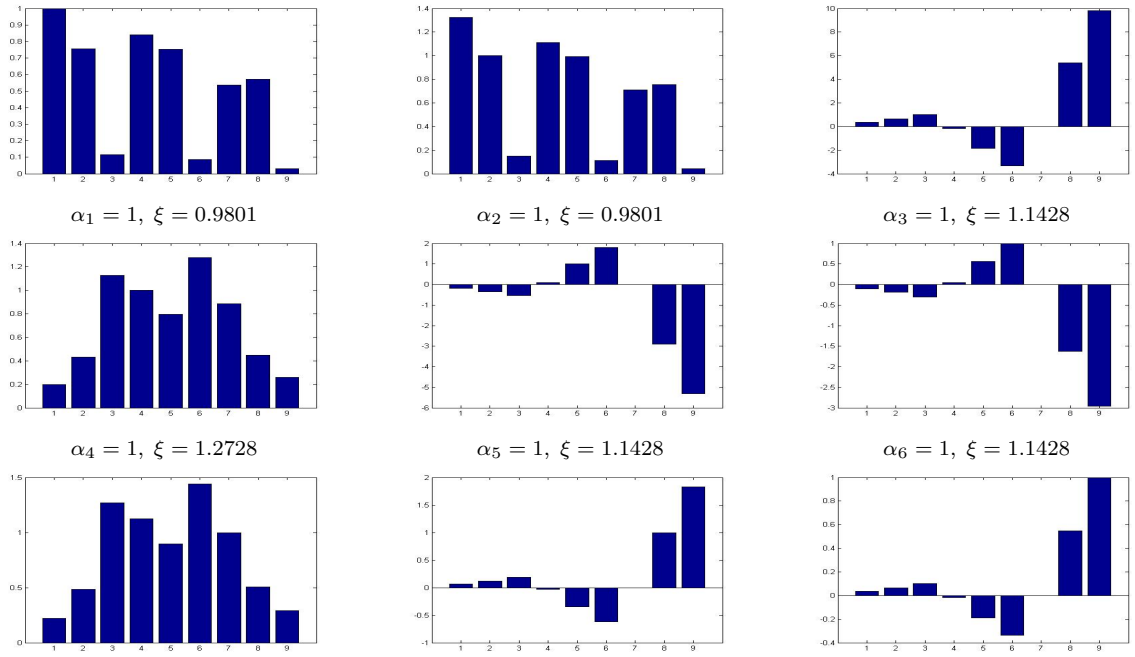

$\alpha_1 = 1,\ \xi = 0.9801$ | $\alpha_2 = 1,\ \xi = 0.9801$ | $\alpha_3 = 1,\ \xi = 1.1428$

$\alpha_4 = 1,\ \xi = 1.2728$ | $\alpha_5 = 1,\ \xi = 1.1428$ | $\alpha_6 = 1,\ \xi = 1.1428$

$\alpha_7 = 1,\ \xi = 1.2728$ | $\alpha_8 = 1,\ \xi = 1.1428$ | $\alpha_9 = 1,\ \xi = 1.1428$

Tab. 3.10: *Three-building city6.5; number of clusters is 3, $M = 5$. The foundation displacements α are depicted as bar graphs, ξ are the wavenumbers.*

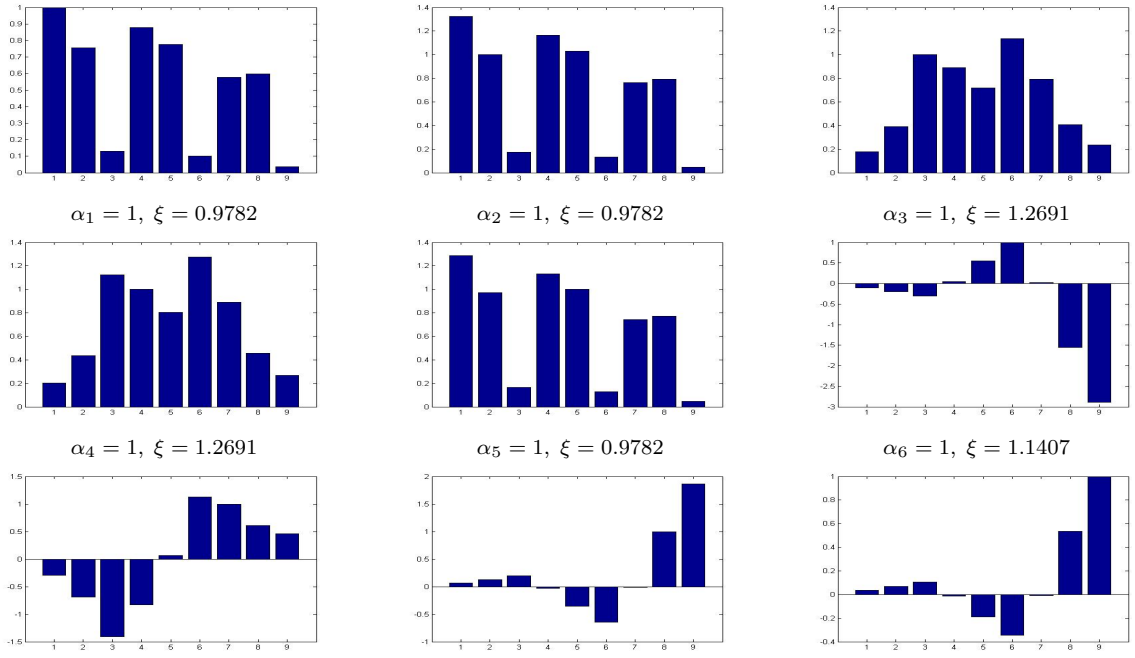

$\alpha_1 = 1,\ \xi = 0.9782$ | $\alpha_2 = 1,\ \xi = 0.9782$ | $\alpha_3 = 1,\ \xi = 1.2691$

$\alpha_4 = 1,\ \xi = 1.2691$ | $\alpha_5 = 1,\ \xi = 0.9782$ | $\alpha_6 = 1,\ \xi = 1.1407$

$\alpha_7 = 1,\ \xi = 1.2159$ | $\alpha_8 = 1,\ \xi = 1.1407$ | $\alpha_9 = 1,\ \xi = 1.1407$

Tab. 3.11: *Three-building city6.5; number of clusters is 3, $M = 10$. The foundation displacements α are depicted as bar graphs, ξ are the wavenumbers.*

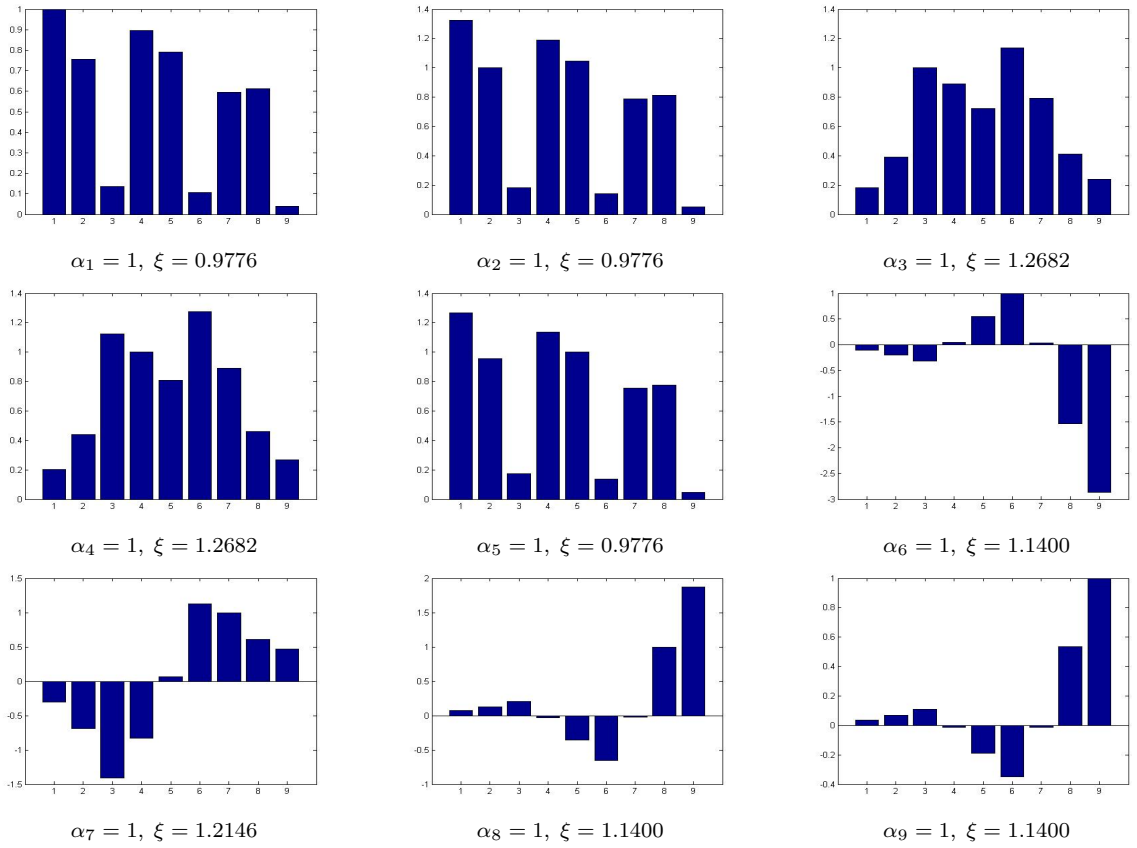

$\alpha_1 = 1,\ \xi = 0.9776$ | $\alpha_2 = 1,\ \xi = 0.9776$ | $\alpha_3 = 1,\ \xi = 1.2682$

$\alpha_4 = 1,\ \xi = 1.2682$ | $\alpha_5 = 1,\ \xi = 0.9776$ | $\alpha_6 = 1,\ \xi = 1.1400$

$\alpha_7 = 1,\ \xi = 1.2146$ | $\alpha_8 = 1,\ \xi = 1.1400$ | $\alpha_9 = 1,\ \xi = 1.1400$

Tab. 3.12: *Three-building city6.5; number of clusters is 3, $M = 20$. The foundation displacements α are depicted as bar graphs, ξ are the wavenumbers.*

M	α_1	α_2	α_3	α_4	α_5	α_6	α_7	α_8	α_9
5	1	0.7559	0.1143	0.8400	0.7516	0.0860	0.5357	0.5703	0.0310
10	1	0.7554	0.1304	0.8795	0.7775	0.1010	0.5771	0.5988	0.0362
20	1	0.7552	0.1362	0.8970	0.7897	0.1068	0.5956	0.6125	0.0382

Tab. 3.13: *Convergence of the foundation displacements α as the number of grid points $2M$ increases; three-building city6.5, $\xi = 0.9776$, number of clusters $N_{cl} = 3$.*

M	5	10	20
ξ_1	0.9801	0.9782	0.9776
ξ_2	1.1428	1.1407	1.1400
ξ_3		1.2159	1.2146
ξ_4	1.2728	1.2690	1.2682

Tab. 3.14: *Convergence of the wavenumbers ξ as the number of grid point $2M$ increases; three-building city6.5, number of clusters $N_{cl} = 3$*

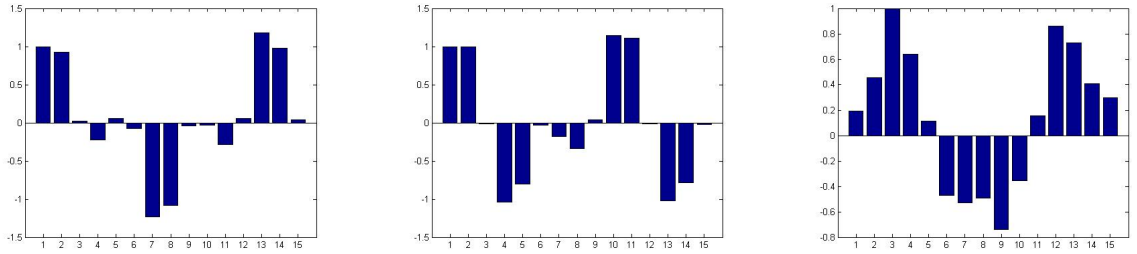

$\alpha_1 = 1,\ \xi = 0.9865$

$\alpha_2 = 1,\ \xi = 0.9906$

$\alpha_3 = 1,\ \xi = 1.2302$

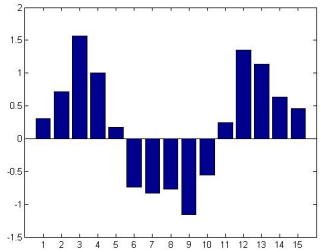

$\alpha_4 = 1,\ \xi = 1.2302$

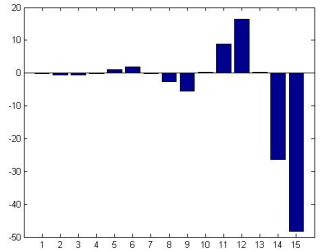

$\alpha_5 = 1,\ \xi = 1.1427$

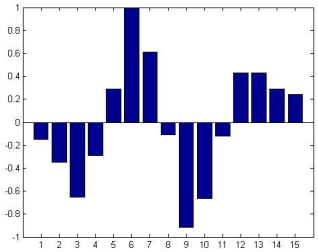

$\alpha_6 = 1,\ \xi = 1.1986$

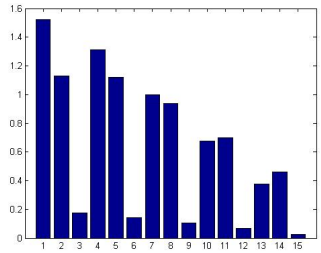

$\alpha_7 = 1,\ \xi = 0.9801$

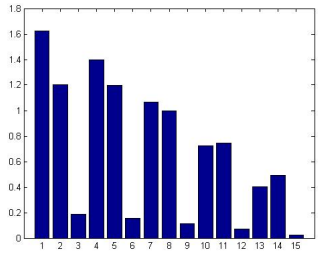

$\alpha_8 = 1,\ \xi = 0.9801$

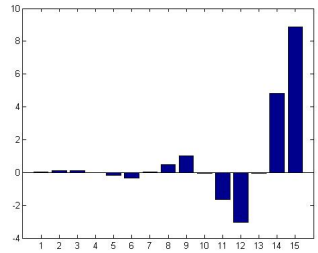

$\alpha_9 = 1,\ \xi = 1.1427$

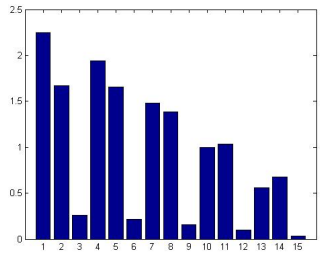

$\alpha_{10} = 1,\ \xi = 0.9801$

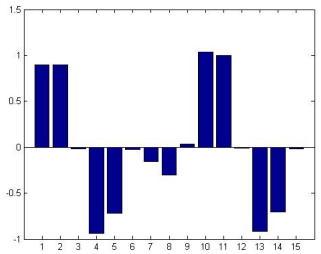

$\alpha_{11} = 1,\ \xi = 0.9906$

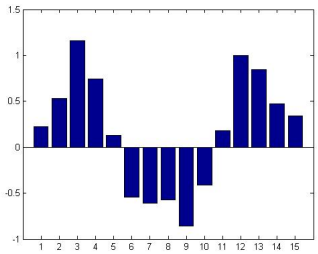

$\alpha_{12} = 1,\ \xi = 1.2302$

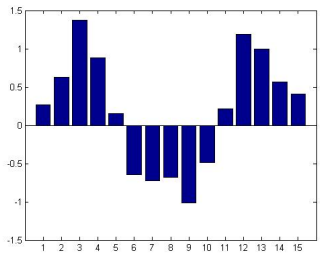

$\alpha_{13} = 1,\ \xi = 1.2302$

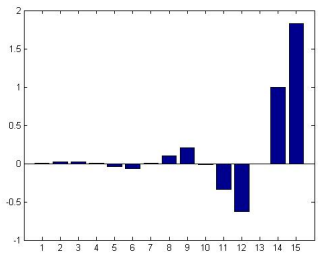

$\alpha_{14} = 1,\ \xi = 1.1427$

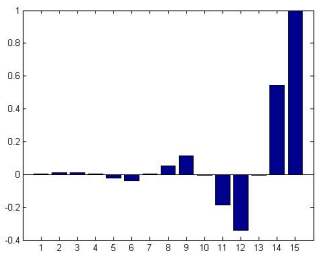

$\alpha_{15} = 1,\ \xi = 1.1427$

Tab. 3.15: *Three-building city6.5; number of clusters is 5, $M = 5$. The foundation displacements α are depicted as bar graphs, ξ are the wavenumbers.*

3.3.2 Periodic case

Just as for the problem with identical buildings, we will now assume that the city is infinite, and a cluster of a few different buildings is repeated throughout the city. The periodic Green's function will be used to find Φ in (3.30). Its period is the length of a single cluster. We assume that $\alpha_j = 1$ for some j, the other displacements of the buildings foundations are unknown, and we will have to solve the system of nonlinear equations (3.30). But, if in the free-space case we had $N_b N_c$ equations, here we solve just for one cluster, which reduces it to only N_b equations. We recall that N_b is the number of buildings in a cluster, and N_c is the number of clusters in the finite case. Below we present the results for the cities we have discussed earlier. As we have already mentioned, their periods are 7.5, 7, and 6.5. In the periodic case it does not matter which foundation displacement is 1, the solution is the same for any j. But it is not unique, and for different initial guesses ξ_0 there *possibly* can appear distinct solutions.

1. City7.5: $a = [-2.5; 1.5],\ b = [-1.5; 3],\ period = 7.5.$
   $\xi_0 = 1,\ M = 5:\ \xi = 1.1594,\ \alpha = [1; -2.1171];$
   $\xi_0 = 1,\ M = 10:\ \xi = 1.1583,\ \alpha = [1; -2.1222];$
   $\xi_0 = 1,\ M = 20:\ \xi = 1.1580,\ \alpha = [1; -2.1241].$
2. City7: $a = [0; 2; 5],\ b = [1.2; 3; 6.7],\ period = 7.$
   $\xi_0 = 1,\ M = 5:\ \xi = 1.0420,\ \alpha = [1; -1.5703; 3.5458];$
   $\xi_0 = 1,\ M = 10:\ \xi = 1.0382,\ \alpha = [1; -1.5103; 3.4610];$
   $\xi_0 = 1,\ M = 20:\ \xi = 1.0368,\ \alpha = [1; -1.4874; 3.4288].$
3. City6.5: $a = [0; 2.2; 4.7]; b = [1.8; 4.2; 6.2],\ period = 6.5.$
   $\xi_0 = 1,\ M = 5:\ \xi = 0.9850,\ \alpha = [1; 0.8109; 0.0919];$
   $\xi_0 = 1,\ M = 10:\ \xi = 0.9822,\ \alpha = [1; 0.8186; 0.1113];$
   $\xi_0 = 1,\ M = 20:\ \xi = 0.9812,\ \alpha = [1; 0.8221; 0.1181];$
   $\xi_0 = 1.5,\ M = 5:\ \xi = 1.2977,\ \alpha = [1; 0.7555; 1.2419];$
   $\xi_0 = 1.5,\ M = 10:\ \xi = 1.2918,\ \alpha = [1; 0.7682; 1.2392].$

From this data we see that the wavenumbers ξ and the foundation displacements α converge as the number of grid points $2M$ increases. We notice that some of the free-space solutions go to the periodic solutions as the number of buildings grows, just as in the case of a homogeneous city, wavenumbers ξ almost coincide. Tables 3.16 and 3.17 illustrate wavenumber convergence, showing one of the free-space solutions for different number of clusters in the city7.5 and city7.

	N=8	N=10	N=12	Periodic
ξ	1.1572	1.1579	1.1584	1.1583

Tab. 3.16: *Convergence of the free-space solution to the periodic solution for city7.5;* $M = 5$ *for free-space case,* $M = 10$ *for periodic case.*

	N=6	N=9	N=12	N=15	Periodic
ξ	1.0116	1.02160	1.0299	1.0349	1.0382

Tab. 3.17: *Convergence of the free-space solution to the periodic solution for city7; $M = 5$ for free-space case, $M = 10$ for periodic case.*

3.3.3 Conclusions

In this section we extended the algorithm introduced in [15] to the case of cities with distinct buildings. The eigenvalue approach is not applicable here, and we have to solve a system of nonlinear equations. Its solution gives us the foundation displacement α and the wavenumber ξ. Our numerical computations support the intuitive idea that both are convergent with respect to the number of grid points $2M$. When we assumed that a city consists of several equal clusters of a few buildings, we observed that ξ is also convergent with respect to the number of such clusters. Also, we noticed that similarly to the free-space case, increase in the number of buildings leads to new solutions. That means the the densely built areas have more frequencies that may cause a resonance.

Even a small number of clusters makes the calculations more difficult and time-consuming compared to the problem for the city with equal buildings. To address this issue, we assume that the city consists of a periodically repeated cluster of buildings. The application of the periodic Green's function becomes even more valuable. We showed that pair α, ξ converges with respect to the number of grid points $2M$. We studied different solutions for both finite and infinite cases, and showed that some wavenumbers of the free-space case go to the corresponding periodic wavenumbers as the number of clusters increases.

Chapter 4

Existence of preferred wavenumbers for the city problem

In this chapter we provide a rigorous mathematical proof for the existence of preferred wavenumbers that effectively couple the vibrations of the underground to the vibrations of the buildings standing on top. This proof is only valid for the antiplane model. Furthemore we only present a proof valid in the free space case in the presence of only one building. More precisely, we prove existence for the solution to problem (1.13)-(1.15) in the case where $N = 1$, and for Φ being the real part of the function Ψ defined by (3.1)-(3.3).
Many of the preliminary results discussed and proved in this chapter have well known analogs in three dimensional space. Those analogs have actually been studied in details by many authors, for instance see [10, 24]. However the results regarding two dimensional spaces are often merely mentioned, and it is hard to find detailed proofs in the literature. This is the reason why in this chapter we chose to study in details exterior Dirichlet to Neumann operators for the Helmholtz equation. Detailed statements and results turn out to be essential tools for proving the existence of a solution to problem (1.13)-(1.15).

4.1 Useful results on Hankel functions

For $n \in \mathbb{N}$ and z in $\mathbb{C}$ we denote by J_n the Bessel function

$$J_n(z) = (\frac{1}{2}z)^n \sum_{k=0}^{\infty} (-\frac{1}{4})^k \frac{z^{2k}}{k!(n+k)!}$$

For $n \in \mathbb{N}$ and z in $\mathbb{C} \setminus \mathbb{R}^{-*}$ we denote by Y_n the Bessel function

$$-\frac{1}{\pi}(\frac{1}{2}z)^{-n} \sum_{k=0}^{n-1} \frac{(n-k-1)!}{k!}(\frac{1}{4}z^2)^k + \frac{2}{\pi}\ln(\frac{1}{2}z)J_n(z)$$
$$-\frac{1}{\pi}(\frac{1}{2}z)^n \sum_{k=0}^{\infty} (\psi(k+1) + \psi(n+k+1))(-\frac{1}{4})^k \frac{z^{2k}}{k!(n+k)!},$$

where the first sum is void if $n = 0$ and the function ψ is defined by

$$\psi(1) = -\gamma,\ \psi(n) = -\gamma + \sum_{k=1}^{n-1} \frac{1}{k},$$

and γ is the Euler constant. The Hankel function of the first kind of order n, that is, $J_n + iY_n$, will be denoted H_n.

Lemma 4.1. *The following equivalence as $n \to \infty$ is uniform for all z in a compact set of $(0, \infty)$*

$$H_n(z) \sim -\frac{i}{\pi}(\frac{1}{2}z)^{-n}(n-1)! \tag{4.1}$$

Proof: Since for any positive z

$$\begin{aligned} |J_n(z)n!(\frac{1}{2}z)^{-n} - 1| &= \frac{1}{n+1}|\sum_{k=1}^{\infty}(-\frac{1}{4})^k \frac{z^{2k}(n+1)!}{k!(n+k)!}| \\ &\leq \frac{1}{n+1}\sum_{k=1}^{\infty}(\frac{1}{4})^k \frac{z^{2k}}{k!} \end{aligned}$$

it is clear that $J_n(z) \sim (\frac{1}{2}z)^n \frac{1}{n!}$ uniformly for all z in a compact set of $(0, \infty)$.
We can show similarily that $Y_n(z) \sim -\frac{1}{\pi}(\frac{1}{2}z)^{-n}(n-1)!$ uniformly for all z in a compact set of $(0, \infty)$. We conclude that (4.1) must hold. □

Lemma 4.2. *For $z > 0$, the following limit as $z \to 0$ is uniform for all integers n different from 0*

$$\lim_{z \to 0^+} -\frac{z}{|n|}\frac{H_n'(z)}{H_n(z)} = 1 \tag{4.2}$$

For the special case $n = 0$ we have,

$$\lim_{z \to 0^+} \frac{zH_0'(z)}{H_0(z)} = 0$$

Proof: We observe that for $n \geq 2$

$$\left(H_n(z)(-\frac{i}{\pi}(\frac{1}{2}z)^{-n}(n-1)!)^{-1} - 1\right)(n-1)$$

can be bounded by a function in z which is continuous on $[0, \infty)$, therefore

$$H_n(z) \sim -\frac{i}{\pi}(\frac{1}{2}z)^{-n}(n-1)! \tag{4.3}$$

as $z \to 0^+$, uniformly on $[0, b]$ for a fixed $b > 0$. Using the formula

$$H_n'(z) = -H_{n+1}(z) + \frac{n}{z} H_n(z) \tag{4.4}$$

we obtain

$$-\frac{z}{n}\frac{H_n'(z)}{H_n(z)} \sim 1$$

as $z \to 0^+$, uniformly on $[0, b]$ for a fixed $b > 0$.
For $n \leq -2$, we can now apply the formula $H_{-n}(z) = (-1)^n H_n(z)$. The remaining three cases can be treated in a straightforward fashion. □

Lemma 4.3. *For any n in $\mathbb{N}$, $|H_n(z)|$ is a decreasing function of z on $(0, +\infty)$.*

Proof: This is due to the formula derived by Nicholson, see[30],

$$J_n^2(z) + Y_n^2(z) = \frac{8}{\pi^2} \int_0^\infty K_0(2z \sinh t) \cosh 2nt dt$$

where $K_0(s) = \displaystyle\int_0^\infty e^{-s \cosh t} dt$. □

Lemma 4.4. *Let a and b be two real numbers such that $0 < a < b$. The following equivalence as $n \to \infty$ is uniform for all complex numbers z in the closed disk of the complex plane centered at b and of radius a*

$$H_n(z) \sim -\frac{i}{\pi}(\frac{1}{2}z)^{-n}(n-1)! \tag{4.5}$$

Proof: The proof is nearly identical to that of lemma 4.1. □

Lemma 4.5. *Denote by St_n the Struve function of order n as defined in [1]. The following formula holds for any $t > 0$*

$$\int_0^t H_0(z) dz = tH_0(t) + \frac{\pi}{2} t(St_0 H_1(t) - St_1 H_0(t)) \tag{4.6}$$

It follows that the semi convergent integral $\displaystyle\int_0^\infty H_0(z) dz$ is exactly equal to 1.

Proof: Integral formula (4.6) is given in [1]. The value of $\int_0^\infty H_0(z) dz$ results from that formula combined to known asymptotics at infinity of Bessel and of Struve functions. One should consult [1] for formulas on Bessel functions, and [30] for their derivation. □

4.2 The boundary Dirichlet to Neumann operator. Continuity with regard to the wavenumber

In this chapter we denote by D the open unit disk of $\mathbb{R}^2$ centered at the origin.

Lemma 4.6. *Let $\kappa > 0$ be a wave number and f be a function in the Sobolev space $H^{\frac{1}{2}}(\partial D)$. The problem*

$$(\Delta + \kappa^2)u = 0 \text{ in } \mathbb{R}^2 \setminus \overline{D} \tag{4.7}$$

$$u = f \text{ on } \partial D \tag{4.8}$$

$$\frac{\partial u}{\partial r} - i\kappa u = o(r^{-1}), \text{ uniformly as } r \to \infty \tag{4.9}$$

has a unique solution. Writing $f = \sum_{n=-\infty}^{\infty} a_n e^{in\theta}$, we have

$$u = \sum_{n=-\infty}^{\infty} a_n e^{in\theta} \frac{H_n(\kappa r)}{H_n(\kappa)}, \tag{4.10}$$

This series and all its derivatives are uniformly convergent on any subset of $\mathbb{R}^2$ in the form $r \geq A$ where $A > 1$.

Proof: Existence and uniqueness for equation (4.7-4.9) are well known, we are chiefly interested here in the convergence properties of the series (4.10). We first note that $H_{-n}(z) = (-1)^n H_n(z)$, so we will establish convergence properties as $n \to \infty$ and the case $n \to -\infty$ will then follow easily. From (4.1) we can claim that

$$\frac{H_n(\kappa r)}{H_n(\kappa)} \sim \frac{1}{r^n},$$

uniformly in r as long as r remains in a compact set of $(0, \infty)$. Fix two real numbers A, B such that $1 < A < B$. Denote $M = \sup |a_n|$. It follows that

$$|a_n e^{in\theta} \frac{H_n(\kappa r)}{H_n(\kappa)}| \leq 2\frac{M}{A^n}$$

for all n large enough, uniformly for all r in $[A, B]$, so the series (4.10) is uniformly convergent on any compact subset of $\mathbb{R}^2 \setminus \overline{D}$.
Next we use the recurrence formula (4.4) to write

$$\kappa \frac{H_n'(\kappa r)}{H_n(\kappa)} = -\kappa \frac{H_{n+1}(\kappa r)}{H_n(\kappa)} + \frac{n}{r} \frac{H_n(\kappa r)}{H_n(\kappa)}$$

The term $\frac{n}{r} \frac{H_n(\kappa r)}{H_n(\kappa)}$ can be estimated as previously. For $\kappa \frac{H_{n+1}(\kappa r)}{H_n(\kappa)}$ use and (4.1) one more time to find

$$\frac{H_{n+1}(\kappa r)}{H_n(\kappa)} \sim \frac{2n+2}{r^{n+2}}$$

uniformly for all r in $[A, B]$. At this stage we can conclude that the r derivative of the series (4.10) is uniformly convergent on any compact subset of $\mathbb{R}^2 \setminus \overline{D}$.

A θ derivative of the series (4.10) corresponds to a multiplication by in so the uniform convergence property holds for that derivative too. Second derivatives can be treated in a similar way to find that the function defined by the series (4.10) is in $C^2(\mathbb{R}^2 \setminus \overline{D})$.
If $r \geq 2$, we combine lemma 4.3 and (4.1) to write

$$|\frac{H_n(\kappa r)}{H_n(\kappa)}| \leq |\frac{H_n(2\kappa)}{H_n(\kappa)}| \leq 2^{-n+1},$$

for all n greater than some N, for all $r \geq 2$. Similarly

$$|\kappa\frac{H_n'(\kappa r)}{H_n(\kappa)}| \leq |\kappa\frac{H_{n+1}(2\kappa)}{H_n(\kappa)}| + |\frac{n}{r}\frac{H_n(2\kappa)}{H_n(\kappa)}| \leq n2^{-n+1},$$

for all n greater than some N, for all $r \geq 2$. Given that a_n is bounded, it follows that the series (4.10) and its r derivative are uniformly convergent for all r in $[2, \infty)$. A similar argument can be carried out for the θ derivative, and all second derivatives.
Next we recall that H_n satisfies the Bessel differential equation

$$y''(r) + \frac{1}{r}y'(r) + (1 - \frac{n}{r^2})y(r) = 0$$

to argue that each function $e^{in\theta}H_n(\kappa r)$ satisfies Helmholtz equation due to the form of the Laplacian in polar coordinates, namely $\partial_r^2 + \frac{1}{r}\partial_r + \frac{1}{r^2}\partial_\theta^2$. All together this shows that the series the function defined by the series (4.10) satisfies (4.7).
To prove (4.9) we first note that each function $e^{in\theta}H_n(\kappa r)$ satisfies that estimate due to the well known asymptotic behavior of Hankel's functions H_n, see [1]. From there (4.9) can be derived using that the series (4.10) and its r derivative are uniformly convergent for all r in $[2, \infty)$.
Finally it is worth mentioning that for any fixed $r \geq 1$ the series in (4.10) is in the Sobolev space $H^{\frac{1}{2}}(\partial D)$ for all $r \geq 1$ and that further applications of lemma 4.3 will show that this series converges strongly to f in $H^{\frac{1}{2}}(\partial D)$ as $r \to 1^+$. $\square$

We now define the linear operator T_κ which maps $H^{\frac{1}{2}}(\partial D)$ into $H^{-\frac{1}{2}}(\partial D)$ by the formula

$$T_\kappa(f) = \sum_{n=-\infty}^{\infty} a_n e^{in\theta}\kappa\frac{H_n'(\kappa)}{H_n(\kappa)}, \tag{4.11}$$

where $f = \sum_{n=-\infty}^{\infty} a_n e^{in\theta}$. T_κ is continuous since fomula (4.4) combined to (4.1) implies that

$$\kappa\frac{H_n'(\kappa)}{H_n(\kappa)} \sim -n, \quad n \to \infty$$

An equivalent way of defining T_κ is to say that it maps f to $\frac{\partial u}{\partial r}|_{r=1}$, where u is the solution to (4.7 - 4.9). We denote by $<,>$ the duality bracket between $H^{\frac{1}{2}}(\partial D)$ and $H^{-\frac{1}{2}}(\partial D)$ which extends the dot product $< f, g >= \int_{\partial D} f\overline{g}$.

Lemma 4.7. *Let f be in $H^{\frac{1}{2}}(\partial D)$. Then $Re < T_\kappa(f), f >\leq 0$.*

Proof:
Set $f = \sum_{n=-\infty}^{\infty} a_n e^{in\theta}$. By definition of T_κ

$$\mathrm{Re} < T_\kappa(f), f >= 2\pi \sum_{n=-\infty}^{\infty} |a_n|^2 \kappa \mathrm{Re}(\frac{H_n'(\kappa)}{H_n(\kappa)}) = 2\pi \sum_{n=-\infty}^{\infty} |a_n|^2 \kappa \frac{\mathrm{Re}(H_n'(\kappa)\overline{H_n(\kappa)})}{|H_n(\kappa)|^2}$$

The result then follows from lemma 4.3. □

Lemma 4.8. *T_κ is real analytic in κ for κ in $(0, \infty)$.*

Proof: Let k_0 and b be two real numbers such that $0 < b < k_0$. Define $D_b(k_0)$ the closed disk in the complex plane centered at k_0 and with radius b. According to [20], chapter 7, to show that T_κ is real analytic in κ for κ in $(0, \infty)$ in operator norm, it suffices to fix f and g in $H^{\frac{1}{2}}(\partial D)$ and to show that $< T_\kappa(f), g >$ is an analytic function of κ in $D_b(k_0)$. Writing $f = \sum_{n=-\infty}^{\infty} a_n e^{in\theta}$, $g = \sum_{n=-\infty}^{\infty} b_n e^{in\theta}$, we have

$$< T_\kappa(f), g >= 2\pi \sum_{n=-\infty}^{\infty} a_n \overline{b_n} \kappa \frac{H_n'(\kappa)}{H_n(\kappa)} \tag{4.12}$$

Given that $\sum_{n=-\infty}^{\infty} n|a_n b_n| < \infty$ and $\kappa \frac{H_n'(\kappa)}{H_n(\kappa)} \sim -|n|, \quad |n| \to \infty$, uniformly for all κ in $D_b(k_0)$, the series in (4.12) is a uniformly convergent sum of analytic functions, thus $< T_\kappa(f), g >$ is analytic in $D_b(k_0)$. □

4.2.1 The limit of the boundary operator T_κ as κ approaches zero

Lemma 4.9. *The operator T_κ converges strongly to the operator T_0 which maps $H^{\frac{1}{2}}(\partial D)$ into $H^{-\frac{1}{2}}(\partial D)$ and is defined by the formula*

$$T_0(f) = \sum_{n=-\infty}^{\infty} -|n| a_n e^{in\theta}, \tag{4.13}$$

where $f = \sum_{n=-\infty}^{\infty} a_n e^{in\theta}$.

Proof: Let $f = \sum_{n=-\infty}^{\infty} a_n e^{in\theta}$ be in $H^{\frac{1}{2}}(\partial D)$. We can write

$$\|T_\kappa(f) - T_0(f)\|_{H^{-\frac{1}{2}}(\partial D)} = \sum_{n=-\infty}^{\infty} \frac{|a_n|^2}{\sqrt{n^2+1}} |\kappa \frac{H_n'(\kappa)}{H_n(\kappa)} - |n||^2$$

and then apply lemma 4.2. □

Lemma 4.10. *Let f be a function in the Sobolev space $H^{\frac{1}{2}}(\partial D)$. The problem*

$$\Delta u = 0 \text{ in } \mathbb{R}^2 \setminus \overline{D} \tag{4.14}$$

$$u = f \text{ on } \partial D \tag{4.15}$$

$$u = O(1), \text{ uniformly as } r \to \infty \tag{4.16}$$

has a unique solution. Writing $f = \sum_{n=-\infty}^{\infty} a_n e^{in\theta}$, we have

$$u = \sum_{n=-\infty}^{\infty} a_n e^{in\theta} r^{-|n|}, \tag{4.17}$$

This series and all its derivatives are uniformly convergent on any subset of $\mathbb{R}^2$ in the form $r \geq u$ where $u > 1$.

Proof: Existence and uniqueness for equation (4.14-4.16) are well known, see [13]. Proving the uniform convergence properties is trivial given how simple the radial terms are. □

We note that an equivalent way of defining T_0 is to say that it maps f to $\frac{\partial u}{\partial r}|_{r=1}$ where u is the solution to (4.14 - 4.16).

4.2.2 Problems in the plane $\mathbb{R}^2$ minus a line segment

We use the following notation in this section: Γ is the line segment $[-\frac{1}{2}, \frac{1}{2}] \times \{0\}$, Ω is the open set $\{x : |x| < 1\} \setminus \Gamma$. ∂D will denote the same boundary as in the previous section. On Γ an upper and a lower trace for all functions in $H^1(\Omega)$ can be defined: even though Γ is an interior boundary of Ω, since Γ is C^1, an adequate version of the trace theorem on Γ holds, see [27].
We denote $H^1_{0,\Gamma}(\Omega)$ the closed subspace of $H^1(\Omega)$ consisting of functions whose upper and lower trace on Γ are zero.
Lemma 4.11. *Let F be a continuous linear functional on $H^1_{0,\Gamma}(\Omega)$. The following variational problem has a unique solution for any $\kappa > 0$:*
find u in $H^1_{0,\Gamma}(\Omega)$ such that

$$\int_\Omega \nabla u \cdot \nabla v - \kappa^2 uv - \int_{\partial D} (T_\kappa u)\, v = F(v), \tag{4.18}$$

for all v in $H^1_{0,\Gamma}(\Omega)$.

Proof: We first prove uniqueness. Assume that u is in $H^1_{0,\Gamma}(\Omega)$ and satisfies (4.18) with $F = 0$. It is clear that u satisfies $(\Delta + \kappa^2)u = 0$ in Ω. Define

$$\Omega^+ = \{(x_1, x_2) \in \Omega : x_2 > 0\}$$

and define Ω^- likewise. By Green's theorem we must have that

$$\operatorname{Im}\int_{\partial\Omega^+} u\overline{\frac{\partial u}{\partial n}} = \operatorname{Im}\int_{\partial\Omega^-} u\overline{\frac{\partial u}{\partial n}} = 0$$

Using the fact that the upper and lower traces of u on Γ are zero we infer that

$$\operatorname{Im}\int_{\partial D} u\overline{\frac{\partial u}{\partial n}} = 0. \tag{4.19}$$

Next we observe that the variational problem (4.18) implies

$$\frac{\partial u}{\partial n} = T_\kappa u \tag{4.20}$$

on the boundary ∂D. Outside D we extend u by setting it equal to the solution of (4.7-4.9) where f is the trace of $u_{|\Omega}$ on ∂D. We can claim thanks to (4.20) that u and $\dfrac{\partial u}{\partial n}$ are continuous across ∂D. By (4.19) u must be zero in $\mathbb{R}^2 \setminus D$ due to Reillich's lemma. Consequently, u and $\dfrac{\partial u}{\partial n}$ are zero on ∂D, and therefore u is also zero in Ω due to the Cauchy Kowalewski theorem.
To show existence define the bilinear functional

$$a_\kappa(u,v) = \int_\Omega \nabla u\cdot\nabla v - \kappa^2 uv - \int_{\partial D}(T_\kappa u)\, v \tag{4.21}$$

a_κ is continuous on $H^1_{0,\Gamma}(\Omega)\times H^1_{0,\Gamma}(\Omega)$. Due to lemma 4.7 we can claim that

$$\operatorname{Re} a_\kappa(u,\overline{u}) \geq \|\nabla u\|^2_{L^2(\Omega)} - \kappa^2\|u\|^2_{L^2(\Omega)}$$

We note that thanks to a generalized version of Poincarré's inequality

$$v \to \|\nabla v\|_{L^2(\Omega)}$$

is a norm on $H^1_{0,\Gamma}(\Omega)$ which is equivalent to the natural norm. Now since the injection of $H^1_{0,\Gamma}(\Omega)$ into $L^2(\Omega)$ is compact we can claim that either the equation $a_\kappa(u,v) = F(v)$ is uniquely solvable or the equation $a_\kappa(u,v) = 0$ has non trivial solutions. Given that we proved uniqueness, we conclude that $a_\kappa(u,v) = F(v)$ is uniquely solvable and that u depends continuously on F. □

Lemma 4.12. *Let F be a continuous linear functional on $H^1_{0,\Gamma}(\Omega)$. The following variational problem has a unique solution for any $\kappa > 0$:*
find u in $H^1_{0,\Gamma}(\Omega)$ such that

$$\int_\Omega \nabla u\cdot\nabla v - \int_{\partial D}(T_0 u)\, v = F(v), \tag{4.22}$$

for all v in $H^1_{0,\Gamma}(\Omega)$.

Proof: Next we observe that due to the definition (4.13) of $T_0 < T_0(f), f >$ is real for all f in $H^{\frac{1}{2}}(\partial D)$ and $< T_0(f), f >\leq 0$. We conclude that problem (4.22) is uniquely solvable and that the solution u depends continuously on F. $\square$

Let φ be a smooth compactly supported function in D which is equal to 1 on Γ and such that $\varphi(x_1, -x_2) = \varphi(x_1, x_2)$. For all $\kappa \geq 0$ we set $\tilde{u}_\kappa$ in $H^1_{0,\Gamma}(\Omega)$ to be the solution to

$$\int_\Omega \nabla \tilde{u}_\kappa \cdot \nabla v - \kappa^2 \tilde{u}_\kappa v - \int_{\partial D} (T_\kappa \tilde{u}_\kappa)\, v = \int_\Omega (\Delta\varphi + \kappa^2 \varphi) v, \quad \forall v \in H^1_{0,\Gamma}(\Omega) \tag{4.23}$$

and we set $u_\kappa = \tilde{u}_\kappa + \varphi$.

Lemma 4.13. *For $\kappa > 0$, u_κ satisfies the following properties:*
(i). u_κ is in $H^1(\Omega)$.
(ii). The upper and lower trace on Γ of u_κ are both equal to the constant 1.
(iii). u_κ can be extended to a function in $\mathbb{R}^2 \setminus \Gamma$ such that, if we still denote by u_κ the extension,

$(\Delta + \kappa^2) u_\kappa = 0$ *in* $\mathbb{R}^2 \setminus \Gamma$,

$\dfrac{\partial u_\kappa}{\partial r} - i\kappa u_\kappa = o(r^{-1})$, *uniformly as* $r \to \infty$

$u_\kappa(x_1, -x_2) = u_\kappa(x_1, x_2)$ *for all* (x_1, x_2) *in* $\mathbb{R}^2 \setminus \Gamma$

$\dfrac{\partial u_\kappa}{\partial x_2}(x_1, 0) = 0$ *if* $(0, x_1) \notin \Gamma$.

(iv). Denoting $\dfrac{\partial u_\kappa}{\partial x_2^-}$ *the lower trace of* $\dfrac{\partial u_\kappa}{\partial x_2}$ *on* Γ,

$$Im \int_\Gamma \frac{\partial u_\kappa}{\partial x_2^-} > 0 \tag{4.24}$$

Proof: Properties (i) and (ii) are clear. The first two items of property (iii) hold simply because we can write $u_{|\partial D} = \sum_{n=-\infty}^{\infty} a_n e^{in\theta}$ and then set $u = \sum_{n=-\infty}^{\infty} a_n e^{in\theta} \dfrac{H_n(\kappa r)}{H_n(\kappa)}$ in $\mathbb{R}^2 \setminus \overline{\Omega}$. We then use Lemma 4.6 in combination to the fact that variational problem (4.23) implies that $T_\kappa u_\kappa$ is the limit of $\dfrac{\partial u_\kappa}{\partial r}$ as $r \to 1^-$.

To show the third item in (iii) we set $\widehat{\tilde{u}_\kappa}(x_1, x_2) = \tilde{u_\kappa}(x_1, -x_2)$ and for any arbitrary v in $H^1_{0,\Gamma}(\Omega)$, $\widehat{v}(x_1, x_2) = v(x_1, -x_2)$. Next we observe that

$$\int_\Omega \nabla \widehat{\tilde{u_\kappa}} \cdot \nabla v - \kappa^2 \widehat{\tilde{u_\kappa}} v = \int_\Omega \nabla \tilde{u}_\kappa \cdot \nabla \widehat{v} - \kappa^2 \tilde{u}_\kappa \widehat{v}$$

In polar coordinates we have the relations $\widehat{\tilde{u_\kappa}}(r, \theta) = \tilde{u_\kappa}(r, -\theta)$ and $\widehat{v}(r, \theta) = v(r, -\theta)$, so

$$\int_{\partial D} (T_\kappa \widehat{\tilde{u_\kappa}})\, v = \int_{\partial D} (T_\kappa \tilde{u_\kappa})\, \widehat{v}$$

Finally, since φ is even in x_2,

$$\int_\Omega (\Delta\varphi + \kappa^2 \varphi) \widehat{v} = \int_\Omega (\Delta\varphi + \kappa^2 \varphi) v$$

Since the solution to problem (4.23) is unique we must have $\widehat{\tilde{u_\kappa}} = \tilde{u_\kappa}$, proving the third item in (iii).

Since u_κ is even in x_2, it follows that $\dfrac{\partial u_\kappa}{\partial x_2}$ is zero on the line $x_2 = 0$ minus the segment Γ, proving the last item in (iii).

Since $u = 1$ on Γ,

$$\mathrm{Im}\int_\Gamma \frac{\partial u_\kappa}{\partial x_2^-} = \mathrm{Im}\int_\Gamma \frac{\partial u_\kappa}{\partial x_2^-}\overline{u} = -\mathrm{Im}\int_{\partial D^-} \frac{\partial u_\kappa}{\partial r}\overline{u}$$

where ∂D^- is the intersection of the circle ∂D and the lower half plane $x_2 < 0$. We use parity one more time to argue that that

$$\mathrm{Im}\int_{\partial D^-} \frac{\partial u_\kappa}{\partial r}\overline{u} = \frac{1}{2}\mathrm{Im}\int_{\partial D} \frac{\partial u_\kappa}{\partial r}\overline{u}$$

Knowing that u_κ is not zero everywhere and using Reillich's lemma we can claim that $\mathrm{Im}\displaystyle\int_{\partial D} \frac{\partial u_\kappa}{\partial r}\overline{u} < 0$. $\square$

Theorem 4.14. *Let $\tilde{u}_\kappa$ be the solution to (4.23) for all $\kappa \geq 0$, and set $u_\kappa = \tilde{u}_\kappa + \varphi$.*
(i). u_κ is analytic in κ for $\kappa > 0$.
(ii). u_κ converges strongly to u_0 in $H^1_{0,\Gamma}(\Omega)$. More precisely there is a constant C such that

$$\|u_\kappa - u_0\|_{H^1(\Omega)} \leq C(\kappa^2 + \|T_\kappa - T_0\|) \tag{4.25}$$

Proof: To show (i) we define an operator A_κ from $H^1_{0,\Gamma}(\Omega)$ to its dual defined by

$$< (A_\kappa u), v >= a_\kappa(u, v)$$

where a_κ was defined in (4.21). Thanks to lemma 4.8 we can claim that A_κ is analytic in κ for $\kappa > 0$. But we showed A_κ is invertible for $\kappa > 0$ and that its inverse is a continuous linear functional. According to [20], chapter 7, A_κ^{-1} is then also analytic in κ for $\kappa > 0$, and so is $A_\kappa^{-1}F$ for any fixed F in the dual of $H^1_{0,\Gamma}(\Omega)$. Note that we have obtained analicity of u_κ relative to the $H^1(\Omega)$ norm.

To prove statement (ii) we first show that $\|\tilde{u}_\kappa\|_{H^1(\Omega)}$ is uniformly bounded for all κ in $[0, B]$ where B is a positive constant. Set $v = \tilde{u}_\kappa$ in (4.23) and use lemma 4.7 to obtain

$$\begin{aligned}\|\nabla\tilde{u}_\kappa\|^2_{L^2(\Omega)} \leq \quad & \kappa^2\|\tilde{u}_\kappa\|^2_{L^2(\Omega)} \\ & +C^2\|\varphi\|_{H^2(\Omega)}\|u_\kappa\|_{L^2(\Omega)},\end{aligned}$$

where C is a positive constant. From there Poincarré 's inequality can show the uniform boundedness of $\|\tilde{u}_\kappa\|_{H^1(\Omega)}$ for all κ in $[0, B]$, as long as B is small enough.

Next we note that $u_\kappa - u_0 = \tilde{u}_\kappa - \tilde{u}_0$ and satisfies for all v in $H^1_{0,\Gamma}(\Omega)$

$$\int_\Omega \nabla(u_\kappa - u_0)\cdot\nabla v - \int_\Omega \kappa^2\tilde{u}_\kappa v - \int_{\partial D}(T_\kappa\tilde{u}_\kappa - T_0\tilde{u}_\kappa)\, v = \int_\Omega \kappa^2\varphi v$$

We re write $\int_{\partial D}(T_\kappa \tilde{u}_\kappa - T_0\tilde{u}_\kappa)\, v$ as

$$\int_{\partial D}(T_\kappa(\tilde{u}_\kappa - \tilde{u}_0))\, v - \int_{\partial D}((T_0 - T_\kappa)\tilde{u}_0)\, v$$

we choose $v = \overline{\tilde{u}_\kappa - \tilde{u}_0}$ and we use that, due to lemma 4.7,

$$\mathrm{Re}\int_{\partial D}(T_\kappa(\tilde{u}_\kappa - \tilde{u}_0))\, v \leq 0$$

to infer the inequality

$$\begin{aligned}\|\nabla(u_\kappa - u_0)\|^2_{L^2(\Omega)} \leq \quad & \kappa^2\|\tilde{u}_\kappa\|_{L^2(\Omega)}\|u_\kappa - u_0\|_{L^2(\Omega)} \\ & + \|T_\kappa - T_0\|\|\tilde{u}_0\|_{H^{\frac{1}{2}}(\partial D)}\|u_\kappa - u_0\|_{H^{\frac{1}{2}}(\partial D)} + \kappa^2\|\varphi\|_{L^2(\Omega)}\|u_\kappa - u_0\|_{L^2(\Omega)}\end{aligned}$$

the result follows since we know that $\|\tilde{u}_\kappa\|_{L^2(\Omega)}$ is bounded for κ in $[0,1]$ and by application of the trace theorem and of Poincarré 's inequality. $\square$.

Lemma 4.15. *Denote* $\dfrac{\partial u_\kappa}{\partial x_2^\pm}$ *the upper and lower traces of* $\dfrac{\partial u_\kappa}{\partial x_2}$ *on* Γ. *Then*
(i).

$$\frac{\partial u_\kappa}{\partial x_2^+} = -\frac{\partial u_\kappa}{\partial x_2^-} \tag{4.26}$$

(ii). Denote $G_\kappa(x,y) = \frac{i}{4}H_0(\kappa|x-y|)$. *For all* x *in* Ω

$$u_\kappa(x) = 2\int_\Gamma G_\kappa(x,y)\frac{\partial u_\kappa}{\partial x_2^-}(y)dy \tag{4.27}$$

Proof: Denote $\Omega^+ = \{(x_1,x_2) \in \Omega : x_2 > 0\}$ and $\Omega^- = \{(x_1,x_2) \in \Omega : x_2 < 0\}$. It is well known from potential theory that if x is in Ω^+

$$u_\kappa(x) = \int_{\partial\Omega^+} G_\kappa(x,y)\frac{\partial u_\kappa}{\partial n}(y) - \frac{\partial G_\kappa(x,y)}{\partial n(y)}u_\kappa(y)dy \tag{4.28}$$

$$0 = \int_{\partial\Omega^-} G_\kappa(x,y)\frac{\partial u_\kappa}{\partial n}(y) - \frac{\partial G_\kappa(x,y)}{\partial n(y)}u_\kappa(y)dy \tag{4.29}$$

where n is the exterior normal vector in each case. If y is in $\partial\Omega^+$ and is such that $y_2 = 0$ it is clear that $\dfrac{\partial G_\kappa(x,y)}{\partial n(y)} = 0$. We also use that u_κ is even in x_2 so that $\dfrac{\partial u}{\partial x_2}(x) = 0$ if $x_2 = 0$ and $x \notin \Gamma$. Combining (4.28) and (4.29) we find that for x in Ω^+

$$u_\kappa(x) = \int_{\partial\Omega} G_\kappa(x,y)\frac{\partial u_\kappa}{\partial n}(y) - \frac{\partial G_\kappa(x,y)}{\partial n(y)}u_\kappa(y)dy \quad - \int_\Gamma G_\kappa(x,y)(\frac{\partial u_\kappa}{\partial x_2^+} - \frac{\partial u_\kappa}{\partial x_2^-})(y)dy$$

But due to point (iii) in lemma 4.13

$$\int_{\partial\Omega} G_\kappa(x,y)\frac{\partial u_\kappa}{\partial n}(y) - \frac{\partial G_\kappa(x,y)}{\partial n(y)}u_\kappa(y)dy \quad = 0,$$

for all x in Ω^+, thus

$$u_\kappa(x) = -\int_\Gamma G_\kappa(x,y)(\frac{\partial u_\kappa}{\partial x_2^+} - \frac{\partial u_\kappa}{\partial x_2^-})(y)dy, \tag{4.30}$$

for all x in Ω^+. The same formula can be derived for all x in Ω^-. By continuity of u_κ and of single layer potentials the formula must also hold if $x_2 = 0$. Next if x is a fixed point in $(-\frac{1}{2}, \frac{1}{2}) \times \{0\}$ taking a ∂_2 deivative in (4.30) and approaching x_2 from Ω^- we obtain using the jump formula for double layer potentials

$$\frac{\partial u_\kappa}{\partial x_2^-}(x) = -\frac{1}{2}(\frac{\partial u_\kappa}{\partial x_2^+} - \frac{\partial u_\kappa}{\partial x_2^-})(x) - \int_\Gamma \frac{\partial G_\kappa(x,y)}{\partial x_2}(\frac{\partial u_\kappa}{\partial x_2^+} - \frac{\partial u_\kappa}{\partial x_2^-})(y)dy$$

We observe that for x and y on Γ, $\dfrac{\partial G_\kappa(x,y)}{\partial x_2} = 0$. It follows that $\dfrac{\partial u_\kappa}{\partial x_2^-}(x) = -\dfrac{\partial u_\kappa}{\partial x_2^+}(x)$ for x on Γ. $\square$

Lemma 4.16. *u_0 is equal to the constant function 1.*

Proof: It can be shown, as in the case where $\kappa > 0$, that u_0 is in $H^1(\Omega)$, the upper and lower trace on Γ of u_0 are both equal to the constant 1, and u_0 can be extended to a function in $\mathbb{R}^2 \setminus \Gamma$ such that, if we still denote by u_0 the extension, $\Delta u_0 = 0$ in $\mathbb{R}^2 \setminus \Gamma$. The condition at infinity for u_0 is different. From (4.17) we infer that $u_0 = a_0 + O(r^{-1})$ and $\partial_r u_0 = O(r^{-2})$. We also note that (4.17) implies that

$$\int_{\partial D} \partial_r u_0 = 0 \tag{4.31}$$

Since $\Delta u_0 = 0$ in Ω, $u = 1$ on Γ, and (4.31) holds, we have

$$\int_\Gamma \frac{\partial u_0}{\partial x_2^+} - \frac{\partial u_0}{\partial x_2^-} = 0 \tag{4.32}$$

but the latter is also equal to

$$\int_\Gamma (\frac{\partial u_0}{\partial x_2^+} - \frac{\partial u_0}{\partial x_2^-})\overline{u_0} = 0 \tag{4.33}$$

so applying Green's formula in combination to the estimates $u_0 = a_0 + O(r^{-1})$ and $\partial_r u_0 = O(r^{-2})$ we find that $\displaystyle\int_{\mathbb{R}^2} |\nabla u_0|^2 = 0$. We infer u_0 is a constant in $\mathbb{R}^2$. That constant can only be 1.$\square$

Lemma 4.17. *The integral Re $\displaystyle\int_\Gamma \frac{\partial u_\kappa}{\partial x_2^-}$ is strictly positive for all $\kappa > 0$ small enough. More precisely we have the estimate as κ approaches 0^+*

$$\int_\Gamma \frac{\partial u_\kappa}{\partial x_2^-} \sim \pi\kappa \frac{H_1(\kappa)}{H_0(\kappa)} \tag{4.34}$$

Consequently, Re $\displaystyle\int_\Gamma \frac{\partial u_\kappa}{\partial x_2^-}$ must be strictly positive for small values of $\kappa > 0$.

Proof: Set $v = 1 - \varphi$ in variational problem (4.23) (note that the trace of v is zero on Γ, as required in the space $H^1_{0,\Gamma}(\Omega)$), to obtain

$$-\int_\Omega \nabla\tilde{u}_\kappa \cdot \nabla\varphi - \int_\Omega \kappa^2 \tilde{u}_\kappa(1-\varphi) - \int_{\partial D} (T_\kappa \tilde{u}_\kappa)\,(1-\varphi) = \int_\Omega (\Delta\varphi + \kappa^2\varphi)(1-\varphi), \quad (4.35)$$

We first observe that $\displaystyle\int_\Omega \kappa^2\varphi(1-\varphi) = O(\kappa^2)$ and due to theorem 4.14, $\displaystyle\int_\Omega \kappa^2\tilde{u}_\kappa(1-\varphi) = O(\kappa^2)$. As φ is zero on ∂D, we have found that

$$-\int_\Omega \nabla\tilde{u}_\kappa \cdot \nabla\varphi + \int_\Omega \Delta\varphi\,\varphi = \int_{\partial D} T_\kappa\tilde{u}_\kappa + O(\kappa^2) \quad (4.36)$$

Next, using Green's theorem,

$$2\int_\Gamma \frac{\partial\tilde{u}_\kappa}{\partial x_2^-} = 2\int_\Gamma \frac{\partial u_\kappa}{\partial x_2^-}\varphi = \int_\Omega \nabla\tilde{u}_\kappa \cdot \nabla\varphi + \int_\Omega \Delta\tilde{u}_\kappa\,\varphi \quad (4.37)$$

Since in Ω, $\Delta\tilde{u}_\kappa = -\Delta\varphi - \kappa^2\tilde{u}_\kappa - \kappa^2\varphi$ combining (4.36) and (4.37) yields

$$2\int_\Gamma \frac{\partial\tilde{u}_\kappa}{\partial x_2^-} = -\int_{\partial D} T_\kappa\tilde{u}_\kappa + O(\kappa^2) \quad (4.38)$$

But $\displaystyle\int_{\partial D} T_\kappa\tilde{u}_\kappa = -\kappa\frac{H_1(\kappa)}{H_0(\kappa)}2\pi a_0(\kappa)$ where $\displaystyle a_0(\kappa) = \frac{1}{2\pi}\int_{\partial D}\tilde{u}_\kappa$, so using again that $\tilde{u}_\kappa$ is strongly convergent to $1-\varphi$ in $H^1(\Omega)$, we claim that

$$\int_{\partial D} T_\kappa\tilde{u}_\kappa \sim -2\pi\kappa\frac{H_1(\kappa)}{H_0(\kappa)} \quad (4.39)$$

as $\kappa \to 0$. Going back to the definition of Bessel functions it easy to see that $\displaystyle\kappa\frac{H_1(\kappa)}{H_0(\kappa)} \sim -(\ln\kappa)^{-1}$ we conclude that $\displaystyle\int_\Gamma \frac{\partial\tilde{u}_\kappa}{\partial x_2^-} \sim -\pi(\ln\kappa)^{-1}$, so Re $\displaystyle\int_\Gamma \frac{\partial u_\kappa}{\partial x_2^-}$ must be strictly positive for all $\kappa > 0$ small enough. □

For illustration, in figure 4.1 we have plotted graphs of $\log_{10}\displaystyle\int_\Gamma \frac{\partial u_\kappa}{\partial x_2^-}$ and $\log_{10}\left(\pi\kappa\frac{H_1(\kappa)}{H_0(\kappa)}\right)$ against the decimal $\log_{10}\kappa$, the imaginary part is on the left, and the real part is on the right.

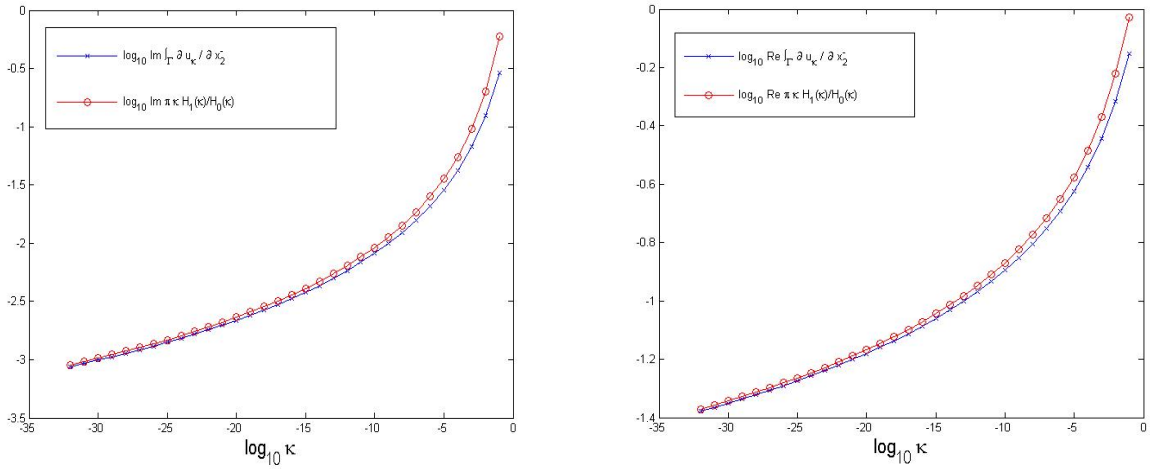

Fig. 4.1: $\log_{10}\int_\Gamma \dfrac{\partial u_\kappa}{\partial x_2^-}$ *(blue) vs* $\log_{10}\left(\pi\kappa\dfrac{H_1(\kappa)}{H_0(\kappa)}\right)$ *(red). Left - the imaginary part, right - the real part.*

4.3 Informal derivation of certain asymptotics for high wavenumbers

We provide in this section an informal derivation of an equivalent for $\displaystyle\int_\Gamma \frac{\partial u_\kappa}{\partial x_2^-}$ as $\kappa\to\infty$, where $u_\kappa=\tilde{u}_\kappa+\varphi$ and $\tilde{u}_\kappa$ solves variational problem (4.23). Denote by $f_\kappa(y_1)$ the value of $\dfrac{\partial u_\kappa}{\partial x_2^-}((y_1,0))$ for y_1 in $[-\frac{1}{2},\frac{1}{2}]$. According to (4.27), f_κ satisfies the integral equation

$$\int_{-\frac{1}{2}}^{\frac{1}{2}} \frac{i}{4}H_0(\kappa|x_1-y_1|)f_\kappa(y_1)dy_1=\frac{1}{2},\quad x_1\in[-\frac{1}{2},\frac{1}{2}] \tag{4.40}$$

Note that as a byproduct of the previous section we know that this integral equation is uniquely solvable as long as the solution is sought in an adequate space. We now integrate equation (4.40) and rescale it to obtain

$$\int_{-\frac{1}{2}}^{\frac{1}{2}}\left(\int_{-\frac{1}{2}}^{\frac{1}{2}}\frac{\kappa}{2}H_0(\kappa|x_1-y_1|)dx_1\right)f_\kappa(y_1)dy_1=-i\kappa$$

Setting $v=\kappa(x_1-y_1)$ we obtain

$$\int_{-\frac{1}{2}}^{\frac{1}{2}}\frac{\kappa}{2}H_0(\kappa|x_1-y_1|)dx_1=\frac{1}{2}\int_{\kappa(-\frac{1}{2}-y_1)}^{\kappa(\frac{1}{2}+y_1)}H_0(|v|)dv$$

For any y_1 in $(-\frac{1}{2}, \frac{1}{2})$ this integral tends to $\frac{1}{2}\int_{-\infty}^{\infty} H_0(|v|)dv$ as $\kappa \to \infty$. According to lemma 4.5, $\frac{1}{2}\int_{-\infty}^{\infty} H_0(|v|)dv = 1$. Define

$$g_\kappa(y_1) = \frac{1}{2}\int_{\kappa(-\frac{1}{2}-y_1)}^{\kappa(\frac{1}{2}+y_1)} H_0(|v|)dv$$

We have $\lim_{\kappa\to\infty}(g_\kappa(y_1) - 1) = 0$, for any y_1 in $(-\frac{1}{2}, \frac{1}{2})$. In some future work we will show that

$$\lim_{\kappa\to\infty}\int_{-\frac{1}{2}}^{\frac{1}{2}}(g_\kappa(y_1) - 1)\frac{f_\kappa}{\kappa}(y_1)dy_1 = 0 \tag{4.41}$$

Note that we will only need to show that $\frac{f_\kappa}{\kappa}$ remains bounded by a fixed function $L^1([-\frac{1}{2}, \frac{1}{2}])$ as $\kappa \to \infty$. Admitting that (4.41) is true and recalling that $\int_{-\frac{1}{2}}^{\frac{1}{2}} g_\kappa(y_1)\frac{f_\kappa}{\kappa}(y_1)dy_1 = -i$, we conclude that

$$\int_{-\frac{1}{2}}^{\frac{1}{2}} f_\kappa(y_1)dy_1 \sim -i\kappa, \tag{4.42}$$

and in particular

$$\mathrm{Re}\int_{-\frac{1}{2}}^{\frac{1}{2}} f_\kappa(y_1)dy_1 = o(\kappa), \tag{4.43}$$

as κ tends to infinity.

For illustration, figure 4.2 shows two graphs of $\frac{1}{\kappa}\int_{-\frac{1}{2}}^{\frac{1}{2}} f_\kappa(y_1)dy_1$ against the wavenumber κ, the imaginary part is on the left, and the real part is on the right.

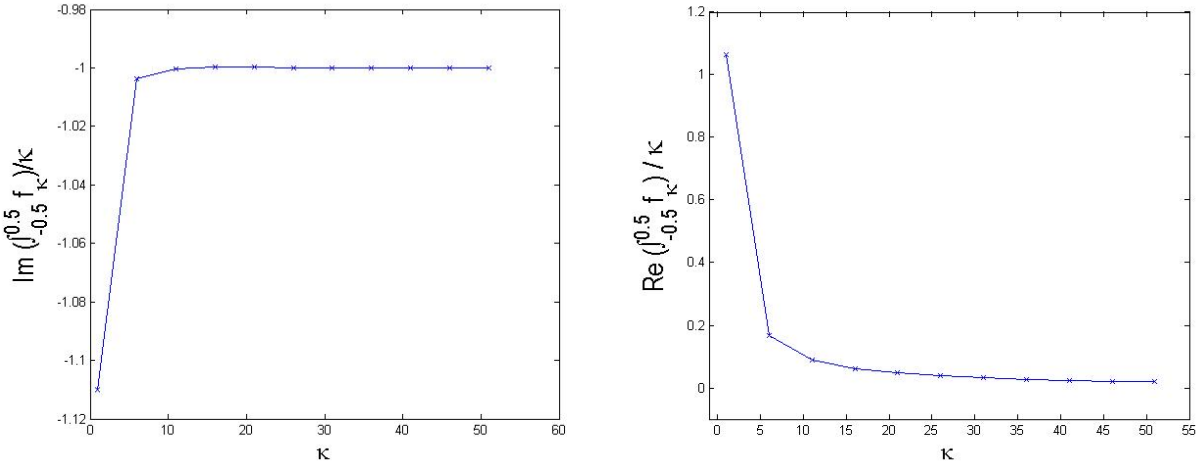

Fig. 4.2: *Left:* $\frac{1}{\kappa} Im \int_{-\frac{1}{2}}^{\frac{1}{2}} f_\kappa(y_1)dy_1 \to -1$ *as* $\kappa \to \infty$. *Right:* $\frac{1}{\kappa} Re \int_{-\frac{1}{2}}^{\frac{1}{2}} f_\kappa(y_1)dy_1 \to 0$ *as* $\kappa \to \infty$.

4.4 Application to the non linear equation (1.15)

We can express the two functions p and q which were defined in (1.12) as

$$p(t) = C_1 t - C_2$$
$$q(t) = C_3 t(-C_4 t + C_5)$$

where all the constants $C_1, ..., C_5$ are strictly positive. In terms of parameters (1.11),

$$C_1 = \frac{2rc_b^2}{f_b},\ C_2 = \frac{c_b^2}{\gamma_b},\ C_3 = (1 + \frac{1}{\gamma_b})b^2 f_b^2,\ C_4 = c_b^2,\ C_5 = b^2 f_b^2.$$

Our problem consists of solving the equation $F(\kappa) = 0$ for $\kappa > 0$ where

$$F(\kappa) = q(\kappa^2) - p(\kappa^2)\mathrm{Re} \int_\Gamma \frac{\partial u_\kappa}{\partial x_2^-} \tag{4.44}$$

and u_κ is defined by $u_\kappa = \tilde{u}_\kappa + \varphi$ where $\tilde{u}_\kappa$ solves (4.23). We know from the previous section that F is analytic in $(0, \infty)$. According to the real part of the estimate (4.34) we have that

$$F(\kappa) \sim -C_2\pi(\ln \kappa)^{-1}, \quad \kappa \to 0^+ \tag{4.45}$$

Recalling estimate (4.43) we claim that

$$F(\kappa) \sim -C_3 C_4 \kappa^4, \quad \kappa \to \infty \tag{4.46}$$

It follows from estimate (4.45) that there is a positive α such that $F(\kappa) > 0$ if κ is in $(0, \alpha)$, and from estimate (4.46) we infer that $\lim_{\kappa\to\infty} F(\kappa) = -\infty$. Since F is continuous in $(0, \infty)$,

we conclude that F must achieve the value zero on that interval. We can also claim that the zeros of F are isolated since F is an analytic function. Due to (4.46) these zeros occur only in some interval $[A, B]$ where A and B are two positive constants. In particular the equation $F(\kappa) = 0$ has at most a finite number of solutions.
For illustration, figure 4.3 shows $\log_{10} F(\kappa)$ and $\log_{10}(-C_2\pi(\ln\kappa)^{-1})$ against $\log_{10}\kappa$ on the left, and $\log_{10}\left|F(\kappa)\right|$ and $\log_{10}(C_3C_4\kappa^4)$ against κ on the right. These graphs were produced using the specific values (3.24), and constants are calculated as $C_1 = 0.4, C_2 = 2/3, C_3 = 5/12, C_4 = 1, C_5 = 0.25$.

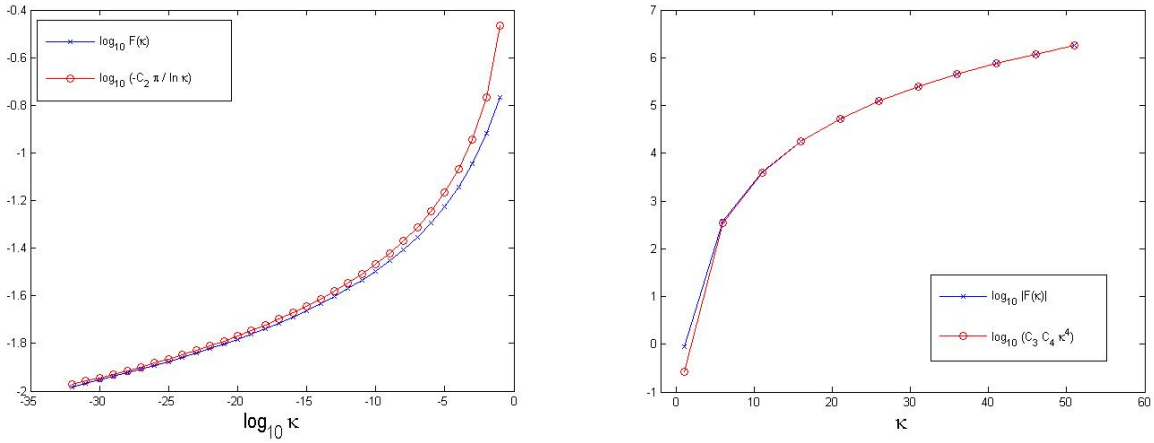

Fig. 4.3: *Left:* $\log_{10} F(\kappa)$ *(blue) vs* $\log_{10}(-C_2\pi(\ln\kappa)^{-1})$ *(red). Right:* $\log_{10}\left|F(\kappa)\right|$ *(blue) vs* $\log_{10}(C_3C_4\kappa^4)$ *(red).*

List of Figures

List of Tables

Appendices

Appendix A

On the C^α regularity of double-layer potentials

A.1 Introduction

In this chapter we first study C^α regularity for double layer potentials defined on boundaries of domains of class C^2 in $\mathbb{R}^2$. Similar regularity results appear in a plethora of texts on potential theory. Folland's textbook [13] covers the case of continuity only. Many textbooks cover exclusively the case of continuity on the boundary only, or as one approaches the boundary in a ***normal*** direction. The closest approach to our work is that found in [9] where the three dimensional analog to our regularity result is proved. We think that our proof has several advantages. In our approach we first focus on the fundamental solution for the Laplace equation and then we extend our results to the Helmholtz equation. The advantage of that approach is that the fundamental solution for the Laplace equation has a very simple expression, and then extending results to the Helmholtz case is rather straightforward. We clearly separate the two well known cases where points are on the boundary only, or the boundary is approached exclusively in a normal direction, so the reader acquainted with those two cases may focus on the remaining cases.

A.2 Double layer potentials for the Laplace operator

Throughout this chapter, let us assume that $D \subset \mathbb{R}^2$ is a bounded domain, ∂D is of class C^2. We will denote ν the exterior normal vector to ∂D throughout this thesis.
We start by defining the function

$$G_{Lap}(x,y) = \frac{1}{2\pi} \ln \frac{1}{|x-y|}, \tag{A.1}$$

where $x, y \in \mathbb{R}^2$, which is a fundamental solution of Laplace's equation in two dimensions. If y is in ∂D we denote by

$$K(x,y) = \frac{\partial G_{Lap}}{\partial \nu(y)}(x,y) = \frac{1}{2\pi} \frac{(x-y)\cdot \nu(y)}{|x-y|^2} \tag{A.2}$$

the integration kernel for the double layer potential associated to G_{Lap}.

We will be using the following Lemma 6.15 from [21], and here we state it without proof.

Lemma A.1. *Let ∂D be of class C^2. Then there exists a positive constant L such that*

$$\left|\big(x-y\big)\cdot \nu(y)\right| \leq L|x-y|^2 \tag{A.3}$$

and

$$|\nu(x) - \nu(y)| \leq L|x-y|^2 \tag{A.4}$$

where $x, y \in \partial D$.

Lemma A.2. *$K(x,y)$ is bounded for x and y on ∂D. Moreover, if x, y and z are on ∂D*

$$|K(x,y) - K(z,y)| \leq C\,|x-z|\, max\left\{\frac{1}{|x-y|},\ \frac{1}{|z-y|},\right\} \tag{A.5}$$

where the positive constant C depends only on ∂D.

Proof:
The boundedness of the function K follows straight from (A.3):

$$|K(x,y)| = \left|\frac{1}{2\pi}\frac{(x-y)\cdot\nu(y)}{|x-y|^2}\right| = \frac{1}{2\pi}\frac{1}{|x-y|^2}\,|(x-y)\cdot\nu(y)| \leq \frac{L\,|x-y|^2}{2\pi\,|x-y|^2} = C.$$

To prove the second part of the statement, we introduce a function

$$f(v) = \frac{(v-y)\cdot\nu(y)}{|v-y|},\ v \in \mathbb{R}^2\backslash\{y\}.$$

Its gradient equals to

$$\nabla f(v) = \frac{|v-y|^2\nu(y) - \{(v-y)\cdot\nu(y)\}\,(v-y)}{|v-y|^3}.$$

In terms of f we write

$$\begin{aligned}\big|K(x,y)-K(z,y)\big| &= \left|\frac{(x-y)\cdot\nu(y)}{2\pi|x-y|^2}-\frac{(z-y)\cdot\nu(y)}{2\pi|z-y|^2}\right| \le \frac{1}{2\pi\,|x-y|}\,|f(x)-f(z)| \\ &+\frac{1}{2\pi\,|z-y|}\,|f(x)-f(z)|+\frac{1}{2\pi}\left|\frac{(z-y)\cdot\nu(y)}{|x-y|\cdot|z-y|}-\frac{(x-y)\cdot\nu(y)}{|x-y|\cdot|z-y|}\right| \\ &\le C\,|f(x)-f(z)|\cdot\max\left\{\frac{1}{|x-y|},\frac{1}{|z-y|}\right\}\end{aligned}$$

Notice that we have not yet used the fact that all the points lie on a smooth boundary. Since ∂D is of C^2, we can introduce an arclength parameterization $\big(s_1(\cdot),s_2(\cdot)\big)$, such that functions s_1 and s_2 are continuously differentiable, and

$$\begin{aligned}\xi(t) &= \big(s_1(t),s_2(t)\big),\\ y(\tau) &= \big(s_1(\tau),s_2(\tau)\big),\end{aligned}$$

where $0\le t,\tau\le A$ for some constant A, $t\neq\tau$, and the unit normal vector to the boundary ∂D is

$$\nu(y)=\nu(\tau)=\big(-s_2'(\tau),s_1'(\tau)\big) \tag{A.6}$$

We compute

$$\begin{aligned}\frac{d}{dt}f\big(\xi(t)\big) &= \frac{\partial f}{\partial\xi_1}\cdot s_1'+\frac{\partial f}{\partial\xi_2}\cdot s_2' \\ &= \frac{\nabla\xi(t)\cdot\nu(\tau)\big|\xi(t)-y(\tau)\big|^2-\big[\big(\xi(t)-y(\tau)\big)\cdot\nu(\tau)\big]\,\big[\big(\xi(t)-y(\tau)\big)\cdot\nabla\xi(t)\big]}{\big|\xi(t)-y(\tau)\big|^3}.\end{aligned}$$

Notice that $\nabla\xi(t)\cdot\nu(\tau)=s_1'(t)s_2'(\tau)-s_2'(t)s_1'(\tau)$, and using Taylor's expansion, it can be shown that

$$\big|\nabla\xi(t)\cdot\nu(\tau)\big|=O\big(|t-\tau|\big).$$

Since ∂D is C^2, then

$$\big|\big(\xi(t)-y(\tau)\big)\cdot\nabla\xi(t)\big|\le\big|\xi(t)-y(\tau)\big|\cdot\sup|\nabla\xi|\,,$$

and

$$|\xi(t)-y(\tau)|=O\big(|t-\tau|\big).$$

Keeping in mind (A.3), we summarize all of these to show

$$\begin{aligned}\big|\frac{d}{dt}f\big(\xi(t)\big)\big| &\le \left|\frac{\nabla\xi(t)\cdot\nu(\tau)}{\big|\xi(t)-y(\tau)\big|}\right|+\left|\frac{\big[\big(\xi(t)-y(\tau)\big)\cdot\nu(\tau)\big]\,\big[\big(\xi(t)-y(\tau)\big)\cdot\nabla\xi(t)\big]}{\big|\xi(t)-y(\tau)\big|^3}\right| \\ &\le |O(1)|+\left|\frac{L\big|\xi(t)-y(\tau)\big|^2\sup\big|\nabla\xi\big|\big|\xi(t)-y(\tau)\big|}{\big|\xi(t)-y(\tau)\big|^3}\right|=C.\end{aligned}$$

We conclude $\big|\frac{d}{dt}f\big(\xi(t)\big)\big|\le C$, which completes the proof. □

Remark A.3. *The choice of an orientation for ∂D does not matter in the previous lemma, but further in this thesis we will choose the vector normal to ∂D to point outward. It is crucial in our numerical examples, and depending on the geometry, we choose between $(-s_2^{'}, s_1^{'})$ and $(s_2^{'}, -s_1^{'})$.*

Lemma A.4. *Let $\varphi \in L^\infty(\partial D)$, $K(x,y)$ and ∂D satisfy the assumptions of Lemma A.2. We define double-layer potential with density φ*

$$\psi(x) = \int_{\partial D} K(x,y)\varphi(y)ds(y).$$

Fix α in $(0,1)$. Then there is a constant C such that for any $x, z \in \partial D$

$$\big|\psi(x) - \psi(z)\big| \le C\big|x - z\big|^\alpha,$$

that is, ψ is of $C^{0,\alpha}(\partial D)$.

Proof:

We denote $\partial D(z;r) = \partial D \cap B\,[z;r]$, where the radius r is sufficiently small and will be specified later.

$$\begin{aligned}\big|\psi(x) - \psi(z)\big| &= \left|\int_{\partial D} K(x,y)\varphi(y)ds(y) - \int_{\partial D} K(z,y)\varphi(y)ds(y)\right. \\ &\le \int_{\partial D(z;r)} \big|K(x,y) - K(z,y)\big| \cdot \big|\varphi(y)\big| ds(y) \\ &+ \int_{\partial D/\partial D(z;r)} \big|K(x,y) - K(z,y)\big| \cdot \big|\varphi(y)\big| ds(y).\end{aligned}$$

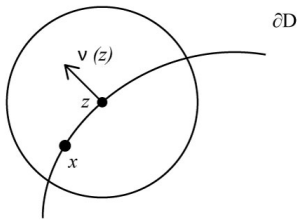

Let $r = 2\,|x - z|$. Then for the first integral we will use the boundedness of K and φ:

$$I_1 := \int_{\partial D(z;r)} |K(x,y) - K(z,y)|\cdot|\varphi(y)|\, ds(y) \le C \int_{\partial D(z;r)} ds(y) \le Cr = C\,|x - z| \le C\,|x - z|^\alpha$$

where $0 < \alpha \le 1$. Now, according to lemma A.2,

$$I_2 := \int_{\partial D/\partial D(z;r)} |K(x,y) - K(z,y)|\cdot|\varphi(y)|\, ds(y) \le C\,|x - z| \int_{\partial D/\partial D(z;r)} \max\left\{\frac{1}{|x-y|},\ \frac{1}{|z-y|}\right\} ds(y)$$

but on $\partial D/\partial D(z;r)$,

$$\max\left\{\frac{1}{|x-y|},\ \frac{1}{|z-y|}\right\} \le \frac{C}{s - \frac{r}{2}},$$

where s is the arclength. So

$$I_2 \le |x - z| \int_r^{C_1} \frac{C}{s - \frac{r}{2}} \le C\,|x - z| \int_r^{C_1} \frac{d\rho}{\rho} =\le C\,|x - z|\,(\ln C_1 - \ln r) \le C\,|x - z|^\alpha,$$

if $r = 2\,|x - z|$. □

Lemma A.5. *Assume z and y are on ∂D and $z \neq y$; let $x = z - h\nu(z)$, where $h > 0$ and $\nu(z)$ is the outward unit normal. Then, provided that h is sufficiently small,*

$$|x-y|^2 \geq \frac{1}{2}\left\{|y-z|^2 + |x-z|^2\right\}. \tag{A.7}$$

Proof:
Keeping in mind that $|x-z|^2 = h^2$, we deduce

$$\begin{aligned} |x-y|^2 &= \left|(x-z)-(y-z)\right|^2 = \left|-h\nu(z)-(y-z)\right|^2 \\ &= h^2 + 2h(y-z)\cdot\nu(z) + |y-z|^2 \\ &\geq h^2 - 2h\left|(z-y)\cdot\nu(z)\right| + |y-z|^2 \end{aligned}$$

Again we use (A.3) to get

$$|x-y|^2 \geq h^2 + (1-2hL)|y-z|^2.$$

Now for a fixed constant L we can choose h sufficiently small, so that $\left(\frac{1}{2} - 2hL\right) \geq 0$, and in this case

$$\begin{aligned} 0 \leq \frac{1}{2}h^2 + \left(\frac{1}{2} - 2hL\right)|y-z|^2 \Leftrightarrow \\ \Leftrightarrow \frac{1}{2}\left(|y-z|^2 + h^2\right) \leq (1-2hL)|y-z|^2 + h^2 \leq |x-y|^2. \end{aligned}$$

□

Proposition A.6. *Let K be given by (A.2). We define the double-layer potential*

$$v(x) = \int_{\partial D} K(x,y)\varphi(y)ds(y), \tag{A.8}$$

for $x \in D$, and extend it as

$$v(z) = \int_{\partial D} K(z,y)\varphi(y)ds(y) - \frac{1}{2}\varphi(z) \tag{A.9}$$

for $z \in \partial D$. If $\varphi \in C^{0,\alpha}(\partial D)$, then $v \in C^{0,\alpha}(\bar{D})$.

Proof:
Proving this proposition will involve separating several cases depending on the position of two points x and z in $\overline{D}$. We first recall that there is a positive constant A such that the exterior normal ν to ∂D can be extended as a C^1 vector field in the compact set

$$E := \{x \in \overline{D} : dist(x, \partial D) \leq A\}$$

. We may choose A small enough such that for each x in E the projection $x_{\partial D}$ of x on ∂D is well defined. In other words for x in E, $|x-y|$ achieves a unique minimum for y on ∂D,

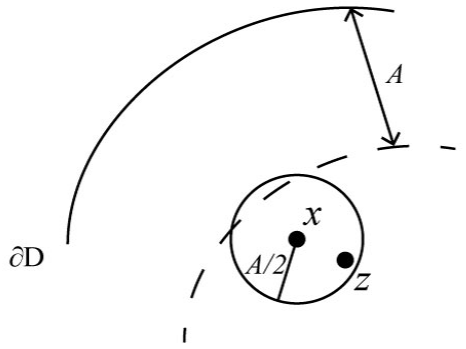

Case 1: $dist(x, \partial D) \geq A,\ |x - z| \leq \frac{A}{2}$.

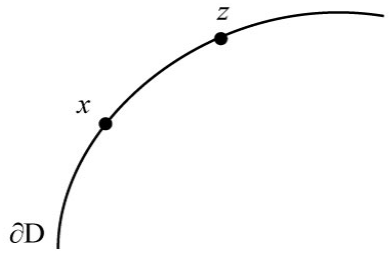

Case 2: $x, z \in \partial D$.

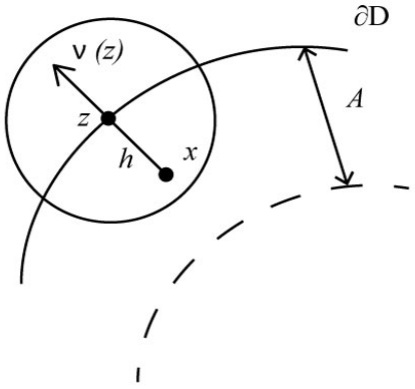

Case 3: $z \in \partial D,\ x = z - h\nu(z)$.

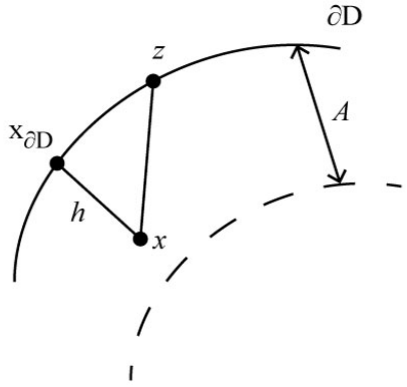

Case 4: $z \in \partial D,\ x \to z$.

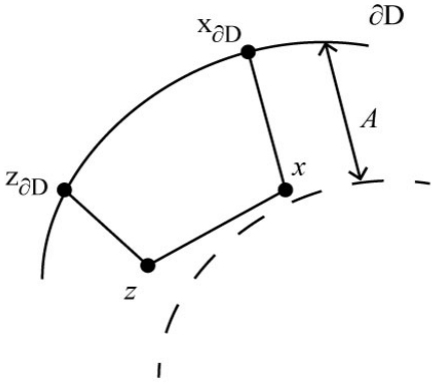

Case 5: $0 < |z - z_{\partial D}| \leq |x - x_{\partial D}| < A$, $|x - z| > \frac{1}{2}|z - z_{\partial D}|$.

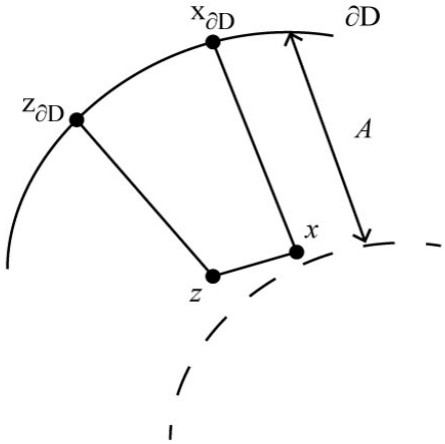

Case 6: $0 < |z - z_{\partial D}| \leq |x - x_{\partial D}| < A$, $|x - z| \leq \frac{1}{2}|z - z_{\partial D}|$

Tab. A.1: *Different cases of Proposition A.6.*

and $x_{\partial D}$ on ∂D is such that $|x - x_{\partial D}| \leq |x - y|$ for all y on ∂D.

1. Assume that x is in D and satisfies $dist(x, \partial D) \geq A$. Let z be in D such that $|x - z| \leq \frac{A}{2}$. Clearly, we must have that $dist(z, \partial D) \geq \frac{A}{2}$. We then use the fact $K(x, y)$ is Lipschitz continuous for (x, y) in

$$\{x \in D : dist(x, \partial D) \geq \frac{A}{2}\} \times \partial D$$

to settle this first case.

2. Assume now that both x and z are on ∂D. The result in this case is a direct consequence of Lemma A.4.

3. Let us now assume that x and z are in E and such that z is on ∂D and $x = z - h\nu(z)$ for h in $(0, A)$.
We note that this case is actually well documented in the literature on potential theory. We only cover it here for the sake of completion. We will use the following two formulas

$$\int_{\partial D} K(z, y) ds(y) = -\frac{1}{2}, \int_{\partial D} K(x, y) ds(y) = -1. \tag{A.10}$$

which are derived by many authors and can be found for example in [21]. According to (A.10)

$$\frac{1}{2}\varphi(z) = -\frac{1}{2}\varphi(z) + \varphi(z) = \int_{\partial D} \varphi(z) K(z, y) ds(y) - \int_{\partial D} \varphi(z) K(x, y) ds(y), \tag{A.11}$$

and using this we deduce:

$$\begin{aligned}
|v(x) - v(z)| &= \left| \int_{\partial D} \varphi(y) K(x, y) ds(y) - \int_{\partial D} \varphi(y) K(z, y) ds(y) + \frac{1}{2}\varphi(z) \right| \\
&= \Big| \int_{\partial D} \varphi(y) K(x, y) ds(y) - \int_{\partial D} \varphi(y) K(z, y) ds(y) \\
&+ \int_{\partial D} \varphi(z) K(z, y) ds(y) - \int_{\partial D} \varphi(z) K(x, y) ds(y) \Big| \\
&= \Big| \int_{\partial D} \{\varphi(y) - \varphi(z)\} \left(K(x, y) - K(z, y)\right) ds(y) \Big| \\
&\leq \int_{\partial D(z,r)} \big|\varphi(y) - \varphi(z)\big| \cdot \big|K(x, y) - K(z, y)\big| ds(y) \\
&+ \int_{\partial D / \partial D(z,r)} \big|\varphi(y) - \varphi(z)\big| \cdot \big|K(x, y) - K(z, y)\big| ds(y) = I_1 + I_2
\end{aligned} \tag{A.12}$$

where $\partial D(z; r) = \partial D \cap B[z; r]$, as in Lemma A.4.
Now we recall Lemma A.5 to claim that $|x - y|^2 \geq \frac{1}{2}\left\{|z - y|^2 + |x - z|^2\right\}$ for $y \in \partial D$ and

h sufficiently small. Using this inequality, we get the bound for the kernel K:

$$|K(x,y)| = \left|\frac{\nu(y)\cdot(z-y)}{2\pi|x-y|^2} + \frac{\nu(y)\cdot(x-z)}{2\pi|x-y|^2}\right| \le \frac{C}{2\pi} + \frac{L|x-z|}{2\pi|x-y|^2}$$
$$\le C_1\left(1 + \frac{|x-z|}{|z-y|^2+|x-z|^2}\right).$$

The first integral in (A.12) can be bounded as follows:

$$\begin{aligned} I_1 &\le C\left\{\int_{\partial D(z,r)} |y-z|^\alpha \cdot \big|K(x,y)\big| ds(y) + \int_{\partial D(z,r)} |y-z|^\alpha \cdot \big|K(z,y)\big| ds(y)\right\} \\ &\le C\left\{\int_0^r \rho^\alpha d\rho + \int_0^r \frac{\rho^\alpha |x-z|}{\rho^2+|x-z|^2} d\rho + \int_0^r \rho^\alpha d\rho\right\} \\ &= C\left\{\frac{1}{\alpha+1}\rho^{\alpha+1}\Big|_0^r + |x-z|^\alpha \int_0^{\frac{r}{|x-z|}} \frac{\bar\rho^\alpha}{\bar\rho^2+1} d\lambda\right\} \\ &\le C\left(r^\alpha + |x-z|^\alpha\right) \le C|x-z|^\alpha \end{aligned} \tag{A.13}$$

if $r = O\big(|x-z|\big)$.

To treat the second integral of (A.12), we introduce function $g(x) = \dfrac{(x-y)\cdot\nu(y)}{|x-y|^2}$. Using the mean-value theorem,

$$|K(x,y) - K(z,y)| = \big|g(x) - g(z)\big| \le \big|\nabla g(\xi)\big||x-z|,$$

for some ξ on the line segment between x and z.
By direct calculations,

$$\left|\frac{\partial}{\partial\xi_1}\big(g(\xi)\big)\right| = \left|\frac{\nu_1(y)|\xi-y|^2 - 2(\xi_1-y_1)(\xi-y)\cdot\nu(y)}{|\xi-y|^4}\right| \le C\frac{1}{|\xi-y|^2}.$$

Similarly, $\left|\dfrac{\partial g}{\partial\xi_2}\right| \le C\dfrac{1}{|\xi-y|^2}$, we have $|\nabla g(x)| \le C\dfrac{1}{|\xi-y|^2}$, and deduce further that $|K(x,y)-K(z,y)| \le C\dfrac{|x-z|}{|\xi-y|^2}$.

We apply lemma A.5 one more time, $|\xi-y|^2 \ge \dfrac{1}{2}\left(|z-y|^2 + |z-\xi|^2\right) \ge \dfrac{1}{2}|z-y|^2$, and

$$|K(x,y) - K(z,y)| \le C\frac{|x-z|}{|z-y|^2}.$$

We are ready to estimate the second integral. Again, if $r = O\big(|x-z|\big)$:

$$\begin{aligned} I_2 &\le C\int_{\partial D/\partial D(z,r)} |y-z|^\alpha \frac{|x-z|}{|y-z|^2} ds(y) \\ &\le C|x-z|\int_r^{C_1} \rho^{\alpha-2} d\rho \le C|x-z|\rho^{\alpha-1}\Big|_\infty^r \\ &= C|x-z|r^{\alpha-1} = C|x-z|^\alpha. \end{aligned} \tag{A.14}$$

Combining (A.13) and (A.14), we get $|v(x) - v(z)| \leq C\,|x - z|^{\alpha}$.

4. Let us now assume that $z \in \partial D$ and $x \in E$. As was pointed out earlier, there exists a unique $x_D \in \partial D$, such that $x = x_{\partial D} - h\nu(x_{\partial D})$, $0 < h < A$. It is obvious that $|x - x_{\partial D}| \leq |x - z|$. We apply lemma A.1 to get

$$|x - z|^2 = |x_{\partial D} - z|^2 - 2h\nu(x_{\partial D}) \cdot (x_{\partial D} - z) + h^2 \geq |x_{\partial D} - z|^2 - 2hL\,|x_{\partial D} - z|^2\,,$$

so that $|x_{\partial D} - z| \leq C|x - z|$ for h small enough. We use the cases **2** and **3** and arrive to:

$$|v(x) - v(z)| \leq \big|v(x) - v(x_{\partial D})\big| + \big|v(x_{\partial D}) - v(z)\big| \leq C|x - x_{\partial D}|^{\alpha} + C|x_{\partial D} - z|^{\alpha} \leq 2C|x - z|^{\alpha}.$$

5. In this case we assume that x and z are in E. Without loss of generality, assume $dist(z, \partial D) \leq dist(x, \partial D)$. Note that without loss of generality, we can also assume that $|x - z|$ is small enough so that $|x_{\partial D} - z_{\partial D}| \leq 2|x - z|$. Now make the assumption specific to this case that $|x - z| > \frac{1}{2}|z - z_{\partial D}|$.
Applying case **2.** and case **3.**

$$\begin{aligned}\big|v(x) - v(z)\big| &\leq \big|v(x) - v(x_{\partial D})\big| + \big|v(x_{\partial D}) - v(z_{\partial D})\big| + \big|v(z) - v(z_{\partial D})\big| \\ &\leq C_1|x - x_{\partial D}|^{\alpha} + C_2|x_{\partial D} - z_{\partial D}|^{\alpha} + C_1|z - z_{\partial D}|^{\alpha} \leq C|x - z|^{\alpha}.\end{aligned}$$

6. We now cover the remaining case where x and z are in E, without loss of generality $0 < dist(z, \partial D) \leq dist(x, \partial D)$, but now $|x - z| \leq \frac{1}{2}|z - z_{\partial D}|$.
We use one more time that

$$\int_{\partial D} K(x_{\partial D}, y)ds(y) = \int_{\partial D} K(z_{\partial D}, y)ds(y) = -\frac{1}{2},$$

to deduce the following:

$$\begin{aligned}v(z) - v(x) &= \frac{1}{2}(\varphi(z_{\partial D}) - \varphi(x_{\partial D})) - \int_{\partial D} (\varphi(y) - \varphi(x_{\partial D}))K(x, y)ds(y) \\ &\quad + \int_{\partial D} (\varphi(y) - \varphi(z_{\partial D}))K(z, y)ds(y) \\ &= \frac{1}{2}(\varphi(z_{\partial D}) - \varphi(x_{\partial D})) - \int_{\partial D} (\varphi(z_{\partial D}) - \varphi(x_{\partial D}))\,K(x, y)ds(y) \\ &\quad + \int_{\partial D} (\varphi(y) - \varphi(z_{\partial D}))\,(K(z, y) - K(x, y))\,ds(y).\end{aligned} \tag{A.15}$$

Since $\varphi \in C^{\alpha}$, K is bounded, and again, we can assume that $|x - z|$ is small enough so that $|x_{\partial D} - z_{\partial D}| \leq 2|x - z|$, we have that

$$\left|\frac{1}{2}(\varphi(z_{\partial D}) - \varphi(x_{\partial D})) - \int_{\partial D} (\varphi(z_{\partial D}) - \varphi(x_{\partial D}))\,K(x, y)ds(y)\right| \leq C|x_{\partial D} - z_{\partial D}|^{\alpha} = C|x - z|^{\alpha}.$$

As was shown in case 3,

$$|K(z,y)-K(x,y)| \le C\frac{|z-x|}{|y-\xi|^2},$$

where ξ is on the line segment between x and z. Due to the positions of x and z relative to ∂D it is clear that in this case (A.16) implies that

$$|K(x,y)-K(z,y)| \le C\frac{|x-z|}{|y-z|^2}$$

By Lemma A.5, provided A is small enough, $|z-y|^2 \ge \frac{1}{2}\left\{|z-z_{\partial D}|^2+|y-z_{\partial D}|^2\right\}$, and we have:

$$\begin{aligned}
&\Big|\int_{\partial D}\big(\varphi(y)-\varphi(z_{\partial D})\big)\big(K(z,y)-K(x,y)\big)ds(y)\Big| \\
&\qquad \le C\int_{\partial D}|y-z_{\partial D}|^{\alpha}\frac{|x-z|}{|z-z_{\partial D}|^2+|y-z_{\partial D}|^2}ds(y) \\
&\qquad = C|x-z|\int_0^{C_2}\frac{s^{\alpha}}{s^2+|z-z_{\partial D}|^2}ds = |x-z|\int_0^{\frac{C_2}{|z-z_{\partial D}|}}\frac{\bar{s}^{\alpha}|z-z_{\partial D}|^{\alpha-1}}{\bar{s}^2+1}d\bar{s} \\
&\qquad \le C\frac{|x-z|}{|z-z_{\partial D}|^{1-\alpha}}\int_0^{\infty}\frac{\bar{s}^{\alpha}}{\bar{s}^2+1}d\bar{s} = C|x-z|^{\alpha}\left(\frac{|x-z|}{|z-z_{\partial D}|}\right)^{1-\alpha} \le C|x-z|^{\alpha},
\end{aligned}$$

where we made a substitution

$$\bar{s} = \frac{s}{|x-x_{\partial D}|}, \tag{A.16}$$

and the last integral converges because $2-\alpha > 1$. Combining the results above, we conclude that $|v(x)-v(z)| \le C|x-z|^{\alpha}$. □

A.3 Double layer potentials for the Helmholtz operator

We start by defining the function

$$G_{sp}(x,y) = \frac{i}{4}H_0(k|x-y|), \tag{A.17}$$

where $k>0$ and H_0 is the Hankel function of the first kind of order zero. H_0 is a combination of entire functions and logarithms, see [1]. More precisely, set

$$J_0(z) = \sum_{k=0}^{\infty}(-\frac{1}{4})^k\frac{z^{2k}}{(k!)^2}$$

and

$$Y_0(z) = \frac{2}{\pi}\ln(\frac{1}{2}z)J_0(z) - \frac{2}{\pi}\sum_{k=0}^{\infty}\psi(k+1)(-\frac{1}{4})^k\frac{z^{2k}}{(k!)^2},$$

where the function ψ is defined by

$$\psi(1) = -\gamma,\ \psi(n) = -\gamma + \sum_{k=1}^{n-1}\frac{1}{k},$$

and γ is the Euler constant. It is well known that G_{sp} is a fundamental solution of the Helmholtz equation in two dimensions. If y is in ∂D we denote by

$$K_{sp}(x,y) = \frac{\partial G_{sp}}{\partial \nu(y)}(x,y)$$

the integration kernel for the double layer potential associated to G_{sp}. Set $K_{diff} = K_{sp} - K$. A simple calculation shows that

$$K_{diff}(x,y) = \ln|x-y|F_1(x,y) + F_2(x,y)$$

where F_1 and F_2 are two entire functions and $F_1(x,x) = 0$ for all x in $\mathbb{R}^2$. It is then easy to see that K_{diff} is Lipschitz continuous on $\overline{D} \times \overline{D}$.

Proposition A.7. *Define the double-layer potential*

$$v(x) = \int_{\partial D} K_{sp}(x,y)\varphi(y)ds(y), \tag{A.18}$$

for $x \in D$, and extend it as

$$v(z) = \int_{\partial D} K_{sp}(z,y)\varphi(y)ds(y) - \frac{1}{2}\varphi(z) \tag{A.19}$$

for $z \in \partial D$. If $\varphi \in C^{0,\alpha}(\partial D)$, then $v \in C^{0,\alpha}(\bar{D})$.

Proof:
Recalling Proposition A.6 and using that $K_{sp} - K$ is Lipschitz continuous on $\overline{D} \times \overline{D}$, this claim is clear. □

The following proposition is the final goal of chapter I. We will use it later in chapter III. The proof uses proposition A.7 and is similar to the proof of the theorem 6.18 from [21]. We omit it here.

Proposition A.8. *For the single-layer potential $u(x) = \int_{\partial D} G_{sp}(x,y)\varphi(y)ds(y),\ x \in \partial D$ with density $\varphi \in C^{0,\alpha}(\partial D)$ we have*

$$\frac{\partial u}{\partial \nu}(z) = \int_{\partial D}\varphi(y)\frac{\partial G_{sp}(z,y)}{\partial \nu(z)}ds(y) - \frac{1}{2}\varphi(z),\ z \in \partial D, \tag{A.20}$$

where

$$\frac{\partial u}{\partial \nu}(z) = \lim_{h \to +0} \nu(z) \cdot \nabla u(z + h\nu(z)).$$

Such extended normal derivative $\dfrac{\partial u}{\partial \nu}$ *is in* $C^{0,\alpha}(\overline{D})$.

Appendix B

Matlab code

B.1 Different building city - free-space case.

- Solving equation (1.15). Here *theta* in the code stands for α in the thesis, and θ_{numi} is assumed to be 1.

```
%%-------------------------------------------------------------
function [ksi, theta] = min_diff(Ni,numi,Mi)
% Ni - quantity of buildings; Mi - grid size

global N_cluster
global M_grid
global num

N_cluster = Ni;
M_grid = Mi;
num = numi;
[a,b,space,l_char] = Init_city;

N_build = N_cluster*length(a);

in_guess = ones(1,N_build);
in_guess(num) = 1;
options=optimset('Display','iter','TolFun',1e-6,'TolX',1e-6);
[x, fval,exitflag] = fsolve(@Get,in_guess,options);
ksi = x(num);
theta=x; theta(num)=1;

function F = Get(x)
```

```
global N_cluster
global M_grid
global num

theta = x;
theta(num) = 1;
[difference] = check(N_cluster,M_grid,x(num),theta);
F = difference;
%%-------------------------------------------------------------
```

- Subtracting right-hand side from left-hand side for a pair of the frequency ksi and the foundations displacements $theta$ in (1.15). Should be zero if solution is correct.

```
%%-------------------------------------------------------------
function [difference] = check(Ni,Mi,ksi,theta)

[a,b,space,l_char]  = Init_city;
% City parameters
quant = length(a);
% Number of buildings in one cluster
freq = ksi;
% Frequency
N_cluster = Ni;
% Quantity of the clusters of the city
N_build = N_cluster*quant;
% Quantity of the buildings
M = Mi;
% Grid size
period = b(end)-a(1)+space(end);
% The length of a periodic city cluster
a_end = zeros(1,N_build); b_end = zeros(1,N_build);
for n=1:N_build
    for j=1:quant
        a_end(j+(n-1)*quant) = a(j)+(n-1)*period;
        b_end(j+(n-1)*quant) = b(j)+(n-1)*period;
    end;
end;
gamma_b = 1.5; f_b = 0.5; b = 1.5; r = 0.1;
c_b=0.5*(b_end-a_end)/l_char;
p_ksi = c_b.^2*freq^2 - (b*f_b)^2;
q_ksi = 2*r*c_b.^2*freq^2/f_b.*(c_b.^2*freq^2-(1+1/gamma_b)*p_ksi);
% City parameteres

p=1:2*M; x_bar = -1+(2*p-1)/(2*M); q=0:2*M; t_bar = -1+q/M;
```

```
Matr = zeros(2*M*N_build,2*M*N_build);
rhs = zeros(2*M*N_build,1);

for q=1:2*M
% asin(t_{q+1})-asin(t_{q}) need to be computed just once,
% and then can be used for each line of the matrix
    darcsin(q) = asin(t_bar(q+1))-asin(t_bar(q));
end;

Matr = syst_matrix(N_cluster,M,ksi);
rhs = zeros(2*N_build*M,1);
for j=1:N_build
    rhs((2*M*(j-1)+1):2*M*j) = theta(j);
end;
phi = Matr\rhs;
for j=1:N_build
    sum = 0;
    for q=1:2*M
        sum = sum + darcsin(q)*phi(q + (j-1)*2*M);
    end;
    T(j) = real(0.5*sum);
    difference(j) = q_ksi(j)*theta(j) - p_ksi(j)*T(j);
end;
%%-----------------------------------------------------------------
```

- Assembling matrix (3.21) for system (3.22).

```
%%-----------------------------------------------------------------
function Matr = syst_matrix(Ni,Mi,ksi)

global a_end
global b_end
global Euler

Euler = 0.5772156649015328;

[a,b,space,l_char]  = Init_city;
quant = length(a);

freq = ksi;
N_build = quant*Ni;
% Quantity of the buildings
M = Mi;
```

```
period = b(end)-a(1)+space(end);
% The length of a periodic city cluster

a_end = zeros(1,N_build); b_end = zeros(1,N_build);
for n=1:N_build
    for j=1:quant
        a_end(j+(n-1)*quant) = a(j)+(n-1)*period;
        b_end(j+(n-1)*quant) = b(j)+(n-1)*period;
    end;
end;

p=1:2*M; x_bar = -1+(2*p-1)/(2*M); q=0:2*M; t_bar = -1+q/M;

Matr = zeros(2*M*N_build,2*M*N_build);
rhs = zeros(2*M*N_build,1);

for q=1:2*M
% asin(t_{q+1})-asin(t_{q}) need to be computed just once,
% and then can be used for each line of the matrix
    darcsin(q) = asin(t_bar(q+1))-asin(t_bar(q));
end;

Matr = zeros(2*M*N_build,2*M*N_build);
for k=1:N_build
  for j=1:N_build
    for p=1:2*M
      for q=1:M
        argum = freq*abs(g_func(k,x_bar(p))-g_func(j,x_bar(q)));
        param1 = (b_end(j)-a_end(j))/2;
        param2 = 0.5*(x_bar(p)*(b_end(k)-a_end(k))+b_end(k)+...
                 a_end(k)-b_end(j)-a_end(j));
        Matr(p+2*M*(k-1),q+2*M*(j-1)) = A_func(argum)/sqrt(1-x_bar(q))*...
             I_integr(param1,-param2,-t_bar(q+1),-t_bar(q)) + ...
             (asin(t_bar(q+1))-asin(t_bar(q)))*(A_func(argum)*log(freq/2)+...
             B_func(argum));
      end;
      for q=(M+1):2*M
        argum = freq*abs(g_func(k,x_bar(p))-g_func(j,x_bar(q)));
        param1 = (b_end(j)-a_end(j))/2;
        param2 = 0.5*(x_bar(p)*(b_end(k)-a_end(k))+b_end(k)+a_end(k)-...
                 b_end(j)-a_end(j));
        Matr(p+2*M*(k-1),q+2*M*(j-1)) = A_func(argum)/sqrt(1+x_bar(q))*...
```

```
                I_integr(param1,param2,t_bar(q),t_bar(q+1)) + ...
                (asin(t_bar(q+1))-asin(t_bar(q)))*(A_func(argum)*log(freq/2)+...
                B_func(argum));
        end;
      end;
    end;
end;

function x=A_func(z)
x = -0.5/pi*besselj(0,z);

function x=B_func(z)
global Euler
if (z~=0)
    x = 0.25*1i*besselh(0,z) + 0.5/pi*besselj(0,z)*log(z/2);
else
    x = 1i/4 - 0.5*Euler/pi;
end;

function x = g_func(j,t)
global a_end
global b_end
x = (b_end(j)-a_end(j))/2*t + (b_end(j)+a_end(j))/2;
%%-----------------------------------------------------------------
```

- Defining city parameters: a, b are the building ends coordinates for one cluster, *space* are the distances between the buildings for one cluster, *l_char* is characteristic length.

```
%%-----------------------------------------------------------------
function [a,b,space,l_char] = Init_city()
a = [0 2.2 4.7]; b = [1.8 4.2 6.2]; space = [0.4 0.5 0.3]; l_char = 1;
%%-----------------------------------------------------------------
```

- Calculating integral (3.23).

```
%%-----------------------------------------------------------------
function g = I_integr(a,b,x_beg,x_end)
% Calculation of int[x_beg,x_end] { ln|at-b| / sqrt(1-t) } dt,
% -1<=end,start<=1

g_1 = 4*(sqrt(1-x_end) - sqrt(1-x_beg));

if (b>a)
    g_2 = func_1(x_end,a,b) - func_1(x_beg,a,b);
else
    if (b<a)
```

```
        g_2 = func_3(x_end,a,b) - func_3(x_beg,a,b);
    else
        g_2 = func_2(x_end,a,b) - func_2(x_beg,a,b);
    end;
end;
g = g_1 - 2*g_2;

function x=func_1(t,a,b)
x = sqrt(1-t)*log(abs(a*t-b)) + 2*sqrt((b-a)/a)*atan(sqrt((a-a*t)/(b-a)));

function x=func_2(t,a,b)
if t==1
    x=0;
else
    x = sqrt(1-t)*log(abs(a*t-a));
end;

function x=func_3(t,a,b)
x = (sqrt(1-t) - sqrt((a-b)/a))*log(abs(a*t-b)) +...
    2*sqrt((a-b)/a)*log(abs(sqrt(a-a*t) + sqrt(a-b)));
%%-----------------------------------------------------------------
```

B.2 Different building city - periodic case.

- Solving equation (1.15). Here *theta* in the code stands for α in the thesis, and θ_{numi} is assumed to be 1.

```
%%-----------------------------------------------------------------
function [ksi,theta] = min_diff(Mi,numi,in_guess)

global N_build
global M_grid
global num
global phi_temp

M_grid = Mi; num=numi;

[a_end, b_end, period, l_char] = Init_geom;
N_build = length(a_end);
options=optimset('Display','iter','TolFun',1e-6,'TolX',1e-6);

[x, fval,exitflag] = fsolve(@Get,in_guess,options);
```

```
for k=1:N_build
    h=(b_end(k)-a_end(k))/(2*M_grid);
    s=a_end+h:h:b_end-h;
end;

ksi = x(num);
theta=x; theta(num)=1;

function F = Get(x)

global N_build
global M_grid
global num
global phi_temp

theta = x;
theta(num) = 1;
[difference,phi_temp] = check(M_grid,x(num),theta);
F = difference;
%%-----------------------------------------------------------------
```

- Subtracting right-hand side from left-hand side for a pair of the frequency *ksi* and the foundations displacements *theta* in (1.15). Should be zero if solution is correct.

```
%%-----------------------------------------------------------------
function [difference] = check(Mi,ksi,theta)

freq = ksi; M = Mi;

[a_end, b_end, period, l_char] = Init_geom;
N = length(a_end);

gamma_b = 1.5; f_b = 0.5; b = 1.5; r = 0.1;
c_b = 0.5/l_char*(b_end-a_end);

p_ksi = c_b.^2*freq^2 - (b*f_b)^2;
q_ksi = 2*r*c_b.^2*freq^2/f_b.*(c_b.^2*freq^2-(1+1/gamma_b)*p_ksi);

p=1:2*M; x_bar = -1+(2*p-1)/(2*M); q=0:2*M; t_bar = -1+q/M;

Matr = zeros(2*M*N,2*M*N);
rhs = zeros(2*M*N,1);

for q=1:2*M
```

```
% asin(t_{q+1})-asin(t_{q}) need to be computed just once,
% and then can be used for each line of the matrix
    darcsin(q) = asin(t_bar(q+1))-asin(t_bar(q));
end;

Matr = syst_matrix(M,ksi);
for j=1:N
    rhs((2*M*(j-1)+1):2*M*j) = theta(j);
end;
phi = Matr\rhs;
for j=1:N
  sum = 0;
  for q=1:2*M
    sum = sum + darcsin(q)*phi(q + (j-1)*2*M);
  end;
  T(j) = real(0.5*sum);
  difference(j) = q_ksi(j)*theta(j) - p_ksi(j)*T(j);
end;
%%-----------------------------------------------------------------
```

- Initializing the city parameters.

```
%%-----------------------------------------------------------------
function [a_end, b_end, period, l_char] = Init_geom;
a_end = [0 1.3 3 4 5.4 6.8]; b_end = [1 2.6 3.5 5 6.2 7.4];
period = 7.9; l_char = 1;
%%-----------------------------------------------------------------
```

-
```
%%-----------------------------------------------------------------
function Matr = syst_matrix(Mi,ksi)

global freq
global fund_zero_out
global a_end
global b_end
global period

Euler = 0.5772156649015328;

freq = ksi;
% Frequency
M = Mi;
% Grid size

[a_end, b_end, period] = Init_geom;
```

```
N_build = length(a_end);
% Quantity of the buildings

fund_zero_out = limit(freq,period);
% Limit of a fundamental solution as its argument goes to zero

p=1:2*M; x_bar = -1+(2*p-1)/(2*M);
q=0:2*M; t_bar = -1+q/M;

Matr = zeros(2*M*N_build,2*M*N_build);

for q=1:2*M
% asin(t_{q+1})-asin(t_{q}) need to be computed just once,
% and then can be used for each line of the matrix
    darcsin(q) = asin(t_bar(q+1))-asin(t_bar(q));
end;

Matr = zeros(2*M*N_build,2*M*N_build);
% Assembling matrix for system (28)
for k=1:N_build
  for j=1:N_build
    for p=1:2*M
      for q=1:M
        argum = freq*abs(g_func(k,x_bar(p))-g_func(j,x_bar(q)));
        param1 = (b_end(j)-a_end(j))/2;
        param2 = 0.5*(x_bar(p)*(b_end(k)-a_end(k))+b_end(k)+a_end(k)-...
                 b_end(j)-a_end(j));
        Matr(p+2*M*(k-1),q+2*M*(j-1)) = A_func(argum)/sqrt(1-x_bar(q))*...
           I_integr(param1,-param2,-t_bar(q+1),-t_bar(q)) + ...
           (asin(t_bar(q+1))-asin(t_bar(q)))*(A_func(argum)*log(freq/2)+...
           B_func(argum));
      end;
      for q=(M+1):2*M
        argum = freq*abs(g_func(k,x_bar(p))-g_func(j,x_bar(q)));
        param1 = (b_end(j)-a_end(j))/2;
        param2 = 0.5*(x_bar(p)*(b_end(k)-a_end(k))+b_end(k)+a_end(k)-...
                 b_end(j)-a_end(j));
        Matr(p+2*M*(k-1),q+2*M*(j-1)) = A_func(argum)/sqrt(1+x_bar(q))*...
             I_integr(param1,param2,t_bar(q),t_bar(q+1)) + ...
             (asin(t_bar(q+1))-asin(t_bar(q)))*(A_func(argum)*log(freq/2)+...
             B_func(argum));
      end;
```

```
    end;
  end;
end;

function x=A_func(z)
x = -0.5/pi*besselj(0,z);

function x=B_func(z)
global freq
global fund_zero_out
global period
if (z~=0)
  x = fundamental(period,freq,0,z/freq,0,0) + 0.5/pi*besselj(0,z)*log(z/2);
else
  x = fund_zero_out;
end;

function x = g_func(j,t)
global a_end
global b_end
x = (b_end(j)-a_end(j))/2*t + (b_end(j)+a_end(j))/2;
%%-------------------------------------------------------------
```

- Code *I_integral.m* to calculate integrals (3.23) is exactly the same as for the free-space case.
- Finding the limit of $B_0(z)$ from (3.29) as $z \to 0$.

```
%%-------------------------------------------------------------
function lim = limit(period,freq)
Euler = 0.5772156649015328;
lim = 1i/4 - 0.5*Euler/pi + 1i/4*bessel0_series(period,freq,5,4,7);
%%-------------------------------------------------------------
```

- Code to calculate (2.21).

```
%%-------------------------------------------------------------
function G = bessel0_series(di,wave_k,M1i,M2i,Ni)

Euler = 0.57721566490153286;
d = di;
% Period
beta = 0;
% Dependence of the incident waves
k = wave_k;
% Wavelength/frequency
```

```
p = 2*pi/d;
M1 = M1i; M2 = M2i; N=Ni; a=3;

sum = 0;
for m=-M1:M1
    beta_m = beta+p*m;
    temp = sqrt(abs(k^2-beta_m^2));
    if (beta_m^2-k^2)>0
        gamma_m = temp;
    else
        gamma_m = -i*temp;
    end;
    sum = sum + erfz(0.5*gamma_m*d/a)/gamma_m;
end;
part1 = 0.5*sum/d;

sum = 0;
for m=-M2:(-1)
    sum1 = 0; coeff=0.5*k*d/a;
    for n=0:N
        sum1 = sum1 + coeff^(2*n)*E_func(n+1,a^2*m^2)/factorial(n);
    end;
    sum = sum + exp(i*m*beta*d)*sum1;
end;
for m=1:M2
    sum1 = 0; coeff=0.5*k*d/a;
    for n=0:N
        sum1 = sum1 + coeff^(2*n)*E_func(n+1,a^2*m^2)/factorial(n);
    end;
    sum = sum + exp(i*m*beta*d)*sum1;
end;
part2 = 0.25*sum/pi;

% if m=0, n>=1
sum = 0;
coeff=0.5*k*d/a;
for n=1:N
    sum = sum + coeff^(2*n)/n/factorial(n);
end;
part3 = sum/(4*pi);

part4 = 0.5*log(0.5*k*d/a)/pi - 1i/4 + 0.25*Euler/pi;
G = (part1 + part2 + part3 + part4)*4/1i;
```

```
%%-------------------------------------------------------------
```

- Fundamental solution of the Helmholtz equation. Periodic case.

```
%%-------------------------------------------------------------
function gr = fundamental(period,freq,x1,x2,y1,y2)
gr = green(period,freq,x1,x2,y1,y2);
%%-------------------------------------------------------------
```

- Code to calculate the periodic Green's function.

```
%%-------------------------------------------------------------
function g = green(period,kappa,xi,yi,ksii,etai)

if abs(xi-ksii) > 1e-1
    g = green_approx(500,period,kappa,xi,yi,ksii,etai);
else
    g = green_approx_ewald(8,3,31,period,kappa,xi,yi,ksii,etai);
end;
%%-------------------------------------------------------------
```

- Spectral form (2.13).

```
%%-------------------------------------------------------------
function alt = green_approx(Mi,di,ki,xi,yi,ksii,etai)
alt = 0;
ksi = ksii; eta = etai;
%Source point
d = di;
% Period
beta = 0;
% Dependence of the incident waves
k = ki;
% Wavelength
p = 2*pi/d; M = Mi; X = xi - ksi; Y = yi - eta;
sum = 0;
for m=-M:M
    beta_m = beta+p*m;
    temp = sqrt(abs(k^2-beta_m^2));
    if (beta_m^2-k^2)>0
        gamma_m = temp;
    else
        gamma_m = -i*temp;
    end;
    sum = sum + exp(-gamma_m*abs(X))*exp(1i*beta_m*Y)/gamma_m;
end;
alt = sum/(2*d);
```

```
%%-------------------------------------------------------------
```

- Ewald's method.

```
%%-------------------------------------------------------------
function G = green_approx_ewald(M1i,M2i,Ni,di,ki,xi,yi,ksii,etai)

d = di;
% Period
beta = 0;
% Dependence of the incident waves
k = ki;
% Wavelength/frequency
M1 = M1i; M2 = M2i; N=Ni;
X = xi - ksii; Y = yi - etai;
p = 2*pi/d;
a=5;

% Calculating E integrals
E = zeros(N+1,2*M2+1);
for m=-M2:M2
    r_m = (X^2+(Y-m*d)^2)^0.5;
    x = (a*r_m/d)^2;
    if x==0
        fprintf('Singularity!!! Some r_m is zero :(');
        break
    else
        E(1,m+M2+1) = expint(x);
    end;
    for n=1:N
        E(n+1,m+M2+1) = exp(-x)/n - x/n*E(n,m+M2+1);
    end;
end;

sum = 0;
for m=-M1:M1
  beta_m = beta+p*m;
  temp = sqrt(abs(k^2-beta_m^2));
  if (beta_m^2-k^2)>0
    gamma_m = temp;
  else
    gamma_m = -i*temp;
  end;
  sum = sum + exp(i*beta_m*Y)/(gamma_m*d)*(exp(gamma_m*X)*...
```

```
        erfz(0.5*gamma_m*d/a+a*X/d)+...
        exp(-gamma_m*X)*erfz(0.5*gamma_m*d/a-a*X/d));
end;
part1 = 0.25*sum;

sum = 0;
for m=-M2:M2
    r_m = (X^2+(Y-m*d)^2)^0.5;
    sum1 = 0;
    for n=0:N
        sum1 = sum1 + (0.5*k*d/a)^(2*n)*E(n+1,m+M2+1)/factorial(n);
    end;
    sum = sum + exp(i*m*beta*d)*sum1;
end;
part2 = 0.25*sum/pi;

G = part1 + part2;
%%-------------------------------------------------------------
```

- Calculation of the complementary error function (2.16) by implementing "A method for calculating the complex complementary error function with prescribed accuracy" by Knut Petras (see [25]).

```
%%-------------------------------------------------------------
function x=erfz(z)
if imag(z)==0
    x = erfc(z);
else
    if abs(z)<4
        % Using formula (2)
        sum = 0;
        for n=0:200
            sum = sum + (-1)^n*z^(2*n+1)/(factorial(n)*(2*n+1));
        end;
        x = 1-2*sum/sqrt(pi);
    else
        % Using formula (4)
        modul = abs(z);
        sum = 1;
        k = (abs(z))^2;
        for n=1:(k-1)
            sum = sum + (-1)^n*odd_fact(n)/(2*z^2)^n;
        end;
        x = sum/(sqrt(pi)*z*exp(z^2));
```

```
    end;

end;

function q=odd_fact(m)
%% Calculating product "odd factorial" 1*3*5*...*(2*m-1)
prod = 1;
for k = 1:m
    prod = prod*(2*k-1);
end;
q = prod;
%%-----------------------------------------------------------------
```

- Calculating the exponential integral (2.17).

```
%%-----------------------------------------------------------------
function E = E_func(n,x)

if (x==0)
    if (n~=1)
        E = 1/(n-1);
    end;
else
    if (n==1)
        E = expint(x);
    else
        if (n==0)
            E = exp(-x)/x;
        else
            E = exp(-x)/(n-1) + x/(1-n)*E_func(n-1,x);
        end;
    end;
end;
%%-----------------------------------------------------------------
```

Appendix C

Maple code

Maple code to calculate limits (2.39) and (2.37).

```
> restart;
> with(linalg);
> assume(t,real);
> assume(tau,real);
> x1 := 0.4*(cos(t) - 0.4*sin(t) - 0.5*sin(2*t));
> x2 :=0.4*cos(t)+0.2*sin(t)+0.5;
> x := <x1,x2>;
> y := eval(x,t=tau);
> z := y-x;
> tang1 := diff(x1,t);
> tang2 := diff(x2,t);
> nu := <tang2,-tang1>;
> nu_tau := eval(nu,t=tau);
> numerator := 2*combine(nu_tau.z);
> denomin := combine(z.z);
> K_2 := simplify(numerator/denomin);
> lim:=limit(K_2,t=tau);
> answer := simplify(lim);
> L_2 := 4*(sin(0.5*(t-tau)))^2/(z.z);
> lim_2 := simplify(limit(L_2,t=tau));
```

Bibliography

[1] M. Abramovitz, I. A. Stegun, Handbook of Mathematical Functions. 10^{th} Printing, National Bureau of Standards, 1972.

[2] P. Y. Bard, J. L. Chazelas, Ph. Gueguen, M. Kham, J. F. Semblat, Site-City Interaction, in: C. S. Oliveira, A. Roca, X. Coula (eds.), Assessing and Managing Risk, 91-114. Springer, 2006.

[3] M. Berger, B. Gostiaux, Differential Geometry: Manifolds, Curves, and Surfaces. Springer-Verlag, 1988.

[4] S. C. Bradford, J. F. Clinton, J. Favela, T. H. Heaton, Results of Millikan library forced vibration testing, *Report No. EERL 2004-3*, Feb. 2004.

[5] D. Bucur, I. R. Ionescu, Asymptotic analysis and scaling of friction parameters. *J. Appl. Math. Phys.* 57 (6) (2006) 1042-1056.

[6] C. Boutin, P. Roussillon, Assessment of the Urbanization Effect on Seismic Response. *Bull. Seism. Soc. Am.*, vol. 94, No. 1 (2004) 251-268.

[7] C. Boutin, P. Roussillon, Wave propagation in presence of oscillators on the free surface. *Int. J. Eng. Sc.*, 44 (2006) 180-204.

[8] F. Capolino, D. R. Wilton, W. A. Johnson, Efficient Computation of the 2-D Green's Function for 1-D Periodic Structures Using the Ewald Method. *IEEE Trans. Antennas Propag.*, vol. 53, No. 9 (2005) 2977-2984.

[9] D. Colton, R. Kress, Integral Equation Methods In Scattering Theory. Wiley, 1983.

[10] D. Colton, R. Kress, Inverse Acoustic and Electromagnetic Scattering Theory. 2^{nd} Ed., Springer, 1998.

[11] S. Erlingsson, A. Bodare, Live load induced vibrations in Ullevi Stadium - dynamic soil analysis, *Soil Dyn. and Earthquake Eng.*, vol. 15, Issue 3 (1996) 171-188.

[12] P. P. Ewald, Die Berechnung optischer und elektrostatischen Gitterpotentiale. *Ann. Phys.* 64 (1921) 253-268.

[13] G. B. Folland, Introduction to Partial Differential Equations, Second Edition, Princeton University Press, 1995.

[14] D. Gilbarg, N. S. Trudinger, Elliptic Partial Differential Equations of Second Order.

Springer, 2001.

[15] M. Ghergu, I. R. Ionescu, Structure-soil-structure coupling in seismic excitation and "city-effect". *Int. J. Eng. Sci.* 47 (2009) 342-354.

[16] I. S. Gradshteyn, I. M. Ryzhik, Table of Integrals, Series, and Products. 7^{th} Ed., Elsevier, 2007.

[17] $http://earthquake.usgs.gov/earthquakes/world/events/1985\_09\_19.php$

[18] $http://eqseis.geosc.psu.edu/\sim cammon/HTML/Classes/IntroQuakes/Notes/seismometers.html$

[19] H. Kanamori, J. Mori, B. Sturtevant, D. L. Anderson, T. Heaton, Seismic excitation by space shuttles, *Shock waves*, 2 (1992) 89-96.

[20] T. Kato, Perturbation Theory for Linear Operators, 2_{nd} edition, Springer, 1995.

[21] R. Kress, Linear Integral Equations, 2^{nd} Ed., Springer, 1999.

[22] P. A. Krutitskii, Dirichlet problem for the Helmholtz equation outside cuts in a plane. *Comp. Math. Math. Phys.*, 34 (1994) 1073-1090.

[23] C. M. Linton, The Green's function for the two-dimensional Helmholtz equation in periodic domains. *J. Engng. Math.* 33 (1998) 377-402.

[24] J.-C. Nédélec, Acoustic and Electromagnetic Equations, Springer, 2001.

[25] K. Petras, A Method for Calculating the Complex Complementary Error Function with Prescribed Accuracy, 2002.

[26] W. Rudin, Real and Complex Analysis. McGraw-Hill, 1970.

[27] Giovanni Maria Troianiello, Elliptic Differential Equations and Obstacle Problems, University Series in Mathematics, 1987.

[28] T. H. V. Phuong, Natural Frequencies of Soil-Foundation Systems and Soil Layers, *HCMUT*, 26 (2011).

[29] D. Volkov, D. T. Papageorgiou, P. G. Petropoulos, Accurate and Efficient Boundary Integral Methods for Electrified Liquid Bridge Problems, *SIAM J. Sci. Comput.*, 26 (6) (2005) 2102-2132.

[30] G. N. Watson, A treatise on the theory of Bessel functions, Cambridge University press, 1922.

[31] A. Wirgin, P.-Y. Bard, Effects of buildings on the duration and amplitude of ground motion in Mexico City, *Bull. Seism. Soc. Am.*, vol. 86 (1996) 914-920.